Stony Brook University

Small Molecule Modulators of Amyloid Formation by Islet Amyloid Polypeptide

A Thesis Presented

by

Harris Noor

To

The Graduate School

in Partial Fulfillment of the

Requirement

For the Degree of

Master of Science

in

Chemistry

Stony Brook University

August 2012

Stony Brook University
The Graduate School

Harris Noor

We, the thesis committee for the above candidate for the Master of Science degree, hereby recommend acceptance of this thesis.

Daniel P. Raleigh, Ph. D. – Thesis Advisor
Department of Chemistry

Elizabeth Boon, Ph.D. – Chairperson
Department of Chemistry

Jessica Seeliger, Ph.D. – Third Member
Department of Pharmacological Sciences

This thesis is accepted by the Graduate School

Charles Taber

Interim Dean of the Graduate School

Abstract of the Thesis

Small Molecule Modulators of Amyloid Formation by Islet Amyloid Polypeptide

By

Harris Noor

Master of Science

In

Chemistry

Stony Brook University

2012

Amyloid formation is involved in many human diseases. Examples include Alzheimer's, Huntington's, and Parkinson's disease, and type-2 diabetes. Islet Amyloid Polypeptide (IAPP) is a protein that is co-secreted with insulin in pancreatic β-cells; however, IAPP is an extremely amyloidogenic protein. There is a considerable amount of interest to develop inhibitors for amyloid formation. A large body of work has been focused on the development of inhibitors for the Aβ peptide of Alzheimer's disease, but fewer inhibitors have been developed for IAPP. In this thesis, small molecules were developed to alter fiber formation kinetics.

This thesis described studies of the ability of Morin Hydrate to inhibit and S-Flurbiprofen to accelerate IAPP amyloid formation. Both of these compounds have been analyzed and proposed to be inhibitors of Aβ, but they have not been tested on IAPP.

Morin hydrate, a hydroxyflavone, can be found in fruits of plants and S-flurbiprofen is a non-steroidal anti-inflammatory drug (NSAID) that is a derivative of naturally occurring molecules found in plants.

It is thought that the toxic intermediates that these amyloidgenic peptides form are the central cause of these amyloidgenic diseases; not necessarily the fibers. These studies demonstrate two different approaches to inhibit amyloid toxicity. One method is to inhibit amyloid formation directly and avoid producing the toxic intermediates. The other method is to accelerate the kinetics at assembly past the toxic oligomeric state straight into fibers. These studies may give a better understanding of the mechanism of amyloid formation and possibly assist in developing effective therapeutic strategies for different amyloidgenic diseases.

Table of Contents

List of Figures

List of Abbreviations

Aβ	The proteolytical fragment of the precursor protein that is responsible for amyloid formation in Alzheimer's disease
AMBI	Aminomethylbenzimidazol
BISA	1-H-Benzimidazole-2-Sulfonic Acid (BISA)
CD	Circular dichroism
DMSO	Dimethyl sulfoxide
EMPB	N-Ethyl-N-Methylamino(phenylazo)benzonitrile
Fmoc	9-Fluorenylmethoxycarbonyl
HBTU	O-benzotriazole-N,N,N',N'-tetramethyluronium hexafluorophosphate
HFIP	Henxafluoroisopropanol
HNDSA	3-hydroxy 2,7-naphthalene disulfonic acid disodium salt
HPLC	High-performance liquid chromatography
IAPP	Islet amyloid polypeptide
MALDI-TOF-MS	Matrix-assisted laser desorption ionization time-of-flight mass spectrometry
PAL-PEG-PS	Pegylated polystyrene support resin, 5-(4'-Fmoc-aminometyl-3', 5-dimethoxyphenol) valeric acid
PC1/3	Prohormone convertase 1/3
PC2	Prohormone convertase 2
preproIAPP	Precursor sequence of proIAPP and mature IAPP
proIAPP	Pro-islet amyloid Polypeptide
t_{50}	Time to 50% completion of fibril formation during a thioflavin-T kinetic assay
TEM	Transmission electron microscopy
TFA	Trifluoroacetic acid

UV	Ultraviolet
v/v	Volume to volume

Acknowledgements

This work could not have been done without the encouragement and support from my advisor Dr. Daniel P. Raleigh. He walked me through everything and helped me come up with creative experiments to perform to verify my findings. He gave me a larger outlook on science and life as well.

Thank you to my committee members, Prof. Elizabeth Boon who taught me a lot through CHE 541 and Prof. Jessica Seeliger for participating in my defense.

Thank you to all of the members of the Raleigh Lab. Thank you to the past members, some of which still help me: Dr. Andisheh Abedini, Trisha Barua, Dr. Humeyra Taskent, Dr. Fanling Meng, Dr. Peter Marek; and present members: Rehana Akter, Ping Cao, Keshav Kalanadhabhatta, Cynthia Li, Olesya Levsh, Bowu Luan, Dr. Wenli Meng, Vadim Patsalo, Ivan Peran, Matthew Watson, Hui Wang, and Dr. Shifeng Xiao. It has been a pleasure to work and learn beside these wonderful people.

Thank you to the Chemistry Department Office Staff. They have helped me, reminded me, and urged me to do well. Without them helping me, I wouldn't have applied for my Masters and pursued this degree.

Thank you to my wife, Esther Noor, for helping, encouraging, and believing in me. Without her and the many things we have been through during these 2-3 years in the Master's Program I don't know what I would have done.

And most of all thank you God for guiding me through this.

1. INTRODUCTION

Amyloids are insoluble proteins aggregates which are involved in many diseases. Amyloids have been known to be involved in more than 20 different human diseases where the accumulation of these peptides or proteins leads to amyloidosis and affects different tissues; examples include Alzheimer's, Huntington's and Parkinson's diseases, and type-2 diabetes mellitus (*1, 2*). Amyloidosis occurs in various tissues, such as the pancreas in type-2 diabetes and the brain in Alzheimer's and Parkinson's disease.

1.1 Features of Amyloid Fibrils

There are many peptides or proteins that can form amyloid. Even though these peptides or proteins have very different amino acid sequences, the structure and physical properties of the amyloid are similar. Populations of amyloid fibrils observed by electron microscopy appeared to be polymorphic in bundles of three protofilaments in a left-handed coil with a pitch of 25-50 nm (*3*). It has been shown through X-ray defraction that amyloid fibers assume cross-β-sheet structures (*4*). A key characteristic feature of amyloid fibrils is that the individual β-sheet strands are aligned perpendicular to the fibrillar axis in which there is an extensive network of hydrogen bonding between the β-sheet strands (*5-7*).

This highly ordered structure of β-sheet enables the binding of histological dyes such as thioflavin-T (*8*). Thioflavin-T has been used as an indirect way to characterize the presence of amyloid fibers. In solution thioflavin-T has low quantum yield; however, when thioflavin-T binds to the fibrils, the quantum yield increases. When a wavelength of approximately 450 nm is used to excite the molecule, and the molecule is bound to the

fiber, the molecule emits a light of around 485nm (*9*). It is unknown how thioflavin-T binds to amyloids fibers, but it is believed that the molecule binds to the grooves on the surface of the amyloid fibrils (Figure 1-1) (*8*).

A number of studies have been performed in order to elucidate the mechanism of amyloid fiber formation; however, the exact mechanism is still not known. Studies have suggested that amyloid formation is in a nucleation-dependent manner which can be affected by seeding (*10-12*). The nucleation dependent model is characterized by a lag phase in which monomers are in solution and sometimes form oligomers. These oligomers slowly convert to fiber nucleus. After the lag phase, there is rapid formation of fibers called the growth phase. After the growth phase, the reaction approaches a plateau where fibers are in equilibrium with soluble monomers (Figure 1-2) (*13*).

1.2 Pancreatic Synthesis of Islet Amyloid Polypeptide (IAPP)

IAPP is a member of the calcitonin-like family of peptides and is found in all mammalian species examined (Figure 1-3) (*14-17*). The 37 residue polypeptide hormone is packaged in the insulin secretory granule and normally acts as an endocrine partner to insulin (*16, 18, 19*). IAPP aggregates to form islet amyloid in type-2 diabetes; a process which is widely believed to contribute to β-cell death in type-2 diabetes (*14, 15, 18, 20-27*). Recent studies also highlight a potentially important role for IAPP amyloid formation in the failure of islet cell grafts (*28-30*). Islet amyloid polypeptide (IAPP, amylin) is normally co-expressed with insulin at a roughly 1:100 ratio of IAPP:insulin, in granules within β-islet cells (*31-33*). The role of IAPP still remains unclear, although, it is thought to be important glycemic regulation by delaying gastric emptying, and

inhibiting of digestive enzyme secretion and glucose intake (*34-36*). IAPP is synthesized as a 89 residue precursor (preproIAPP) (*37, 38*). The precursor is proteolytically removed to create a 67 residue proIAPP. proIAPP is processed by proprotein convertase enzyme PC1, PC2, and PC3 (*39*). The residues at the C-terminus are removed by carboxypeptidase E and the removal of glycine and amidation of the Tyr-37 by peptidylglycine alpha-amidating onooxygenase (PAM). The formation of the disulfide bond between the Cys-2 and Cys-7 form the mature and fully functional IAPP. The primary sequence of IAPP and processing is shown in Figure 1-4.

There are two major types of diabetic-patients. Type-1diabetes results from destruction of the islets. Type-2 diabetic-patients develop the disease mostly over a 40-year period where the body develops insulin resistance. Type-2 diabetes is also characterized by a deficiency of insulin secretion. Amyloid deposition is a characteristic feature of type-2 diabetes (*20*). Islet amyloid deposits may play an important role in β-cell loss and insulin secretion in type-2 diabetic-patients, and has been implicated as a cause of the failure of islet cell transplants (*40*).

1.3 Inhibition of Amyloid Formation

Inhibitors of amyloidgenic peptides can provide important insights into the properties of amyloid fiber formation and have obvious therapeutic potential. There is a wide interest in developing inhibitors of amyloid formation and a great deal of effort has been devoted to the Aβ peptide, which is the amyloidgenic peptide that causes amyloid formation in Alzheimer's disease; although, less effort has been devoted to design inhibitors of IAPP amyloid formation.

This thesis described studies of the ability of hydroxyflavones to inhibit and non-steroidal anti-inflammatory drugs (NSAIDs) to accelerate IAPP amyloid formation. Both of these compounds have been analyzed and proposed to be inhibitors of other amyloid forming proteins (*41, 42*). Many of the hydroxyflavones can be found in the fruits of plants (*43*) and of course NSAIDs are commonly found as over the counter drugs; most of which are from plants or are derivatives of naturally occurring molecules. It is thought that the toxic intermediates of these amyloidgenic proteins from soluble peptides into insoluble fibers are the central cause of these amyloidgenic diseases (*44*); not necessarily the fibers itself. Two different approaches to inhibit amyloid toxicity are analyzed. One method is to inhibit amyloid formation directly and avoid producing the toxic state of the amyloidgenic protein. The other method is to accelerate the kinetics at assembly past the toxic oligomeric state straight into fibers. The ability of these compounds to inhibit IAPP amyloid formation has yet to be examined. This prompted us to examine the ability of a number of hydroxyflavones and NSAIDs to inhibit amyloid formation by IAPP.

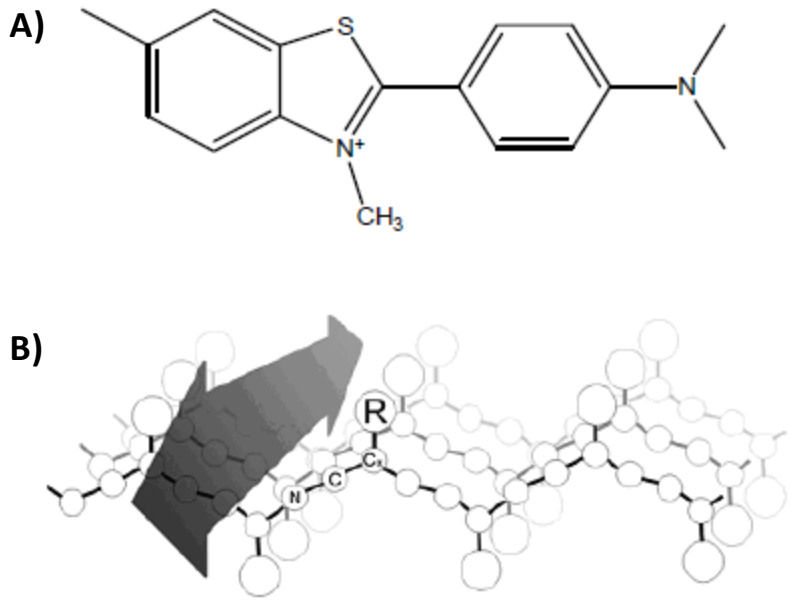

Figure 1-1: Schematic of thioflavin-T binding to β-sheet fibers. **A)** The structure of thioflavin-T. **B)** Model of thioflavin-T binding within a β-sheet channel formed by surface sidechains. It is likely that one face of the sheet would be solvent exposed. Figure adapted from (*8*).

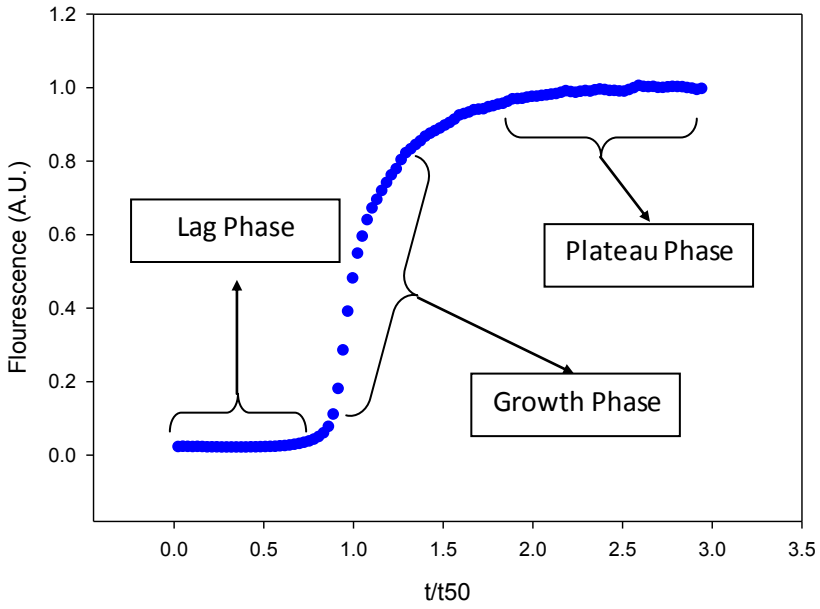

Figure 1-2: A typical thioflavin-T curve to demonstrate the pathway to fiber formation. *Lag phase*: The beginning time points where no detectable fibers are formed. *Growth phase*: Rapid growth of fibers where oligomers act as a nucleus for fiber growth. *Plateau phase*: Fibrillization reaction reaches a plateau where fibers are in equilibrium with soluble monomers.

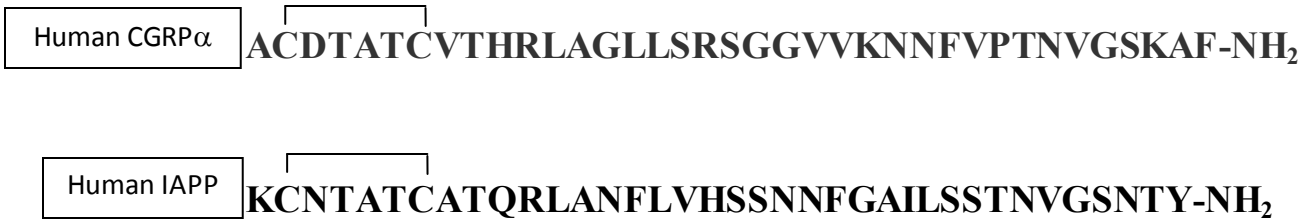

Figure 1-3: A figure comparing the sequence of Human CGRPα and mature human IAPP. **A)** Primary sequence of CGRPa. It contains an amidated C-terminus and a C2-C7 disulfide bridge. **B)** Primary sequence of IAPP. It also contains an amidated C-terminus and a C2-C7 disulfide bridge.

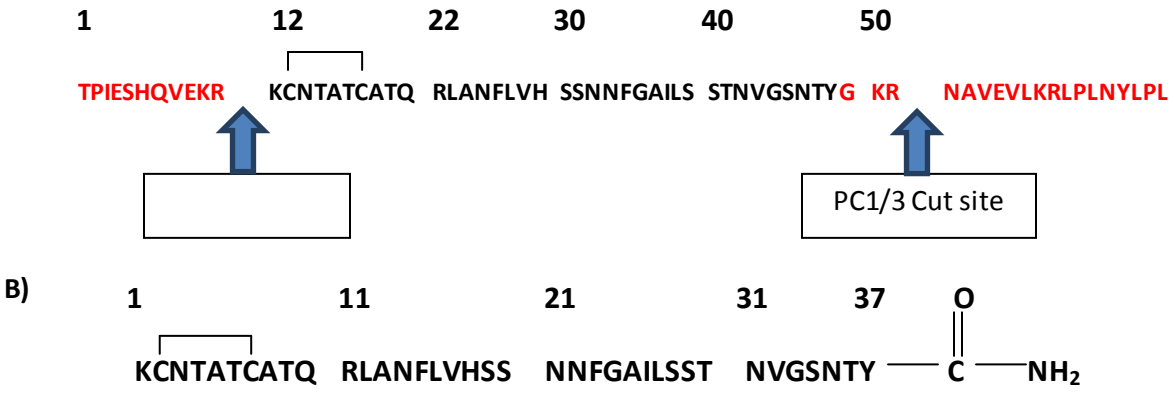

Figure 1-4: A) The primary sequence and processing of the 67-residue proIAPP peptide. The N-terminal and C-terminal flanking regions of pro-IAPP are shown in red which is cleaved by pro-hormone convertases (PC1/PC2/PC3). Cleavage of pro-IAPP occurs at two dibasic sites (Lys-10=Arg-11 and at Lys-50=Arg-51). The N-terminal cleavage is initiated by PC2 and the C-terminal cleavage is initiated by PC1/3. The mature IAPP sequence is shown in black. **B)** The primary sequence of the mature 37 residue IAPP protein with the disulfide bond between Cys-2 and Cys-7, and an amidated C-terminus. The numbering used in (A) cooresponds to the prosequence.

2. Morin Hydrate Inhibits Amyloid Formation by Islet Amyloid Polypeptide and Disaggregates Amyloid Fibers

ABSTRACT

The polypeptide hormone Islet Amyloid Polypeptide (IAPP, amylin) is responsible for islet amyloid formation in type 2 diabetes and in islet cell transplants, where it may contribute to graft failure. Human IAPP is extremely amyloidogenic and fewer inhibitors of amyloid formation by IAPP have been reported than for the Alzheimer's Aβ peptide or for α-synuclein. The ability of a set of hydroxyflavones to inhibit IAPP amyloid formation was tested. Fluorescence detected thioflavin-T binding assays are the most popular method for interpreting the kinetics of amyloid formation and for screening potential inhibitors; however, we show that they can lead to false positives with hydroxyflavones. Several of the compounds inhibit thioflavin-T fluorescence, but not amyloid formation; a result which highlights the hazards of relying solely on thioflavin-T assays to screen potential inhibitors. Transmission electron microscopy shows that Morin hydrate (2′,3,4′,5,7-Pentahydroxyflavone) inhibits amyloid formation by human IAPP and disaggregates pre-formed IAPP amyloid fibers. In contrast, Myricetin, Kaempferol and Quercetin, which differ only in substitutions on the B ring, are not effective inhibitors. Morin hydrate represents a new type of IAPP amyloid inhibitor and the results with the other compounds highlight the importance of the substitution pattern on the B ring.

NOTE: This work presented in this chapter has been published (Harris Noor, Ping Cao, Daniel P. Raleigh. "Morin hydrate inhibits amyloid formation by islet amyloid polypeptide and disaggregates amyloid fibers" (2012) *Protein Science* **21** 373-382). This chapter contains direct excerpts from that paper.

2.1 INTRODUCTION

The search for inhibitors of amyloid fiber formation is an active area of research and particular attention has been paid to flavanoids (*27, 45-66*). In this chapter I examine the ability of a set of hydroxyflavones to inhibit amyloid formation by Islet Amyloid Polypeptide (IAPP, amylin).

There is widespread interest in developing inhibitors of amyloid formation and compounds which can disaggregate pre-formed amyloid. Much of this work has focused on the Aβ peptide of Alzheimer's disease or on α-synuclein, the protein which plays a central role in Parkinson's disease, but fewer inhibitors of IAPP amyloid formation have been reported (*27, 45-66*). IAPP is extremely amyloidogenic and is thus a challenging target for inhibition studies. Certain hydroxyflavones have been reported to be effective inhibitors of amyloid formation by the Aβ polypeptide, although there are conflicting reports about their effectiveness (*67-69*). Their ability to inhibit amyloid formation by IAPP has not yet been examined. I tested the ability of a set of four related hydroxyflavones, Morin hydrate (2′,3,4′,5,7-Pentahydroxyflavone), Myricetin (3,3′,4′,5,5′,7-Hexahydroxyflavone), Kaempferol (3,4′,5,7-Tetrahydroxyflavone) and Quercetin (3,3′,4′,5,6-Pentahydroxyflavone), to inhibit amyloid formation by IAPP and to disaggregate already assembled IAPP amyloid fibers. Morin hydrate is shown to be effective inhibitor while the other compounds are not as effective. I also show that these compounds can compromise standard fluorescence assays of amyloid formation and, in some cases, can lead to false positives in inhibitor screens.

2.2 MATERIALS AND METHODS

2.2.1 Peptide Synthesis

IAPP was synthesized using a CEM Liberty Automatic Microwave Peptide Synthesizer and 9-fluornylmethoxycarbonyl (Fmoc) solid phase peptide Chemistry. FMOC-PAL-Polyethylene-Glycol-Polystyrene (FMOC-PAL-PEG-PS) resin was used and standard Fmoc reaction cycles were employed. Pseudoprolines were used to assist the synthesis as described (*70*). The peptide was cleaved from the resin using standard trifluoroacetic acid (TFA) methods and was then lypholized for 24-48 hours. To increase the solubility of the peptides for later stages of purification, the crude material was dissolved in 20% acetic acid for 2-3 hours and lyophilized. The crude peptides were oxidized in dimethyl sulfoxide (DMSO) (*71*). Peptides were purified using reverse-phase high performance liquid chromatography (HPLC) using a Vydac C18 preparative column with a 2-buffer system. Buffer A, contained 0.045% HCl in distilled deionized (DDI) water and buffer B, contained 0.045% HCl in 80% acetonitrile (ACN) and 20% DDI water. The peptide eluted at 50% buffer B. The identity of the pure peptide was confirmed using Matrix-Assisted Laser Desorption/Ionization Time-of-Flight Mass Spectroscopy (MALDI-TOF MS). IAPP expected 3904.8 daltons; observed 3903.9 daltons.

Myricetin, Quercetin, Morin hydrate and Kaempferol were obtained from Sigma-Aldrich and dissolved in dimethyl sulfoxide (DMSO) to a final concentration of 15.8 mM, determined by weight for experiments in which the compound was added at the 1:1

ratio and 130 mM for experiments in which it was added at a higher ratio. The small molecules were dissolved in DMSO the day of the experiment.

2.2.2 Thioflavin-T Fluorescence Assays

Fluorescence experiments were performed on a Beckman model D880 plate reader. The thioflavin-T studies used excitation and emission filters of 430 nm and 485 nm, respectively. The experiments were performed in 96-well plates at 25 ^{o}C.

IAPP was dissolved in hexafluoroisopropanol (HFIP) to a final concentration of 1.58 mM, determined by weight. The stock solution of IAPP in HFIP was filtered using a 0.45 μm syringe filter. Aliquots of filtered stock solution were pipetted into eppendorf tubes and lypholized. All of the thioflavin-T assays were prepared by dissolving the dried samples of IAPP in Tris-HCl buffer (20 mM, pH 7.4) immediately before measurements. The final peptide concentration was 32 μm in 0.25% DMSO, 20 mM Tris HCl buffer at pH 7.4 and 32 μM thioflavin-T with or without inhibitors. For experiments with the inhibitor, concentrated stock solutions of compounds in DMSO were used and were diluted into the thioflavin-T IAPP solution. The data was analyzed using Sigma-Plot v11.

2.2.3 Transmission Electron Microscopy (TEM)

Aliquots were removed from the fluorescence assays and were analyzed by TEM. Samples were prepared by pipetting 15 μl of the solution onto carbon-coated Formvar 300 mesh copper grids. The grids are stained using saturated uranyl acetate for 1 minute. An FEI Technai12 BioTwinG^2 Transmission Electron Microscope was used and the grids were viewed at a magnification of 98000X (high voltage: 80kV).

2.2.4 Amyloid Disaggregation Experiments

Normal procedures for forming fibers were performed, as described above. Morin hydrate was added at approximately 45 hours after the initiation of fiber formation. Aliquots of the assay were periodically removed from the solution for TEM analysis.

2.3 RESULTS AND DISCUSSION

2.3.1 Hydroxyflavones Can Interfere With Standard Fluorescence Assays of Amyloid Formation.

The structures of the compounds examined in this study are displayed in Figure 2-1 together with the primary structure of IAPP. The compounds share the same core structure; they are poly-hydroxylated and consist of a 12 membered heterocyclic ring linked to the 6 membered aromatic B-ring (Figure 2-1).

Amyloid formation by IAPP displays a lag phase during which no detectable amyloid fibrils are formed followed by a growth phase which leads to a steady state in which amyloid fibrils are in equilibrium with soluble peptide (Figure 2-2A). The rate of amyloid formation is typically measured using fluorescence detected thioflavin-T binding assays. Thioflavin-T is thought to bind to the surface of amyloid fibers in grooves formed by the alignment of side chains in the cross β-sheet structure. Binding to an amyloid fiber increases the fluorescence quantum yield of the dye by restricting the rotation of the benzaminic and benzothiozole rings and thus reducing self-quenching (*72*). Thioflavin-T assays are simple and convenient, but problems may arise in studies of inhibitors since

compounds which appear to inhibit amyloid formation could just be inhibitors of thioflavin-T fluorescence. This may occur because they absorb strongly and lead to inner filter effects, or because they quench the bound thioflavin-T fluorescence, or because they inhibit thioflavin-T binding to amyloid (*73, 74*).

The compounds under study here have the potential to interfere with thioflavin-T assays. Absorbance spectra of the compounds are shown in Figure 2-2. Since the excitation and emission filters of 430 nm and 485 nm are used, respectively the absorbance spectra indicate that there is a large absorbance at 430 nm wavelength numbers. This indicates that there is a high possibility that inner filter effects can affect the final fluorescence levels. Figure 2-3 shows the results of a thioflavin-T monitored kinetic experiment in the presence of Myricetin. In the absence of the compound, a typical IAPP kinetic curve is observed (Figure 2-3A, solid circle curve). Very different behavior is observed in its presence. There is only a very small change in fluorescence over the entire time course of the experiment (Figure 2-3A, open square curve). Taken alone, these results could imply that Myricetin is a potent amyloid inhibitor. However, transmission electron microscopy (TEM) images collected from samples removed at the end of the reaction revealed the presence of amyloid fibers in the IAPP control sample (Figure 2-3B) and in the 1:1 mixture of Myricetin and IAPP (Figure 2-3C). Thus Myricetin is actually not an effective amyloid inhibitor. Similar results were obtained with Kaempferol and Quercetin (Figure 2-5, 2-6, 2-7). We suspect that similar effects might account for some of the discrepancy in the literature on the potency of this class of compounds in inhibiting other amyloids (*67-69*). Experiments in which Myricetin is added to a sample which contains IAPP amyloid fibers and thioflavin-T provide

additional evidence that Myricetin infers with thioflavin-T assays. When the compound is added an immediate drop in fluorescence is observed, but TEM confirm that fibers are still present (Figure 2-8).

The experiments described in the previous section clearly show that thioflavin-T based inhibitor assays are not reliable for these hydroxyflavones. Thus we tested their ability to inhibit IAPP amyloid formation using TEM. Compounds were incubated with IAPP for 48 hours and TEM images were recorded. The incubation period is longer than that required for IAPP to form amyloid under these conditions (Figure 2-3A black curve) and dense collections of amyloid fibers are observed in a control sample of IAPP without compound (Figure 2-4A). Some aggregated material is observed in the 1:1 mixtures of IAPP with all four of the compounds (Figure 2-4B-E). Amyloid fibers are visible in the TEM images of Kaempferol, Quercetin and Myricetin (Figure 2-4B-D); however, the objects detected in the presence of Morin hydrate are thinner and they appear to be less abundant (Figure 2-4E). This encouraged us to examine the effect of different concentration of Morin hydrate on amyloid formation by IAPP.

The TEM micrographs displayed in Figure 2-9 compare the results of 1:1, 1:2, 1:5 and 1:10 mixtures of IAPP and Morin hydrate. In all cases Morin hydrate was added at time equal zero and the samples were incubated for 48 hours. Dense mats of fibers are observed in the control sample of IAPP without Morin hydrate (Figure 2-9A). Adding Morin hydrate in a two-fold excess leads to more pronounced effects than was observed with the 1:1 mixture (compare Figure 2-9B and 2-9C). The objects which are detected are even thinner and less abundant in the 2 fold excess sample relative to the 1:1 sample. Addition of a five or ten fold excess of Morin hydrate led to even more pronounced

changes. Very short objects together with some amorphous aggregates are detected on the grids (Figure 2-9D, 2-9E). We also examined the other compounds at higher ratios, but they still failed to inhibit amyloid formation by IAPP (Fig 2-5, 2-6, 2-7).

We also conducted right angle light scattering experiments in order to obtain an independent test of the ability of Morin hydrate to inhibit IAPP amyloid formation and to confirm that these compounds can interfere with thioflavin-T assays. The curve recorded in the absence of inhibitor shows a sigmoidal transition which closely follows the time course of the thioflavin-T studies (Figure 2-10A). TEM confirms that amyloid fibers are formed (Figure 2-10B). Very different results were obtained when Morin hydrate was present at in a five-fold excess relative to IAPP. No change in signal was observed over the course of the experiment, and TEM confirmed the lack of amyloid (Fig, 2-10A, 2-10C). We also used right angle light scattering to examine the effects of Myricetin on IAPP amyloid formation. The light scattering curve recorded in the presence of Myricetin resembles the curve obtained from the sample of pure IAPP and is very different from the data obtained in the presence of Morin hydrate. TEM confirms that amyloid fibers are formed (Figure 2-10D). These experiments further verify that Myricetin is not an effective inhibitor of IAPP amyloid formation and, even more importantly, confirm that Morin hydrate is an inhibitor.

2.3.2 Morin Hydrate Disaggregates IAPP Amyloid Fibers.

We next examined the ability of Morin hydrate to disaggregate preformed IAPP fibers (Figure 2-11). A sample of IAPP was incubated for 45 hours and a five-fold excess of Morin hydrate was added (Figure 2-11A, black arrow). Note the thioflavin-T curve is

included simply to illustrate that the amyloid reaction had reduced the plateau region before the compound was added. Thioflavin-T fluorescence cannot be used to follow the kinetics of disassembly because the hydroxyflavones interfere with thioflavin-T assays. TEM images of a sample removed just before the addition of the compound revealed dense mats of amyloid fibers (Figure 2-11B). Additional aliquots were removed for TEM analysis starting one hour after addition of Morin hydrate (Figure 2-11A, colored arrows). No fibers were detected in the TEM images of these samples (Figure 2-11).

Morin hydrate also disaggregates IAPP amyloid fibers when it is added at a 1:1 ratio. In this case, the dense collection of amyloid fibers is disrupted to produce a smaller amount of thinner and shorter fibers (Figure 2-12) which bear some resemblance to the species observed when Morin hydrate is added to an IAPP solution at time equals zero. However, disaggregation does not have to be the reverse of amyloid fiber formation and has been shown to be different for at least one inhibitor (*59*).

2.4 CONCLUSION

The results presented here highlight the difficulty of using thioflavin-T based assays to test for amyloid inhibitors and for compounds which disaggregate amyloid fibers. They reiterate the importance of conducting experiments which directly test for the presence of amyloid fibers. Here we used TEM to test for the presence of amyloid and light scattering to monitor the kinetics of aggregation. The data shows that Morin hydrate inhibits amyloid formation by IAPP and demonstrates that it can disassemble IAPP amyloid fibers. The compound represents a new class of IAPP amyloid inhibitors. The ability of this class of compounds to inhibit amyloid formation by IAPP appears to be

strongly dependent upon the substitution pattern in the B-ring since the other compounds tested were much less effective.

There are compounds that inhibit amyloid formation by both IAPP and Aβ (*45, 54, 59*). In contrast, some of the hydroxyflavones studies here have different effects on the Aβ peptide. In particular, Myricetin has been reported to inhibit Aβ amyloid formation (*67-69*), but the data presented here shows it is not effective against IAPP. Several hydroxyflavones in addition to Myricetin have been tested for their ability to inhibit amyloid formation by the Aβ peptide and there are differing reports of their effectiveness (*67-69*). The difficulty of quantitatively interpreting thioflavin-T fluorescence intensities in the presence of the hydroxyflavones may contribute to the apparent differences. These compounds interfere with thioflavin-T assays of amyloid formation by IAPP, thus perhaps they could also interfere or partially interfere with assays of Aβ amyloid formation.

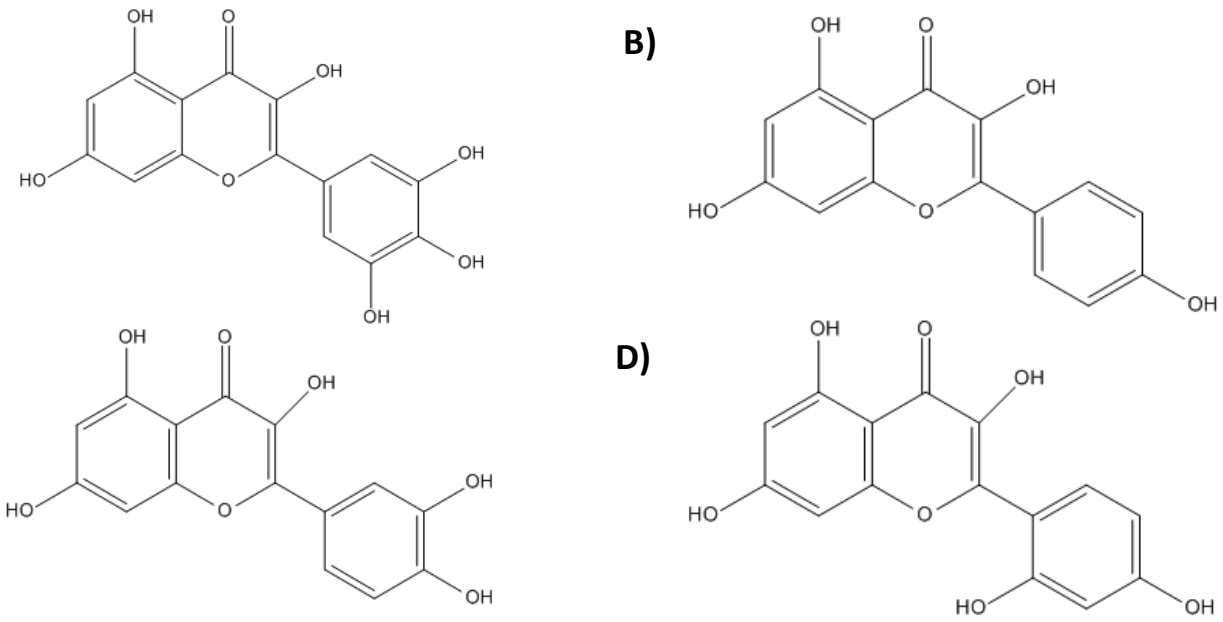

E)

1 10 20 30 37

NH_3^+- KCNTATCAT QRLANFLVHS SNNFGAILSS TNVGSNTY - C- NH_2

Figure 2-1: Structures of the compounds studied together with the primary sequence of IAPP. **A)** Myricetin. **B)** Kaempferol. **C)** Quercertin. **D)** Morin hydrate. **E)** Primary structure of human IAPP. The peptide has an amidated C-terminus and a disulfide bond involving Cys-2 and Cys-7.

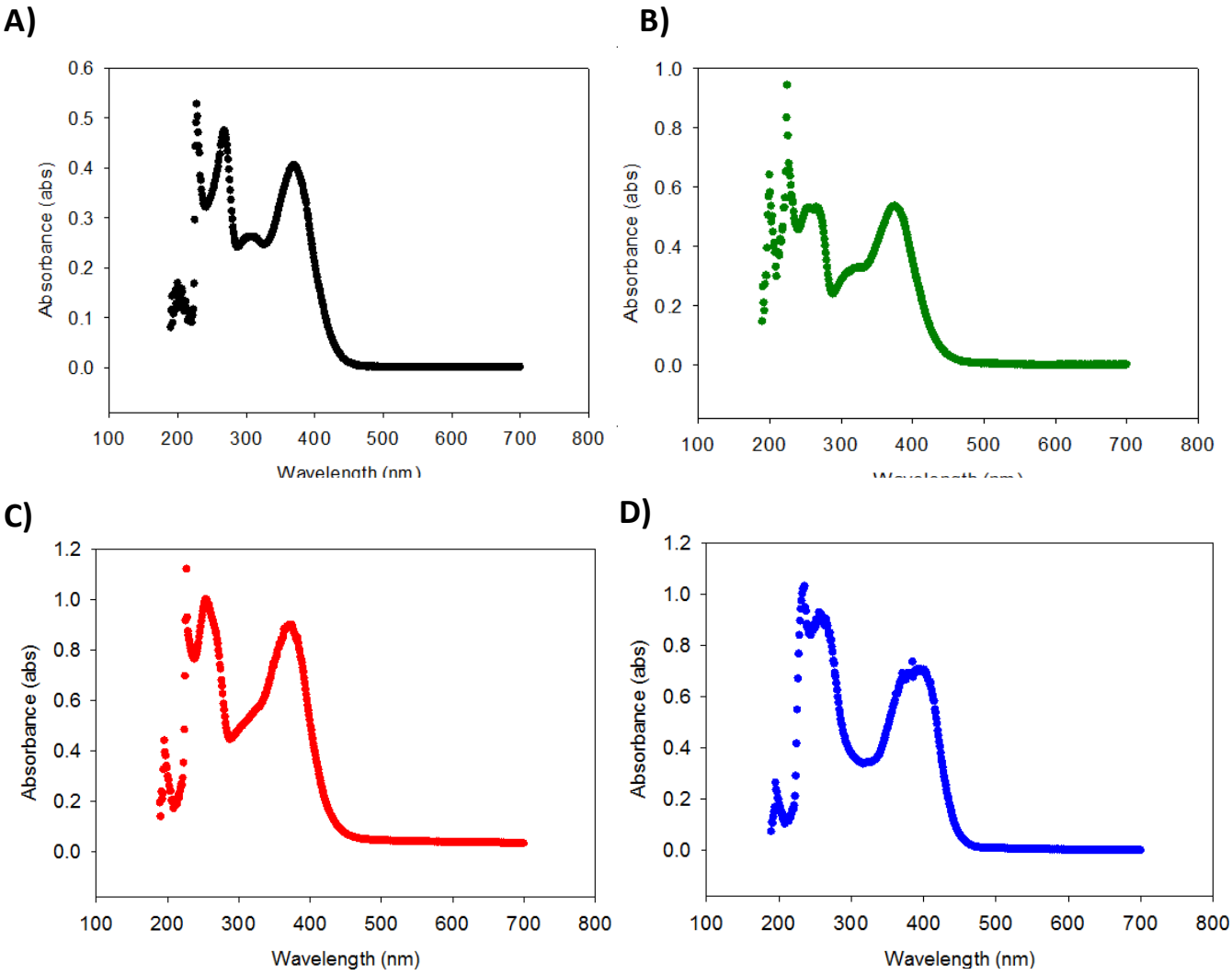

Figure 2-2: UV absorbance spectra of the compounds evaluated. **A)** Kaempferol **B)** Myricetin. **C)** Quercetin. **D)** Morin Hydrate. All experiments were performed in 20 mM Tris-HCl buffer pH 7.4, 0.25% (v/v) DMSO, and 32 µM of the small molecule.

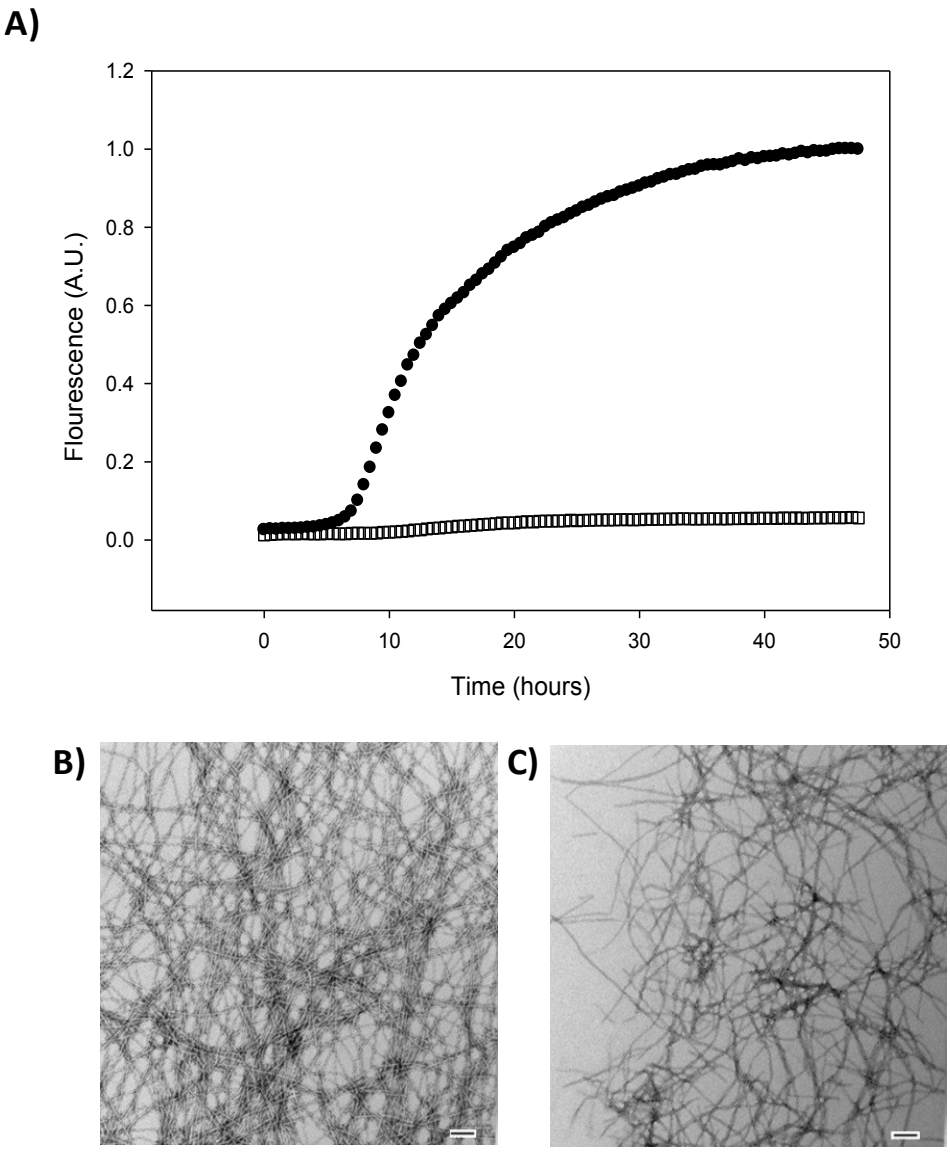

Figure 2-3: Hydroxyflavones interfere with thioflavin-T based assays. **A)** Thioflavin-T monitored kinetic experiments. Black circles; IAPP alone. Black open squares; IAPP plus an equimolar amount of Myricetin. **B)** TEM image collected at the end of the reaction for the IAPP sample. **C)** TEM image collected at the end of the reaction for the 1:1 mixture of IAPP and Myricetin. Scale bars represented 100nm. Experiments were conducted at 25^{o} C, pH 7.4, 20 mM Tris HCl, 32 μM IAPP, 0.25% DMSO (v/v).

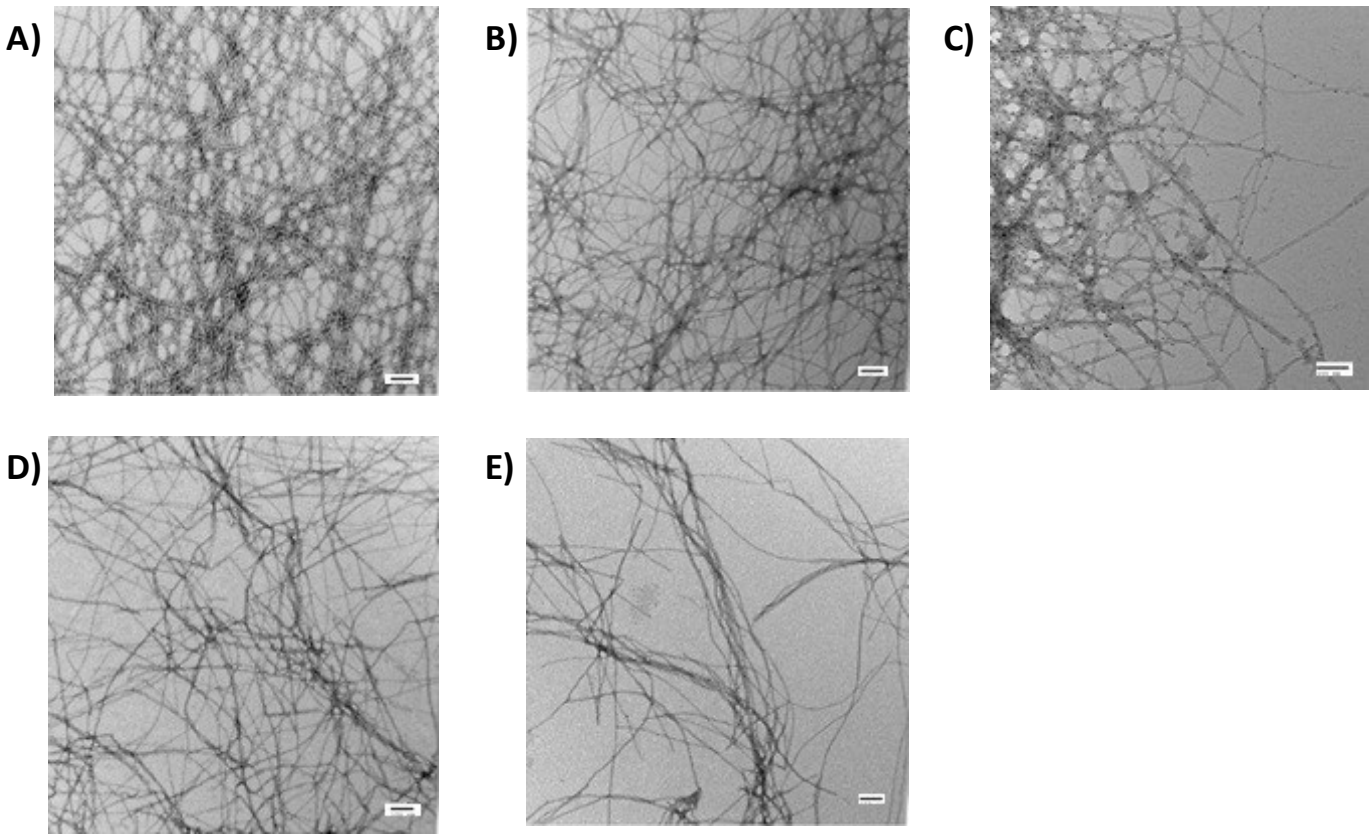

Figure 2-4: Morin Hydrate, but not Myricetin, Kaempferol or Quercetin, inhibits amyloid formation by IAPP. TEM images are shown of samples collected 48 hours after the initiation of amyloid formation. **A)** IAPP alone. **B)** IAPP:Myricetin 1:1. **C)** IAPP:Kaempferol. 1:1 **D)** IAPP:Quercertin 1:1 **E)** IAPP:Morin hydrate 1:1. Experiments were conducted at 25° C, pH 7.4, 20mM Tris HCl, 32 μM IAPP, 0.25% DMSO (v/v). Inhibitors, when present were at 32 μM. Scale bars represent 100 nm.

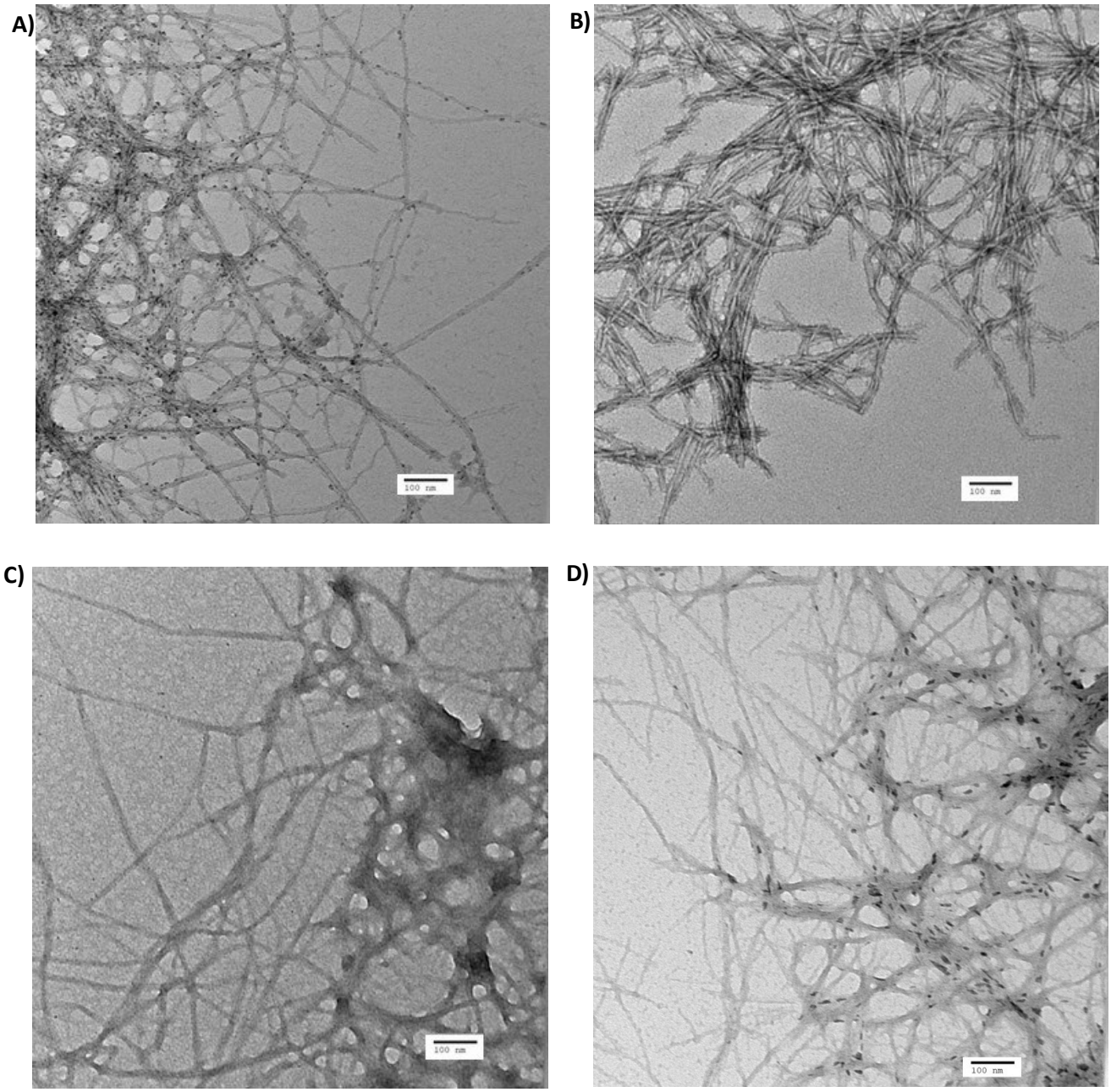

Figure 2-5: TEM images of IAPP Kaempferol mixtures at various ratios of IAPP to Kaempferol. **A)** 1:1. **B)** 1:2. **C)** 1:5. **D)** 1:10. Experiments were performed as described for the data shown in figure 2-3 in the thesis, except that higher concentrations of Kaempferol were used. Scale bars represent 100nm. Experiments were conducted at 25° C pH 7.4 in 20 mM Tris HCl, 0.25% DMSO (v:v) at 32 μM IAPP. The concentration of Kaempferol ranged from 32 to 320 μM.

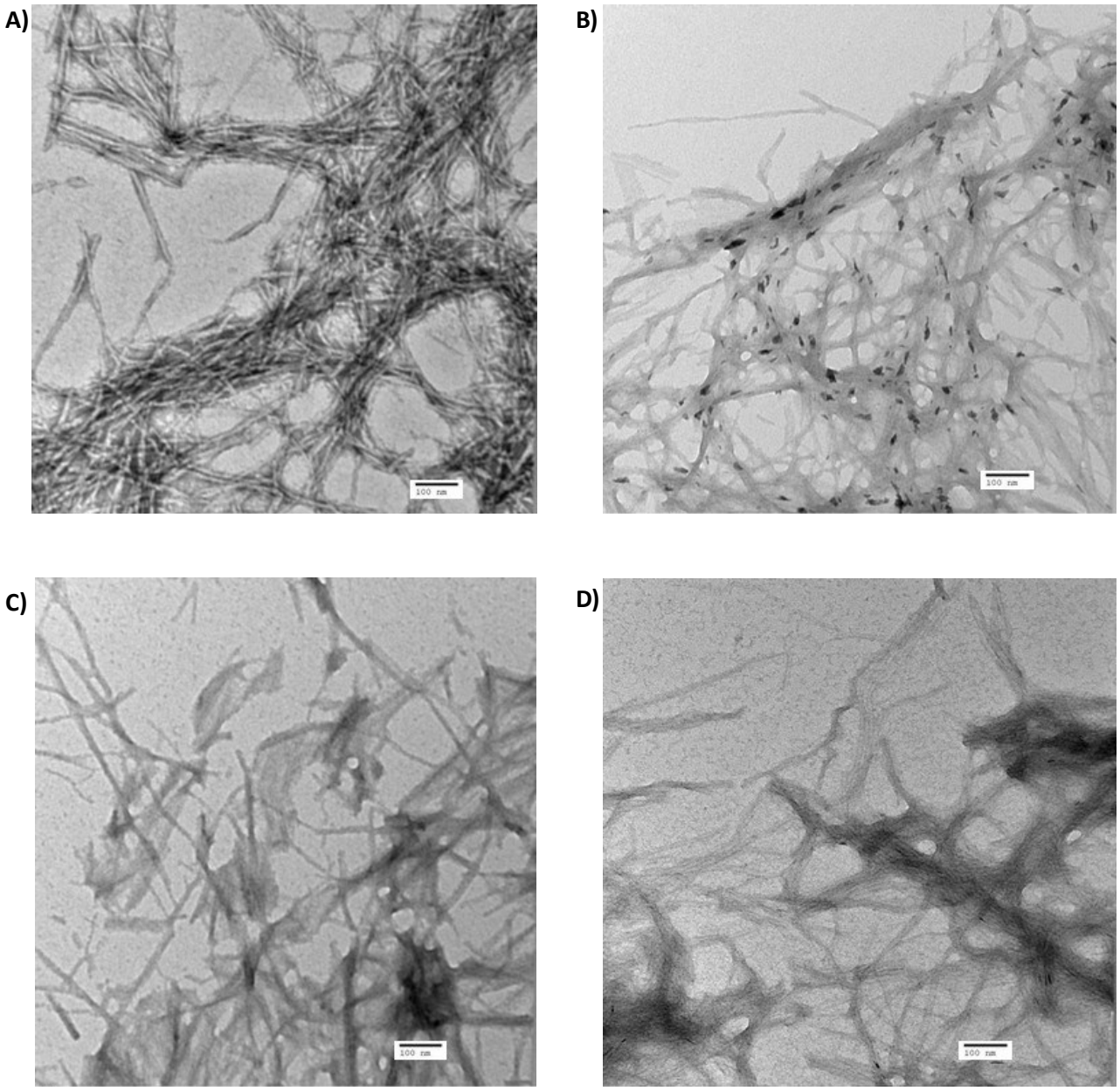

Figure 2-6: TEM images of IAPP Myricetin mixtures at various ratios of IAPP to Myricetin. **A)** 1:1. **B)** 1:2. **C)** 1:5. **D)** 1:10. Experiments were performed as described for the data shown in figure 2-3 in the thesis, except that higher concentrations of Myricetin were used. Scale bars represent 100nm. Experiments were conducted at 25° C pH 7.4 in 20 mM Tris HCl, 0.25% DMSO (v:v) at 32 μM IAPP. The concentration of Myricetin ranged from 32 to 320 μM.

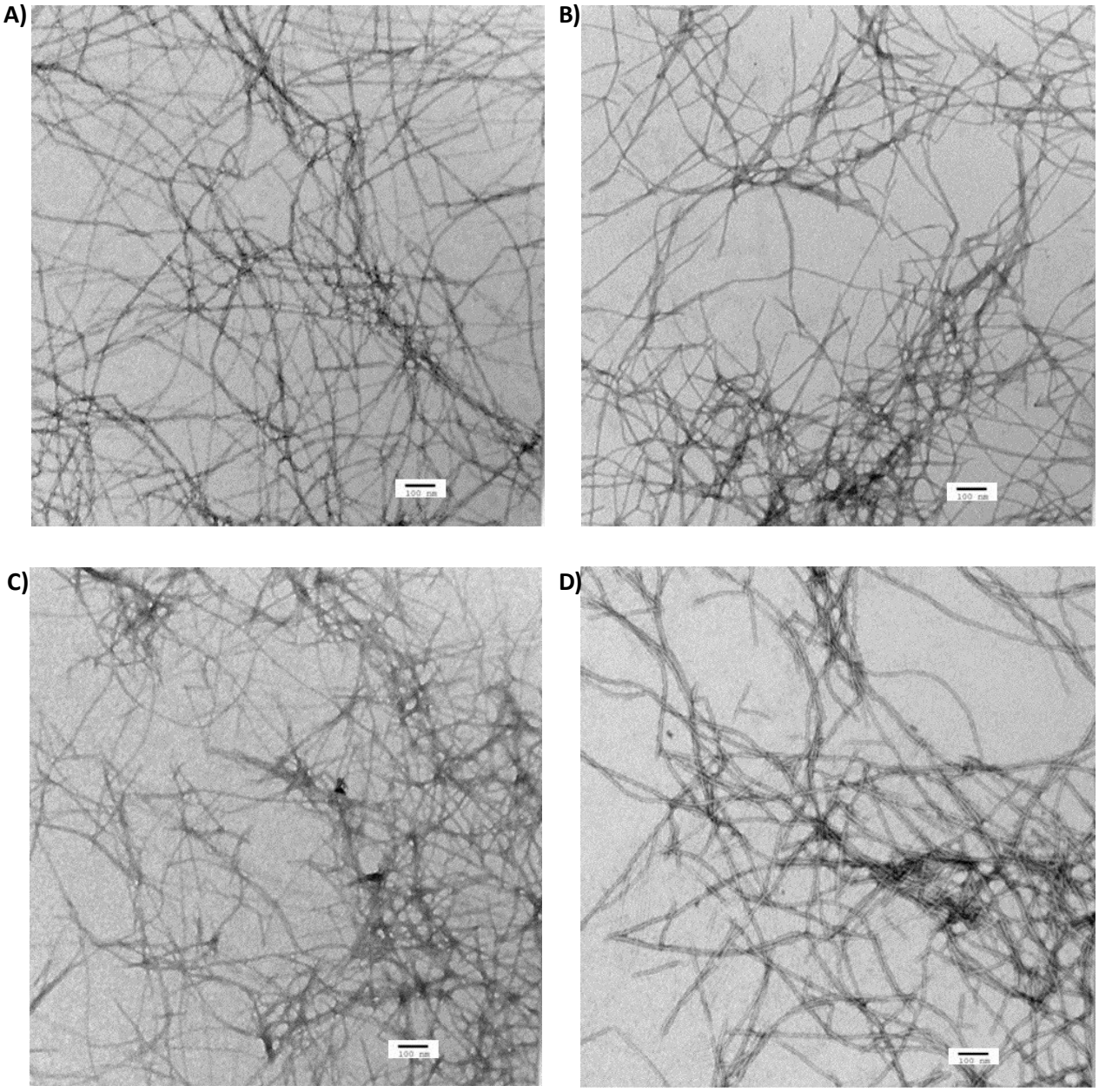

Figure 2-7: TEM images of IAPP Quercetin mixtures at various ratios of IAPP to Quercetin. **A)** 1:1. **B)** 1:2. **C)** 1:5. **D)** 1:10. Experiments were performed as described for the data shown in figure 2-3 in the thesis, except that higher concentrations of Quercetin were used. Scale bars represent 100nm. Experiments were conducted at 25° C pH 7.4 in 20 mM Tris HCl, 0.25% DMSO (v:v) at 32 μM IAPP. The concentration of Quercetin ranged from 32 to 320 μM.

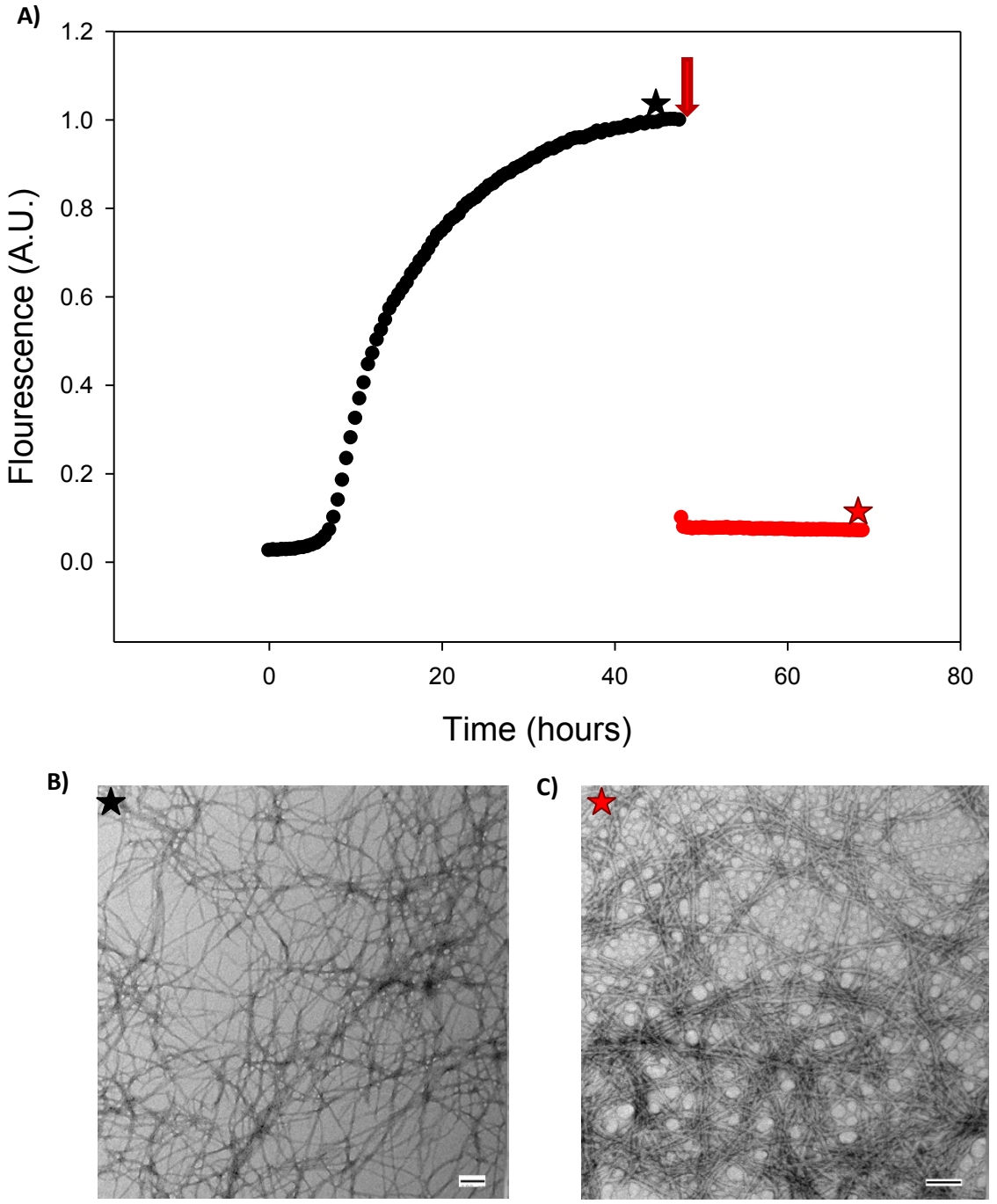

Figure 2-8: Myricetin does not significantly inhibit amyloid formation by IAPP, but does interfere with thioflavin-T assays. A thioflavin-T curve for IAPP is shown. **A)** Myricetin is added at the time point indicated by the red arrow and an immediate loss of thioflavin-T fluorescence is observed. The experiment confirms that Myricetin interferes with thioflavin-T fluorescence studies. The curve does not reflect the actual time course of disaggregation. **B)** A TEM image recorded at t = 45 hours (black star) prior to the addition of Myricetin. **C)** A TEM image recorded at t = 60 hours (red star) confirms the presence of amyloid fibers. Experiments were conducted at 25° C pH 7.4 in 20 mM Tris HCl, 0.25% DMSO (v:v) at 32 μM IAPP and 32 μM Myricetin (concentration after addition). Scale bars represent 100nm.

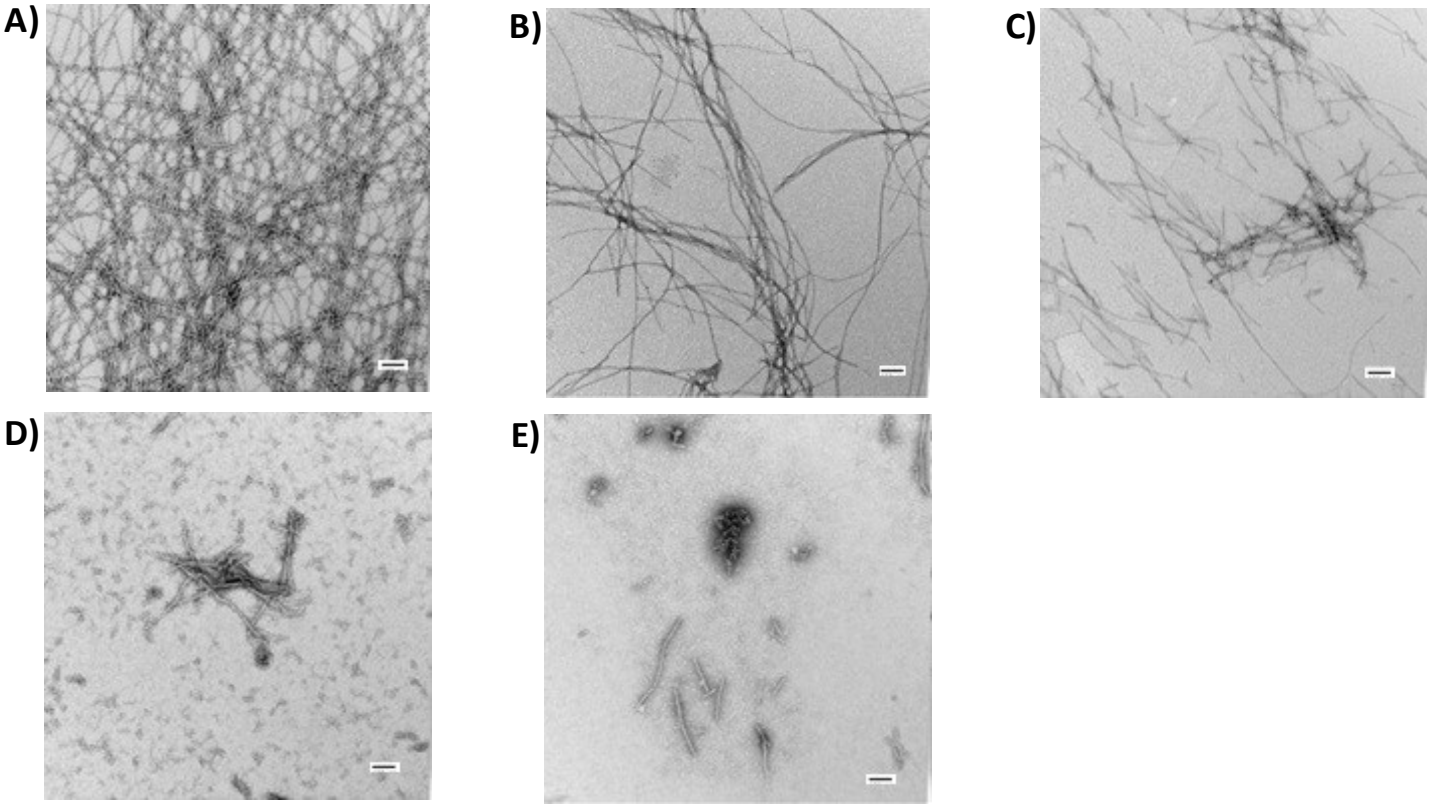

Figure 2-9: The effects of Morin hydrate are concentration dependent. TEM images are shown of samples collected 48 hours after the initiation of amyloid formation **A)** IAPP alone. **B)** 1:1 Mixture of IAPP and Morin hydrate. **C)** 1:2 Mixture of IAPP and Morin hydrate. **D)** 1:5 Mixture of IAPP and Morin hydrate. **E)** 1:10 Mixture of IAPP and Morin hydrate. Experiments were conducted at pH 7.4, 20mM Tris HCl, 32 μM IAPP, 0.25% DMSO (v/v). The concentration of Morin hydrate, when present, ranged from 32 μM to 320 μM.

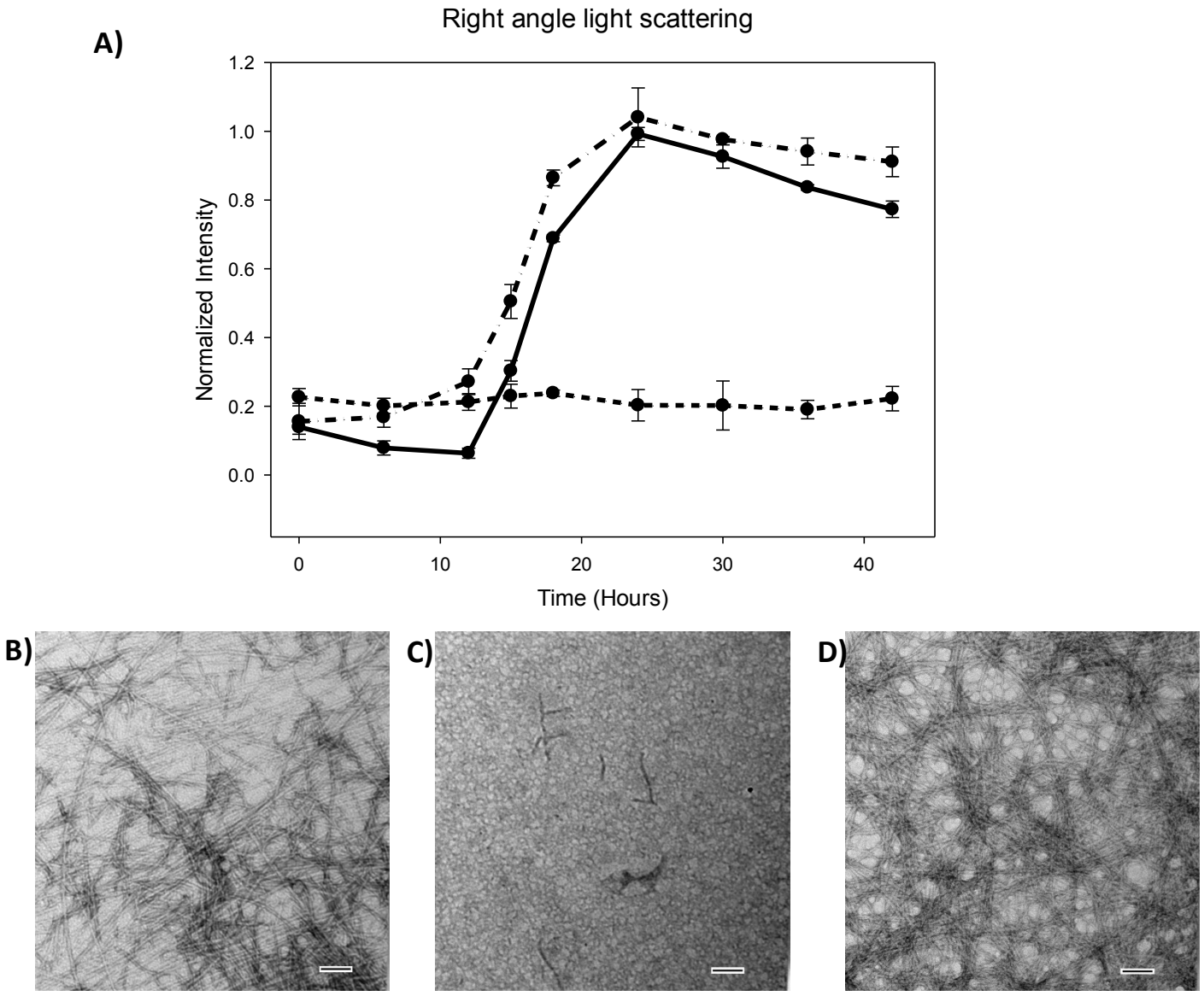

Figure 2-10: Right angle light scattering confirms that Morin hydrate, but not Myricetin inhibits IAPP amyloid formation. **A)** Light scattering. Solid line (▬) IAPP alone, dashed line (▬ ▬) IAPP plus Morin hydrate, dashed-dotted line (▬●▬) IAPP plus Myricetin. **B)** TEM image of the sample of IAPP without compound. Sample was removed at 42 hours. **C)** TEM image of a sample from the experiment conducted in the presence of Morin hydrate in five-fold excess. Sample was removed at 42 hours. **D)** TEM image of a sample from the experiment conducted in the presence of Myricetin in five-fold excess. Sample was removed at 42 hours. All samples contained 32 μM IAPP, 0.25% DMSO (v/v) 20 mM Tris-HCl, pH 7.4. The signal was monitored at 500 nm. Experiments were conducted at 25 °C Scale bars in TEM images represent 100 nm. The light scattering data is the result of 3 separate measurements for each sample. The error bars represent the standard deviation of each data point.

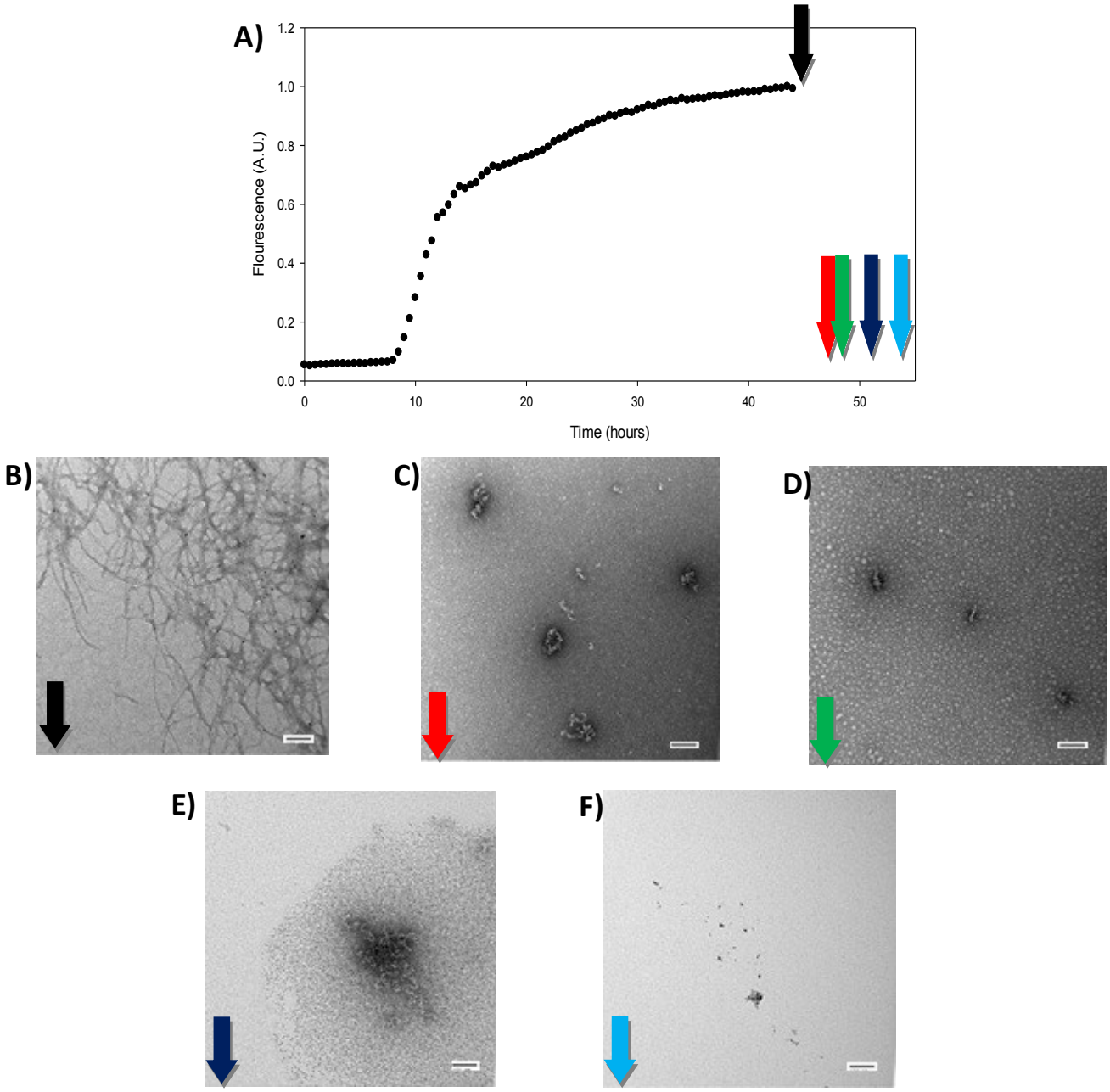

Figure 2-11: Morin hydrate disaggregates human IAPP amyloid fibers. **A)** A thioflavin-T monitored kinetic experiment in the absence of Morin hydrate. Morin hydrate was added in five-fold excess at the time point indicated by the black arrow **B)** TEM image of a sample removed just prior to the addition of Morin hydrate (black arrow). **C)** TEM image one hour after addition of Morin hydrate (red arrow). **D)** TEM image two hours after addition of Morin hydrate (green arrow). **E)** TEM image four hours after addition of Morin hydrate (dark blue arrow). **F)** TEM image six hours after addition of Morin hydrate (light blue arrow). Experiments were conducted at 25° C, pH 7.4, 20mM Tris HCl with 32μM IAPP, 0.5% DMSO (v/v) The concentration of Morin hydrate was 160μM. Scale bars represent 100nm.

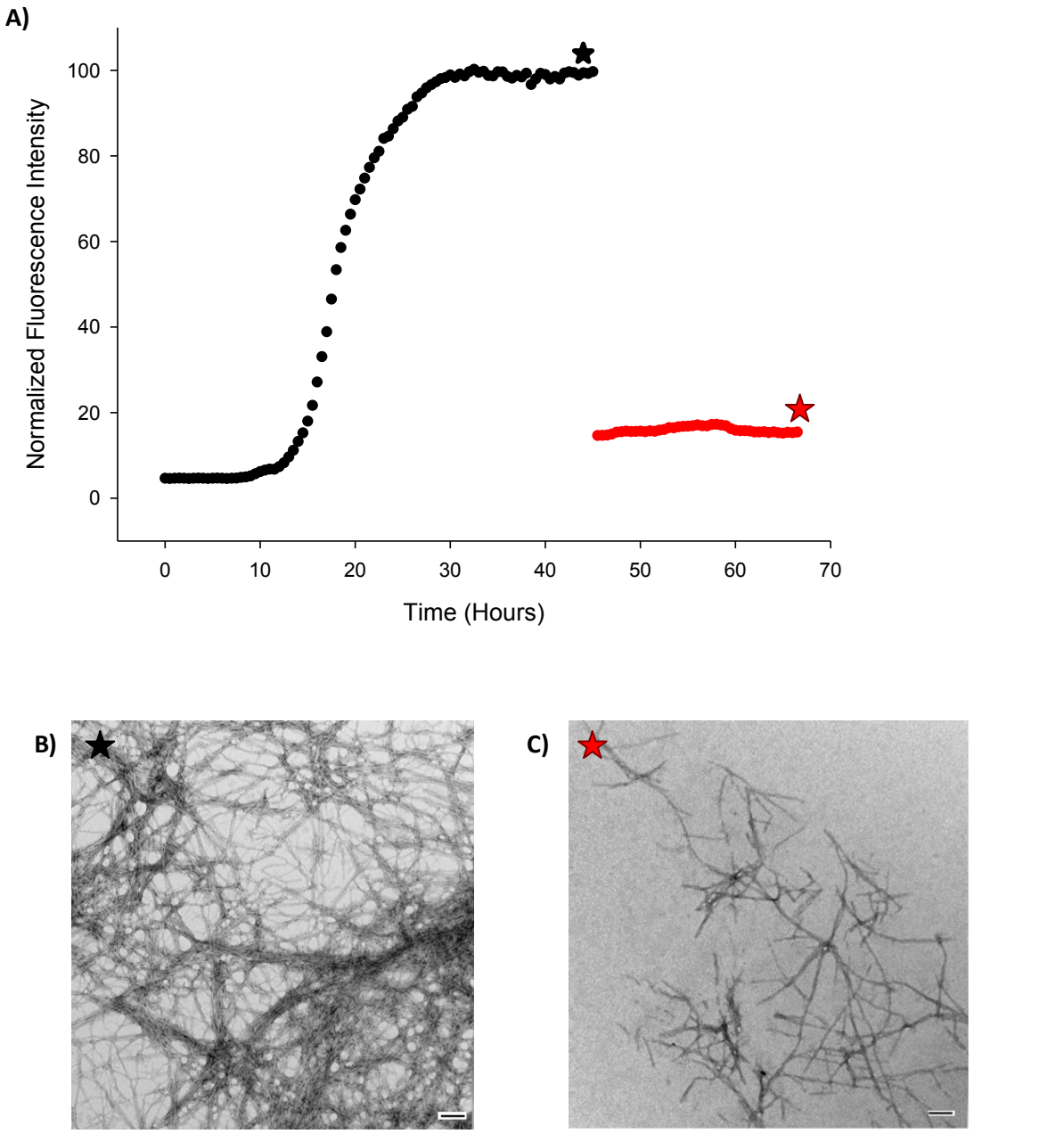

Figure 2-12: Morin hydrate disaggregates IAPP amyloid fibers when added at a 1:1 ratio **A)** A thioflavin-T kinetic curve. Morin hydrate was added after amyloid fiber formation was complete (black star). **B)** A TEM image recorded before addition of Morin hydrate. An aliquot was removed at the time point indicated by the black star for TEM analysis. **C)** TEM image recorded after addition of Morin Hydrate. An aliquot was removed at the time point indicated by the red star for TEM analysis. The thioflavin-T time course is shown to illustrate when the compound was added, the thioflavin-T signal rapidly drops after addition of compound, but this does not reflect the kinetics of disaggregation since hydroxyflavone interferes with thioflavin-T assays. Experiments were conducted at 25° C pH 7.4 in 20 mM Tris HCl, 0.25% DMSO (v:v) at 32 uM IAPP and 32 uM Morin hydrate (concentration after addition). Scale bars represent 100nm.

3. Flurbiprofen Accelerates Amyloid Formation by Islet Amyloid Polypeptide (IAPP)

3.1 INTRODUCTION

Amyloidosis plays a major role in many diseases such as Alzheimer's disease and type-2 diabetes. The formation of amyloid plays a critical role in toxicity. Studies of patients who have used non-steroidal anti-inflammatory drugs (NSAIDs) for long-term periods suggest a reduced risk of Alzheimer's disease (*27*). The ability of these NSAIDs to inhibit Aβ amyloid formation has been studied; however, like many other inhibitors, their effects have on IAPP have not been evaluated. Here we examine the ability of several NSAIDs to alter amyloid formation kinetics by IAPP.

IAPP monomers self-assemble into amyloid fibrils in a nucleation dependent manner. The formation of these fibers is a complex process consisting of multiple intermediates, some of which are associated with cell toxicity. The intermediates are not well defined and are thought to involve the assembly of transient oligomeric species (*44*). Developing inhibitors of the formation of fibrils is an interesting field to explore, but being able to prevent formation of toxic intermediates and being able to investigate these oligomeric intermediates or reduce their population is even more important.

As previously shown, IAPP amyloid formation can be manipulated using point mutation mutants to accelerate amyloid formation (*75*). However, little attention has been paid to the use of small molecules to accelerate IAPP amyloid formation. Here I use kinetic assays, transmission electron microscopy (TEM) show that a common NSAID, 2-(2-fluorobiphenyl-4-yl)propanoic acid (flurbiprofen), has the ability to accelerate amyloid

formation by IAPP. Preliminary data collected by Dr. Andisheh Abedini in the laboratory of Professor Ann-Marie Schmidt at NYU Medical Center shows it may have the ability to protect cultured rat INS-1 β-cells against the toxic effects of IAPP amyloid formation.

3.2 MATERIALS AND METHODS

3.2.1 Peptide Synthesis

Human IAPP was synthesized using a CEM microwave peptide synthesizer by 9-fluorenylmethoxycarbonyl (Fmoc) chemistry. Pseudoproline dipeptide derivatives were used to assist in the synthesis. Fmoc- PAL-Polyethylene-Glycol-Polystyrene (Fmoc-PAL-PEG-PS) resin was used and standard Fmoc reaction cycles were employed. Double couplings were performed for the first residue attached to the resin, β-branched residues, and pseudoprolines. Peptides were cleaved from the resin using trifluoroacetic acid (TFA). Crude peptide was dissolved in 20% acetic acid (v/v) and lypholized to increase solubility. The peptide was then oxidized in dimethyl sulfoxide (DMSO) in order to oxidize the disulfide bond between Cys-2 and Cys-7 (*71*). The peptide was incubated for 24 hours at room temperature. IAPP was purified by using reverse-phase HPLC using a Vydac C18 preparative column. A two buffer system was used: buffer A consists of 100% H2O and 0.045% HCl (v/v) and buffer B consists of 80% acetonitrile (ACN), 20% H2O, and 0.045% HCl. HCl was used as an ion-pairing agent instead of TFA, since TFA can influence aggregation kinetics (*76*). A 10-70% buffer B gradient in 60 minutes was used. The pure peptide eluted at approximately 50% buffer B (which is around 40 minutes). The identity of the pure peptide was confirmed using matrix-assisted laser

desorption/ionization time-of-flight mass spectrometry (MALDI-TOF MS) (observed 3904.4, expected 3904.8)

3.2.2 Sample Preparation

A 1.58 mM peptide solution was prepared in 100% hexafluoroisopropanol (HFIP) and stored at -20 ^{o}C. S-Flurbiprofen was obtained from Cayman Chemical (Item number 10004207). R-Flubiprofen (54570), flurbiprofen mixture (F8514), aspirin (A2093), and naproxen (N8280) were obtained from Sigma Aldrich. Flurbiprofen mixture and naproxen were dissolved in HFIP. S-flurbiprofen, R-flurbiprofen, and aspirin were dissolved in DMSO at varying concentrations.

All IAPP peptide solutions were filtered through a 0.45-μm syringe filter. The IAPP peptide solution was measured into an eppendorf tube, frozen in liquid nitrogen, and lypholized. Samples were prepared by adding Tris-HCl buffer (pH 7.4, 20 mM Tris) to the dry lypholized peptide. The final concentration of IAPP in the solutions was 32 μM.

3.2.3 Thioflavin-T Assays

Preliminary fluorescence experiments were performed using an Applied Photontechnology Fluorescence Spectrophotometer. A 1 cm cuvette was used to carry the solution and each point was averaged for 1 minute. An excitation wavelength of 450 nm and an emission wavelength of 485 was used to evaluate these thioflavin-T studies. Solutions were prepared by diluting filtered peptide solution into a Tris-HCl buffer and thioflavin-T solution. The solution was stirred in order to increase the rate of amyloid

formation and maintain sample homogeneity. The final concentrations were 32 μM IAPP, 32 μM thioflavin-T, and 2% HFIP.

Other fluorescence experiments were performed on a Beckman model D880 plate reader. The Thioflavin-T studies used excitation and emission filters of 430 nm and 485 nm, respectively. The experiments were performed in 96-well plates at 25 ^{o}C. IAPP was dissolved in hexafluoroisopropanol (HFIP) to a final concentration of 1.58 mM. The stock solution of IAPP in HFIP was filtered using a 0.45 μm syringe filter. Aliquots of filtered stock solution were pipetted into eppendorf tubes and lypholized.

All of the thioflavin-T assays were prepared by dissolving the dried samples of IAPP in Tris-HCl buffer (20 mM, pH 7.4) immediately before measurements. The final peptide concentration was 32 μM in 0.25% DMSO, 20 mM Tris HCl buffer at pH 7.4 and 32 mM thioflavin-T with or without inhibitors. For experiments with the inhibitor, concentrated stock solutions of compounds in DMSO were used and were diluted into the thioflavin-T IAPP solution. The data was analyzed using Sigma-Plot v11.

3.2.4 Transmission Electron Microscopy (TEM)

15 ml aliquots of the solution at the end of the fluorescence measurements were taken at the end of the kinetic reactions and blotted on a carbon-coated Formvar 300-mesh copper grid for 1 minute and then negatively stained with saturated uranyl acetate for 1 minute. TEM analyses were performed at the life science microscopy center at Stony Brook University.

3.2.5 Dynamic Light Scattering (DLS)

Dynamic light scattering experiments were performed on a 90Plus particle size analyzer at 25 ^{o}C. The flurbiprofen stock solution was prepared as previously mentioned. The particle size distribution was determined at a flurbiprofen concentration of 640 mM in filtered 20 mM Tris-HCl buffer at pH 7.4. The buffer solution was filtered through a syringe filter with 0.45 μM membrane prior to dilution of flurbiprofen. The measured intensity autocorrelation function was converted to an effective size distribution using the software supplied by the manufacturer.

3.2.6 Cytotoxicity Assays

These experiments were conducted by Dr. Abedini at NYU Medical School and the following protocol was used. Transformed rat insulinoma (INS-1) β-cells were used to assess the ability of S-flurbiprofen to protect cells against the toxic effects of human IAPP. INS-1 cells were grown on RPMI 1640 supplemented with 10% fetal bovine serum (FBS), 11 mM glucose, 10 mM Hepes, 2 mM L-glutamine, 1 mM sodium pyruvate, 50 μM β-mercaptoethanol, 100 U/ml penicillin, and 100 U/ml strptomycin. Cells were grown at 37 ^{o}C and supplemented with 5% CO_2. The viability assays were conducted with cells at a density of 30,000 cells per well in 96-well plates and cultured for 24 hours prior to addition of solutions. Solutions of IAPP:S-flurbiprofen at 1:1 and 1:20 molar ratio (30 μM IAPP) were prepared by adding the Tris-HCl buffer (pH 7.4) to dried IAPP and adding concentrated stock solution of S-flurbiprofen in DMSO to the solution to obtain the desired concentration. Peptide samples and samples of peptide and S-flurbiprofen in Tris-HCl buffer (pH 7.4 and 0.25% DMSO) were directly added to cells after 11 hours of incubation at room temperature. Alamar Blue was used to assess cell

viability and was diluted 10-fold in culture media and cells were incubated for an additional 5 hours at 37 ^{o}C before readout. Fluorescence (excitation: 530 nm, emission: 590 nm) was measured using a Beckman model D880 plate reader.

3.3 RESULTS AND DISCUSSION

3.3.1 Naproxen Has No Effect on Amyloid Formation but Flurbiprofen Accelerates Amyloid Formation

The structure of flurbiprofen, aspirin, naproxen, and IAPP are shown in Figure 3-1 A-D. Each of the NSAIDs tested are non-selective cyclooxygenase inhibitors. Like many other amyloidgenic peptides, IAPP aggregation experiences a lag phase, followed by an elongation phase, and ending with the plateau phase. Preliminary data were recorded on the Applied Photontechnology Fluorescence Spectrophotometer. In the cuvette the solution contains 20 mM Tris-HCl buffer at pH 7.4, 2% HFIP, 32 μM IAPP, 32 μM thioflavin-T, and the presence of or absence of the small molecule. Experiments were performed in stirring conditions. Both HFIP and sheer force effects are both known to have the ability to accelerate amyloid formation (*77, 78*). So experiments performed under these conditions can be completed in a short time period. The thioflavin-T experiments were performed at different concentrations of naproxen and flurbiprofen mixture.

The data with different concentrations of naproxen show that even at 2-fold and 5-fold molar excess of naproxen there were not significant effects on the thioflavin-T kinetics (Figure 3-2A). At the end of the thioflavin-T experiments, aliquots of the assays were used to obtain transmission microscope images. These images show that the fibers

formed are similar to the fibers of wild type IAPP (Compare Figure 3-2 B-D and Figure 3-2 E). When the same experiments were performed with a mixture of R and S flurbiprofen there is an acceleration of the fiber formation. The lag phase of fiber formation is shortened for the 5:1 flurbiprofen:IAPP solution (Figure 3-3 A). This was an interesting discovery so transmission electron microscope images were taken (Figure 3-3 B-D). The morphology of the fibers formed in the presence of the flurbiprofen mixture changes significantly as the concentration of flurbiprofen is increased. The fibers seem somewhat shorter and twisted compared to the wild type fibers (Figure 3-3 E). The change in morphology and the acceleration of IAPP were enough evidence to pursue more detailed studies.

It has been shown that different enantiomers of flurbiprofen can affect Aβ formation differently (*79*). The stock solution we obtained is a mixture of the R and S isomers. As a result, two separate isomers were tested to see the effects the different enantiomers have on amyloid formation (Figure 3-4 D-E). Both enantiomers of flurbiprofen had the ability to shorten the lag phase (Figure 3-4 A). TEM images also show comparable IAPP fibers between the S-flurbiprofen and R-flurbiprofen assays (Figure 3-4 B-C). S-flurbiprofen was chosen arbitrarily to continue future studies.

The thioflavin-T monitored curves of IAPP in the absence and in the presence of S-flurbiprofen are shown in Figure 3-5. These experiments were performed on a plate reader, where the presence of sheer force effects from a stir bar and HFIP are not present. HFIP evaporates quickly and was not a suitable co-solvent for this experiment since the normal lag time of IAPP is 10 hours. The co-solvent was that used as a replacement was DMSO. Experiments performed in the presence of S-flurbiprofen show a significantly

different result. At a 1:1 ratio of IAPP:S-flurbiprofen there is not a significant change in the sigmoidal curve. The lag phase is approximately the same length and the final florescence is the same. However, at higher ratios of IAPP:S-flurbiprofen the lag phase shortens and the final fluorescence is significantly higher. This suggests that S-flurbiprofen accelerates amyloid formation and somehow increases the amount of fibers or the affinity for thioflavin-T to binding to amyloid fibers. It is important to confirm the results of thioflavin-T binding assays and we used TEM to do so. Figure 3-6 A-B depicts wild-type IAPP in the absence of S-flurbiprofen. The image recorded shows extensive amyloid fibrils with a morphology typical of normal wild-type IAPP *in vitro*. The images of the IAPP:S-flurbiprofen mixture recorded (Figure 3-6 C-J) show that there are still extensive amyloid fibrils; however, the appearance of the fibers changes as the S-flurbiprofen concentration increases. The TEM images indicate that S-flurbiprofen has a significant effect on the morphology of IAPP fibers.

3.3.2 S-Flurbiprofen Possibly Protects INS-1 β-cells Against the Toxic Effects of IAPP.

Dr. Abedini, in the laboratory of Professor Ann-Marie Schmidt, compared the effects of 30 μM human IAPP, a 1:1 mixture of 30 μM human IAPP and 30 μM S-flurbiprofen, and a 1:20 mixture of 30 μM human IAPP and 600 μM S-flurbiprofen to determine whether S-flurbiprofen was able to protect INS-1 β-cells from the toxic effects of human IAPP (Figure 3-7). Rat INS-1 cell-line is a transformed β-cell line which is widely used to study β-cell toxicity. The data is preliminary, but it suggests that S-flurbiprofen protects INS-1 β-cells at 15 hours. S-flurbiprofen by itself was not toxic to the cells even at the highest concentration. After incubation of 30 μM IAPP fibers for 15

hours on bench, the INS-1 β-cells are exposed to these fibers. Toxicity decreased cell viability 55% relative to the untreated control. In the 1:1 mixture of IAPP:S-flurbiprofen the percentage of viable cells increased to 97% and at the 1:20 mixture of IAPP:S-flurbiprofen the percentage of viable cells were at 89%.

3.3.3 S-Flurbiprofen Does Not Aggregate

Aggregation of some small molecules has been implicated in playing a role in the ability to inhibit protein aggregation. The small-molecule can form micelle-like structures which bind the amyloidgenic proteins (*80*). Due to the solubility issues of S-flurbiprofen in water, the aggregation of S-flurbiprofen is possible.

Thus we used dynamic light scattering (DLS) to analyze the ability of S-flurbiprofen to aggregate. The DLS study was conducted on a sample of S-flurbiprofen which was at 640 μM concentration. There were no detectable aggregates in solution. The apparent effective diameter of the molecules detected were 0.0 nm at the beginning of the experiment at time = 0 hours and also at time = 48 hours. These reflect the detection limit of the instrument. These experiments show that there were no detectable particles with the effective diameter greater than 1 nm, which is the detection limit of the instrument.

3.3.4 Aspirin Does Not Alter the Kinetics of Amyloid Formation by IAPP

Aspirin, another NSAID commonly used, was tested on the effects of amyloid formation. The thioflavin-T assays indicate that there was no effect even at a 20 fold excess of aspirin (Figure 3-8 A). Although the thioflavin-T assays indicate that there was no effect on thioflavin-T kinetics, TEM images were taken to further verify this finding.

TEM images indicate that the morphology at the 20-fold excess were similar to that of wild-type (Figure 3-8 E). The TEM images of the other concentrations were also shown for completeness (Figure 3-8 B-D).

3.4 CONCLUSION

The data presented here demonstrates that S-Flurbiprofen accelerates *in vitro* amyloid formation by IAPP and changes the morphology of IAPP fibers. S-flurbiprofen is one of the first NSAIDs shown to have the ability to affect IAPP amyloid formation. S-flurbiprofen is clearly affecting the aggregation of IAPP, but it is not possible to deduce if it is accelerating each step of the aggregation pathway, selective steps, or is changing the pathway taken. The effect of S-flurbiprofen on the t_{50} of IAPP amyloid formation may saturate as S-flurbiprofen's concentration is increased (Figure 3-5 B). Although the fibers formed in the presence of flurbiprofen looks different from normal IAPP fibers in the absence of flurbiprofen, it is extraordinarily difficult to characterize the species of the final product at the molecular level. It is also very difficult to prove if flurbiprofen traps IAPP in an on or off pathway species of IAPP (*81, 82*). Interruption studies could be performed to provide more information. An interruption study is performed by allowing IAPP to form mature fibers and the small molecule is added at the top of the plateau. The interruption study will provide information on the effect that S-flurbiprofen has on mature IAPP amyloid fibers and will tell us whether it could change mature fibers to a morphology similar to that found when of S-flurbiprofen is added at t=0.

The cytotoxicity data demonstrates that S-flurbiprofen protects INS-1 β-cells from the cytotoxic effects at 15 hours. These are preliminary experiments and will be

repeated. Future studies could involve a time course cytotoxicity assay where shorter intervals data points are taken. This could capture the interval from the start of the experiment to t=15 hrs and test if flurbiprofen protects cells from early toxic intermediates.

Another useful experiment for the future is to use another NSAID other than flurbiprofen to ensure that it is not the anti-inflammatory characteristic of flurbiprofen that is affecting the INS-1 cells. This data in this chapter also show that aspirin and naproxen do not alter amyloid formation (Figure 3-2 and 3-9)

A)

B)

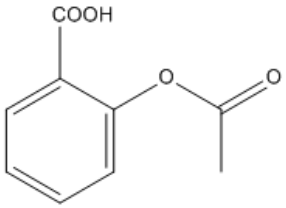

C)

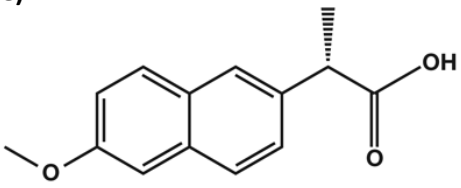

D)

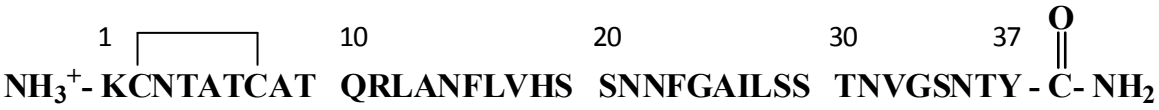

Figure 3-1: A) Structure of flurbiprofen. **B)** Structure of Aspirin. **C)** Structure of Naproxen. **D)** Primary structure of mature human wild-type IAPP.

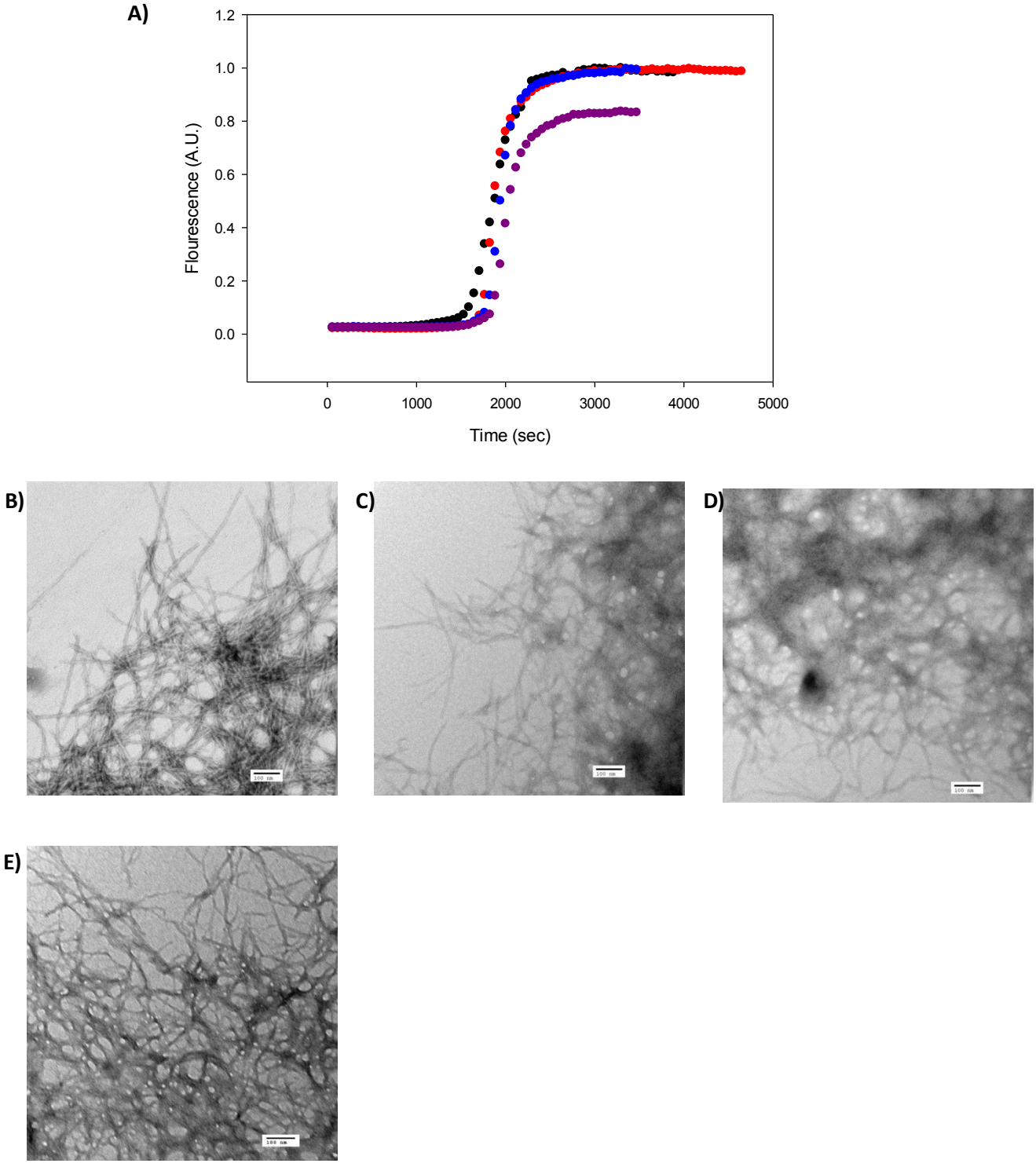

Figure 3-2: A) Thioflavin-T curves of 32 μM IAPP in the absence of small molecule (black), 32 μM IAPP in the presence of naproxen at a 1:1 ratio (red), 1:2 ratio (blue), and 1:5 ratio (purple) of IAPP:naproxen. Experiments were conducted at 25° C, pH 7.4, 20mM Tris HCl, 32 μM IAPP, 2% HFIP (v/v). **B)** TEM image of the 1:1 mixture of IAPP:naproxen. **C)** TEM image of the 1:2 mixture of IAPP:naproxen. **D)** TEM image of the 1:5 mixture of IAPP:naproxen. **E)** TEM image of IAPP in the absence of the small molecule. Scale bar represents 100

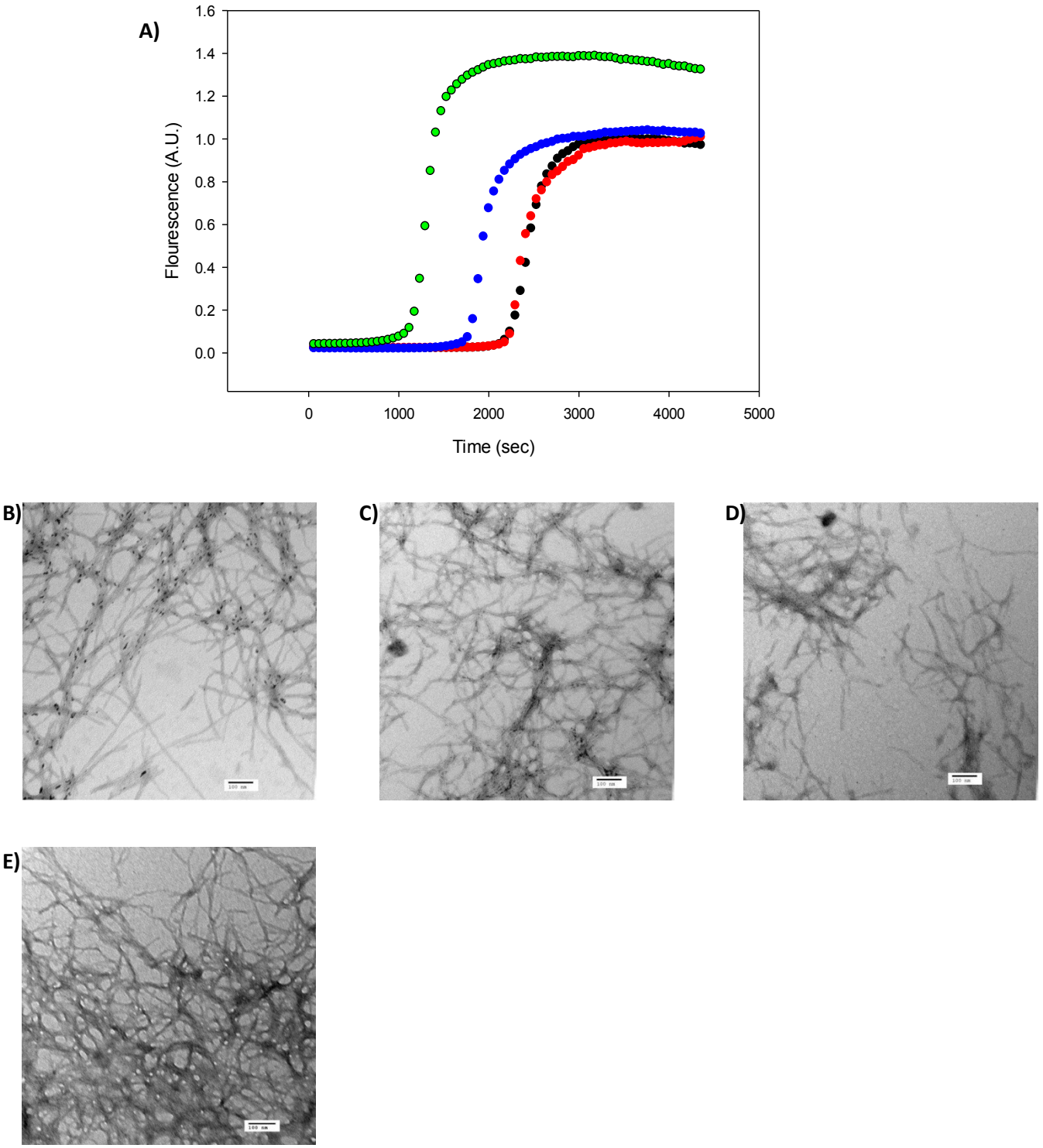

Figure 3-3: A) Thioflavin-T curves of 32 mM IAPP in the absence of flurbiprofen mixture (black), 32 µM IAPP in the presence of flurbiprofen at a 1:1 ratio (red), 1:2 ratio (blue), and 1:5 ratio (green) of IAPP:flurbiprofen. . Experiments were conducted at 25° C, pH 7.4, 20mM Tris HCl, 32 µM IAPP, 2% HFIP (v/v). **B)** TEM image of the 1:1 mixture of IAPP:flurbiprofen. **C)** TEM image of the 1:2 mixture of IAPP:flurbiprofen. **D)** TEM image of the 1:5 mixture of IAPP:flurbiprofen. **E)** TEM image of IAPP in the absence of the small molecule. Scale bar represents 100 nm.

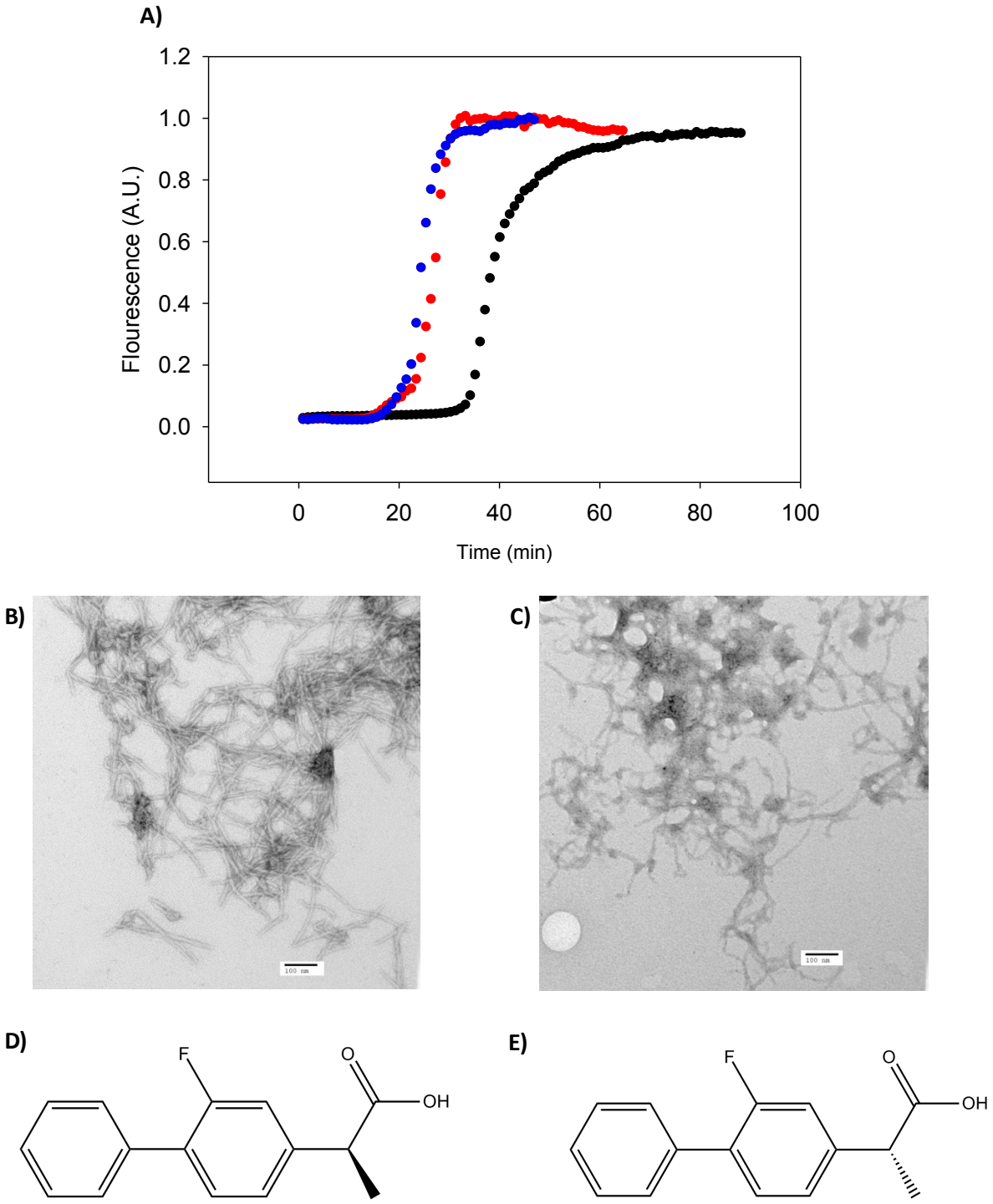

Figure 3-4: A) Thioflavin-T curves of 32 μM IAPP in the absence of small molecule (black), 32 μM IAPP in the presence of small molecule at a 1:10 ratio IAPP to S-flurbiprofen (red), 1:10 ratio IAPP to R-flurbiprofen (blue). Experiments were conducted at 25° C, pH 7.4, 20mM Tris HCl, 32 μM IAPP, stirring, and 2% HFIP (v/v). **B)** TEM image of IAPP fibers at the end of the thioflavin-T assay with S-flurbiprofen. **C)** TEM image of IAPP fibers at the end of the thioflavin-T assay with R-flurbiprofen. **D)** Structure of S-flurbiprofen. **E)** Structure of R-flurbiprofen

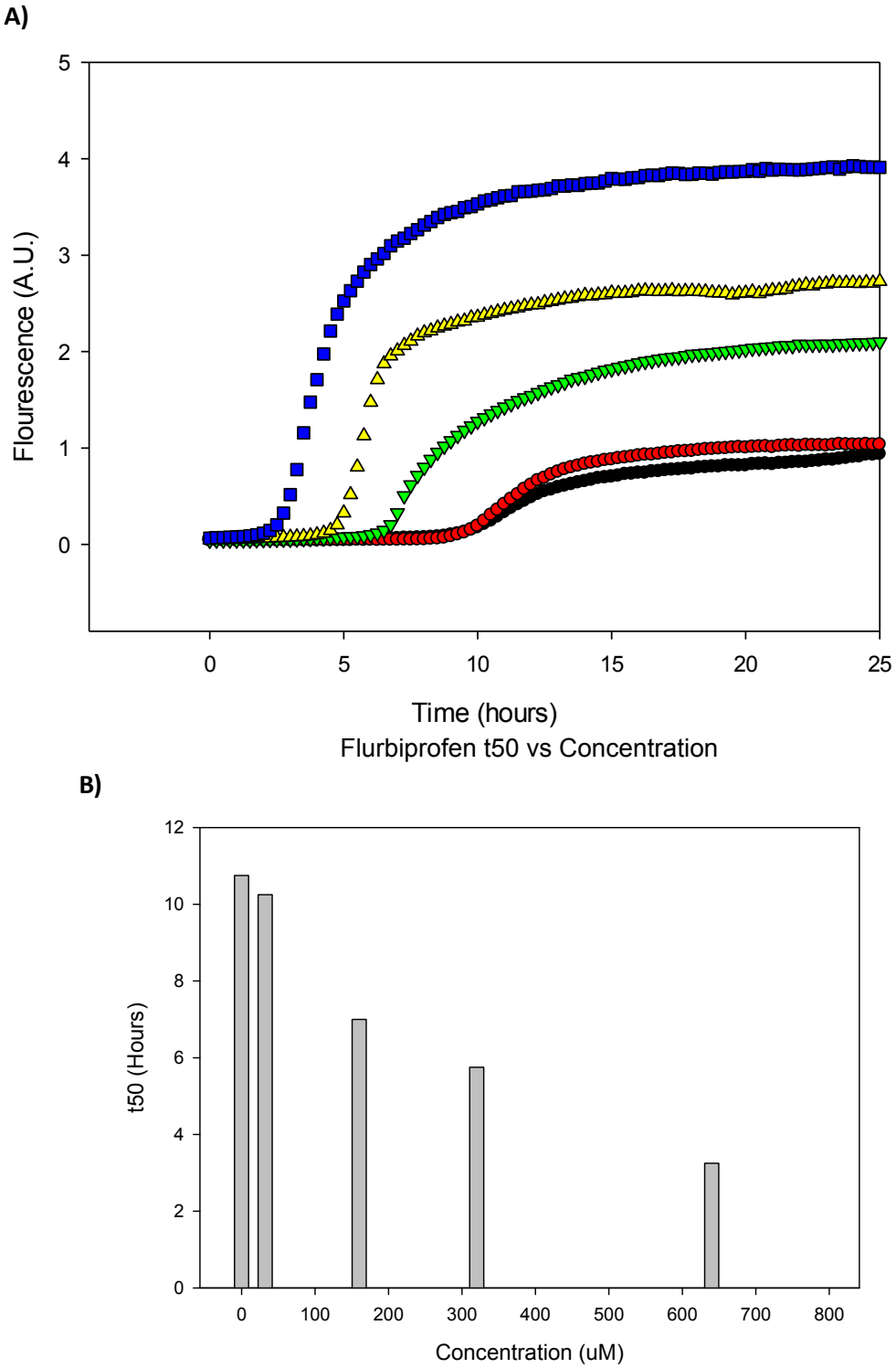

Figure 3-5: A) Thioflavin-T curves of 32 mM IAPP in the absence of small molecule (black), 32 μM IAPP in the presence of small molecule at a 1:1 ratio (red), 1:5 ratio (green), 1:10 ratio (yellow), and 1:20 ratio (blue) of IAPP to S-flurbiprofen. Experiments were conducted at 25° C, pH 7.4, 20mM Tris HCl, 32 μM IAPP, no stirring and trace amounts of DMSO (0.25%) (v/v). **B)** t_{50} plotted in a concentration dependent manner.

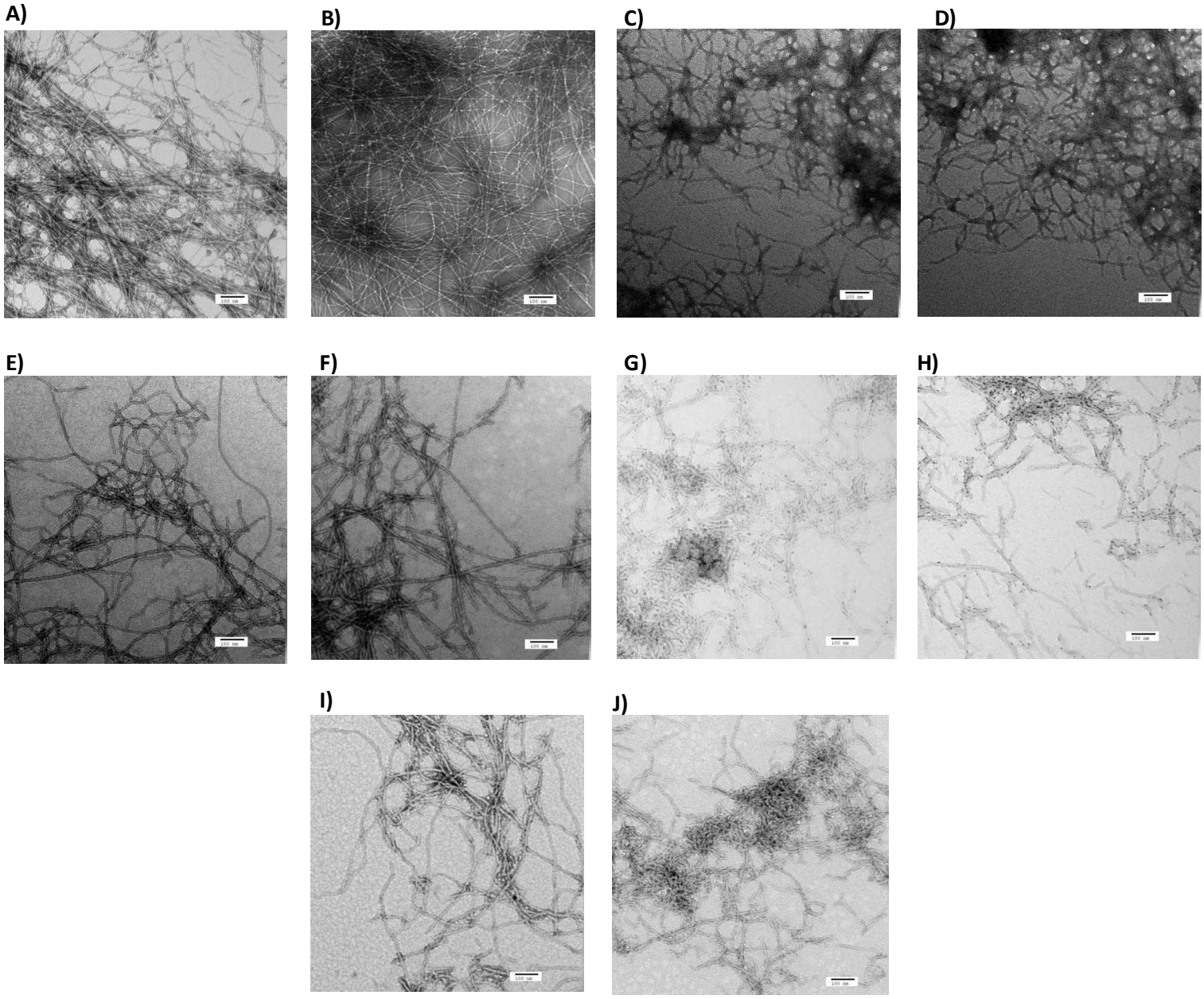

Figure 3-6: S-Flurbiprofen accelerates amyloid formation and changes fiber morphology in a concentration dependent manner. TEM images show IAPP fibers at different concentrations of S-Flurbiprofen. All TEM grids were staind at the end of each run once fibers were fully formed. **A-B)** 32 μM IAPP control in the absence of S-Flurbiprofen. **C-D)** 32 μM IAPP in the presence of 32 μM S-Flurbiprofen. **E-F)** 32 μM IAPP in the presence of 160 μM S-Flurbiprofen. **G-H)** 32 μM IAPP in the presence of 320 μM S-Flurbiprofen. **I-J)** 32 μM IAPP in the presence of 640 μM S-Flurbiprofen. Scale bars represent 100 nm

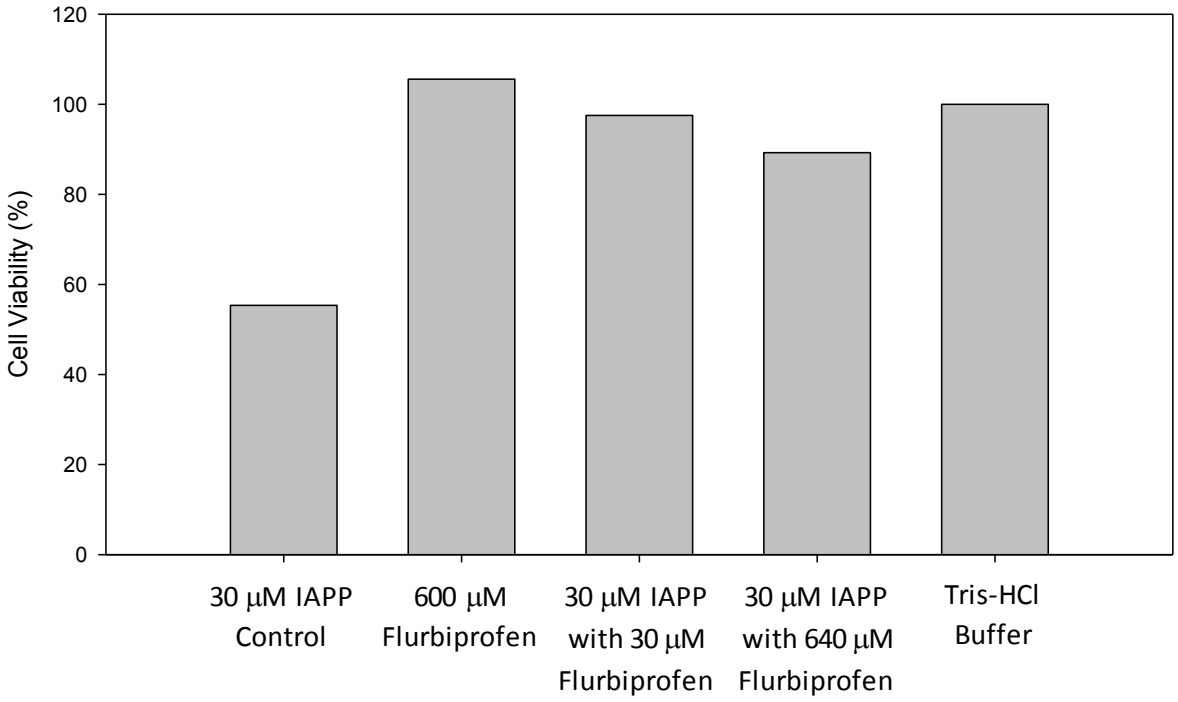

Figure 3-7: Preliminary tests suggest that flurbiprofen protects rat INS-1 cells against the toxic effects of human IAPP at 15 hours after initiation of amyloid formation. Cell viability as determined via Alamar blue assays, plotted as percent viability. From left to right. The effect of the addition of human IAPP (30 μM). The effect of flurbiprofen (600 μM). The effect of IAPP and flurbiprofen at a 1:1 ratio (30 μM IAPP:30 μM flurbiprofen). The effect of IAPP and flurbiprofen at a 1:20 ratio (30 μM IAPP:600 μM flurbiprofen). All solutions were incubated at room temperature for 11 hours and then applied to rat INS-1 cells in 96-well plates.

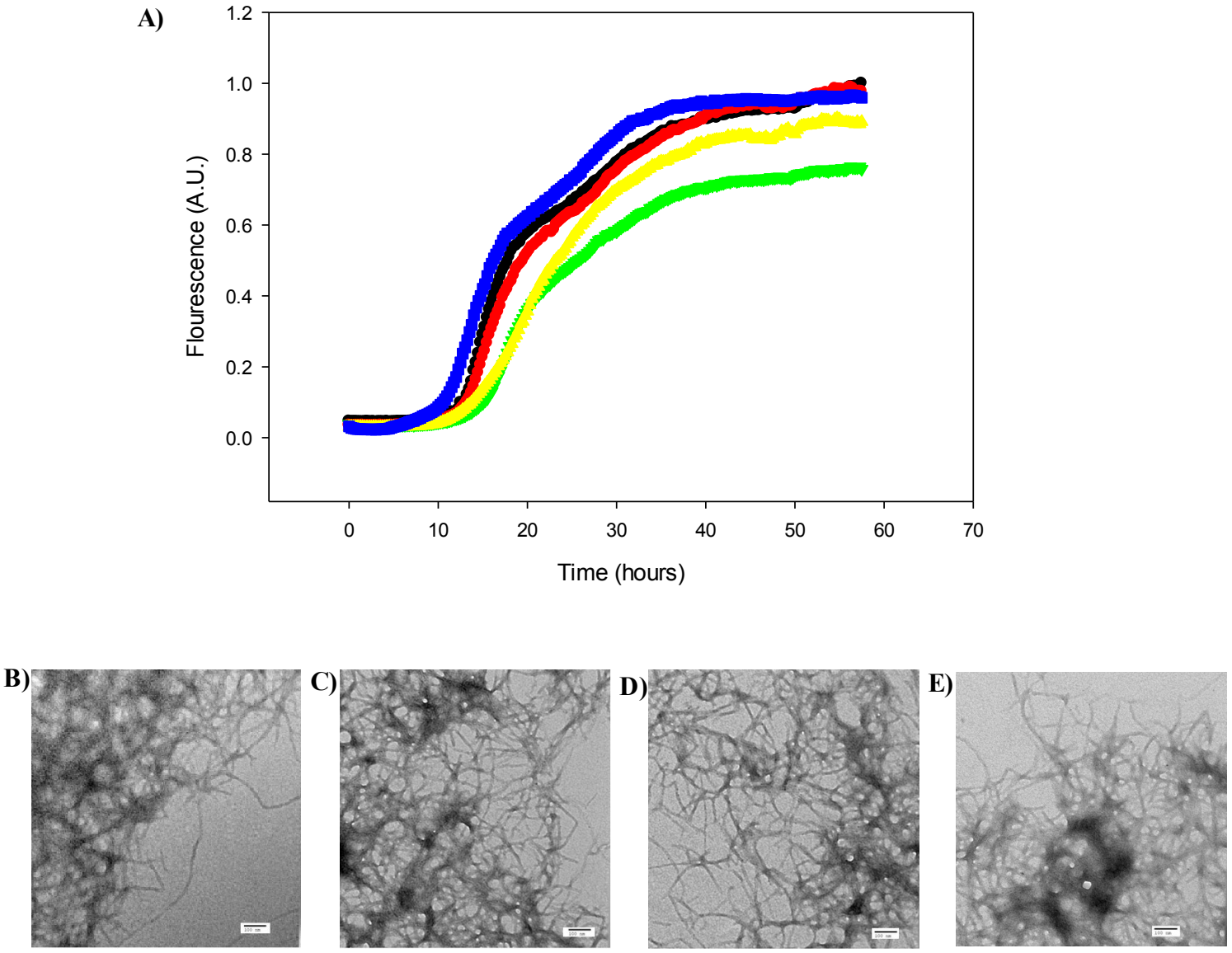

Figure 3-8: Aspirin does not inhibit IAPP amyloid formation. A) Thioflavin-T assays of IAPP and varying concentrations of Aspirin. The black curve represents 32 μM IAPP Control in the absence of Aspirin. The red curve represents 32 μM IAPP in the presence of 32 μM Aspirin. The green curve represents 32 μM IAPP in the presence of 320 μM Aspirin. The yellow curve represents 32 μM IAPP in the presence of 640 μM Aspirin. Conditions were 20 mM Tris-HCl buffer, pH 7.4, 0.25% DMSO, 32 μM IAPP, 32 μM thioflavin-T, and varying concentrations of Aspirin. **B)** TEM image of wild-type IAPP. **C)** IAPP:Aspirin 1:1. **D)** IAPP:Aspirin 1:10. **E)** IAPP:Aspirin 1:20. Scale bar represents 100 nm.

4. APPENDIX

4.1 List of Other Compounds Tested as IAPP Inhibitors and a Summary of the Experimental Results

This chapter describes the results of testing a range of compounds for their ability to inhibit IAPP amyloid formation. They were chosen either because they have been shown to inhibit α-synuclein or Aβ amyloid formation, or because they chemically resemble known inhibitors.

4.1.1: Ponceau SS

Ponceau SS (Figure 4-1 A) was obtained from Sigma Aldrich (Product Number: 199745). In Figure 4-1 B, the absorbance spectrum also shows that there is a significant amount of absorbance at 450 nm and 485 nm; so inner filter effects play a large role in thioflavin-T kinetics. These experiments were performed in 20 mM Tris-HCl buffer pH 7.4 2% HFIP (v/v) with stirring and 16 μM IAPP. This makes thioflavin-T kinetics difficult to analyze. So it may seem like the thioflavin-T assay shows that there was inhibition of amyloid fibers (Figure 4-1 C); however, the physical aggregation can be observed in Figure 4-2 C after the turbidity assay performed in Figure 4-2 A. This compound has been reported to inhibit tau filament formation (*41*).

4.1.2: 2,3,4-Trihydroxybenzophenone

Trihydroxybenzophenone (Figure 4-3 A) was obtained from Sigma Aldrich (Product Number 260576). The thioflavin-T curve for Trihydroxybenzophenone suggests that there is barely any inhibition. These experiments were performed in 20 mM Tris-HCl

buffer pH 7.4 2% HFIP (v/v) with stirring and 16 μM IAPP. The CD scans and TEM images support this claim (Figure 4-3 D-E and Figure 4-4 A-C). This compound has been reported to inhibit tau filament formation (*41*).

4.1.3: 4,4'-Dihydroxybenzophenone

Dihydroxybenzophenone (Figure 4-5 A) was obtained from Sigma Aldrich (Product Number: D110507). The thioflavin-T curve for Dihydroxybenzophenone suggests that there is no inhibition. These experiments were performed in 20 mM Tris-HCl buffer pH 7.4 2% HFIP (v/v) with stirring and 16 μM IAPP. Both the CD scans and TEM images indicate that fibers similar to wild type are shown (Figure 4-5 D-E and Figure 4-6 A-C). This compound was chosen based on the resemblance to known inhibitors for tau and Aβ protein (*41, 53*).

4.1.4: 3-Hydroxy 2,7-Naphthalene Disulfonic Acid Disodium Salt

Hydroxy-Naphthalene Disulfonic Acid (HNDSA) (Figure 4-7 A) was obtained from Sigma Aldrich (Product Number: R396850). The thioflavin-T curve indicates that there is not a significant effect of fiber kinetics (Figure 4-7 C). These experiments were performed in 20 mM Tris-HCl buffer pH 7.4 2% HFIP (v/v) with stirring and 16 μM IAPP. CD spectra and TEM images support this claim (Figure 4-7 D-E and Figure 4-8 A-C). HNDSA units are found in a number of more complicated compounds which are known to inhibit Aβ and tau protein, one of which is Ponceau SS (*41, 53*).

4.1.5: Azobenzene

Azobenzene (Figure 4-9 A) was obtained from Sigma Aldrich (Product Number: 424633). The thioflavin-T assay suggests that there is a significant amount of inhibition occurring (Figure 4-9 C), however, the CD scans indicate that the amount of β-sheet fibers is equivalent in the 1:1 assay and the 1:10 assay (Figure 4-9 D-E), when the thioflavin-T curves suggests otherwise. These experiments were performed in 20 mM Tris-HCl buffer pH 7.4 2% HFIP (v/v) with stirring and 16 μM IAPP. Azobenzene units are found in a number of more complicated compounds which are known to inhibit Aβ and tau protein, one of which is Ponceau SS (*41, 53*).

4.1.6 4-(4-(N-Ethyl-N-Methylamino)phenylazo)benzonitrile

4-(4-(N-Ethyl-N-Methylamino)phenylazo)benzonitrile (EMPB) (Figure 4-10 A) was obtained from Sigma Aldrich (Product Number: S930717). EMPB has a large absorbance at 450 nm and 485 nm (Figure 4-10 B) which means that inner filter effects play a significant part in the thioflavin-T assay. These experiments were performed in 20 mM Tris-HCl buffer pH 7.4 2% HFIP (v/v) with stirring and 16 μM IAPP. CD scans suggest that there is still β-sheet formation occurring (Figure 4-10 D-E). EMPB units are found in a more complicated molecule, Ponceau SS, which has been known to inhibit tau protein fiber growth (*41, 53*).

4.1.7 Orcein

Orcein (Figure 4-11 A) was obtained from Sigma Aldrich (Product Number: O7380). Orcein has a small amount of absorbance at 450 nm and 485 nm (Figure 4-11 B), so inner filter effects may be plausible. The thioflavin-T assay indicate that the small

molecule is inhibiting thioflavin-T kinetics (Figure 4-11 C); however, CD scans and TEM images indicate that fibers are still present (Figure 4-11 D-E and Figure 4-12 A-C). These experiments were performed in 20 mM Tris-HCl buffer pH 7.4 2% HFIP (v/v) with stirring and 16 μM IAPP. Orcein has been shown to accelerate Aβ fiber formation and decrease toxicity (*44*).

4.1.8 Azure A

Azure (Figure 4-13 A) was obtained from Sigma Aldrich (Product Number: A6270). Figure 4-13 B suggests that there are some inner filter effects at 450 nm and 485 nm. So the thioflavin-T curve (Figure 4-13 C) is not reliable. These experiments were performed in 20 mM Tris-HCl buffer pH 7.4 2% HFIP (v/v) with stirring and 16 μM IAPP. The CD scans suggests that there are still β-sheets formed (Figure 4-13 D-F). TEM images show that there is a small change in morphology (Figure 4-14 A-D). A turbidity experiment was performed using a UV Spectrophotometer set at wavelength 400 nm (Figure 4-15). The assay indicates that fibers/aggregate species are being formed. An interruption study was performed using Azure A and adding it approximately to preformed IAPP fibers. An instantaneous drop in fluorescence is observed (Figure 4-16 A); however, TEM images indicate that fibers are still formed (Figure 4-16 C). Azure A has been shown to inhibit tau filamentous growth (*41*).

4.1.9: Benzathiazoles

Riluzole (Product Number: R3772), 1-H-Benzimidazole-2-Sulfonic Acid (BISA) (Product Number: 530646), Aminomethylbenzimidazol (AMBI) (Product Number: 412546), Benzimidazole (Product Number: 194123), and Thiabenzdazole (Product

Number: T8904) were all obtained from Sigma Aldrich (Figure 4-17 A-E). The UV absorbance spectra indicate that for all 5 small molecules there are no inner filter effects (Figure 4-18 A-E). The thioflavin-T curves indicate that there was no effect on fiber formation (Figure 4-19). These experiments were performed in 20 mM Tris-HCl buffer pH 7.4 2% HFIP (v/v) with stirring and 16 μM IAPP. These banzathiazoles show structural similarities to thioflavin-T which can bind within the groove of β-sheets

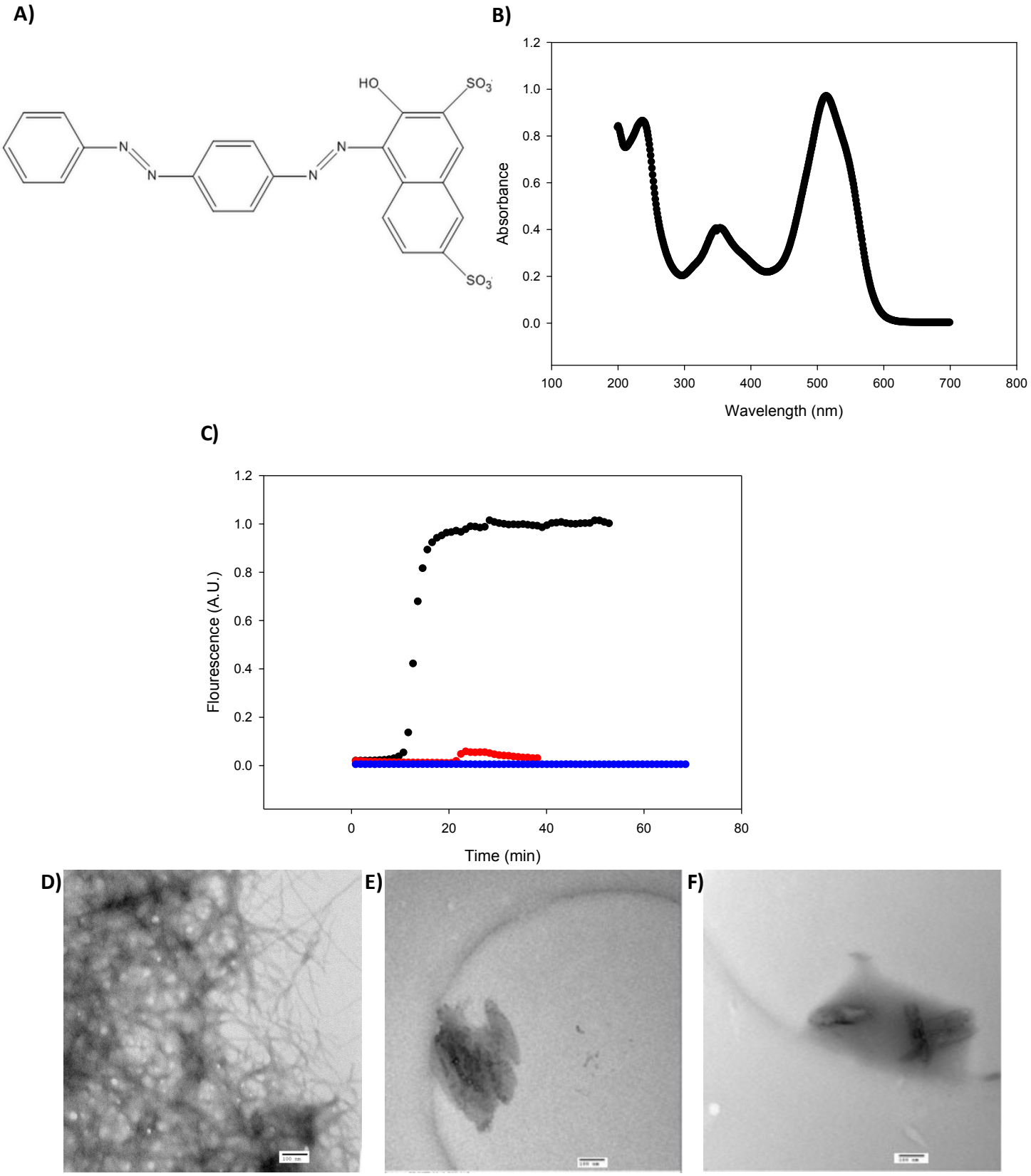

Figure 4-1: A) Structure of Ponceau SS. **B)** UV Absorbance Spectra of Ponceau at 16 μM concentration in 2% HFIP (v/v). **C)** Thioflavin-T based assay of Ponceau SS with IAPP. Black is IAPP control at 16 μM. Red indicates IAPP in the presence of Ponceau SS at a 1:1 ratio of IAPP:Ponceau SS. Blue indicates IAPP in the presence of Ponceau SS at a 1:10 ratio of IAPP:Ponceau SS. **D)** TEM image of IAPP in the absence of Ponceau SS. **E)** TEM image of IAPP:Ponceau SS at a 1:1 ratio. **F)** TEM image of IAPP:Ponceau SS at a 1:10 ratio. Scale bars represent 100 nm. All experiments were performed in 20 mM Tris-HCl buffer at pH 7.4 and 2% HFIP.

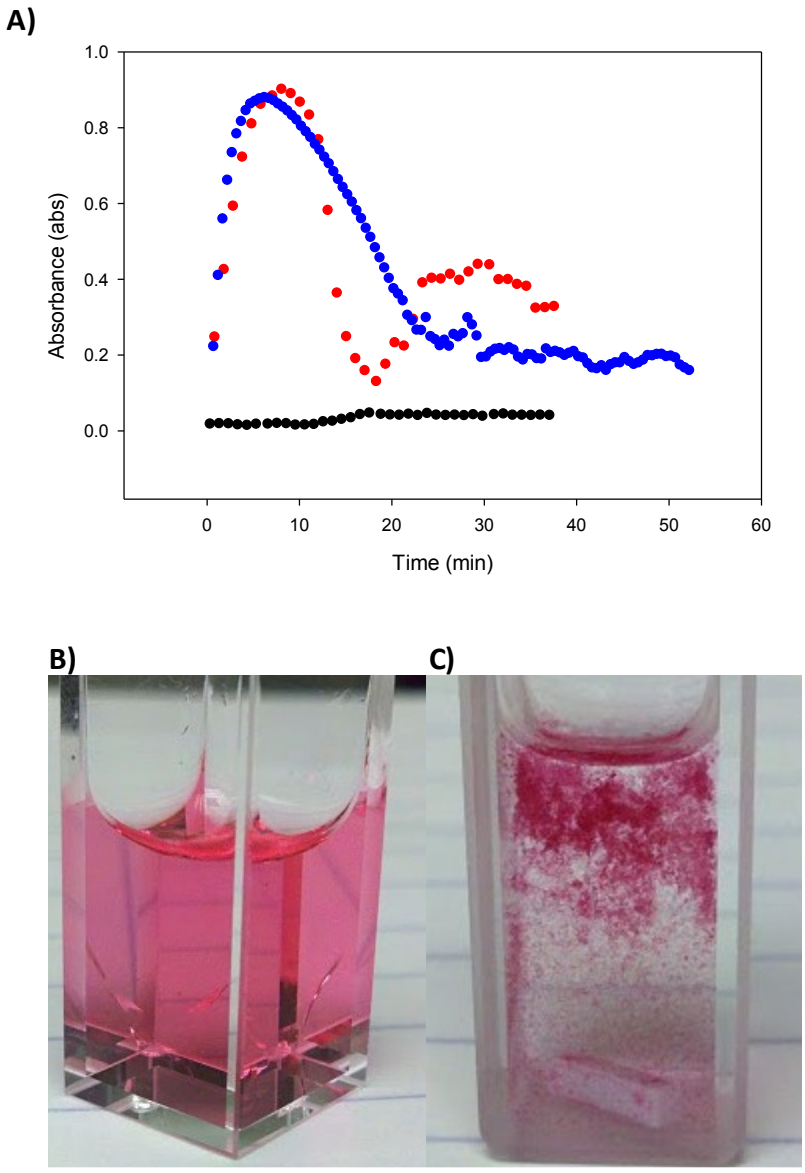

Figure 4-2: Turbidity experiment performed using Ponceau SS at a 1:1 ratio of IAPP:Ponceau SS. **A)** Turbidity assay performed at 600 nm wavelength. Black curve represents 16 μM IAPP Control. Red and blue curve indicate two independent runs using Ponceau SS at a 1:1 ratio of IAPP:Ponceau SS. **B)** A physical picture of the 1:1 ratio of IAPP:Ponceau SS at the beginning of the run. **C)** A physical picture of the 1:1 ratio of IAPP:Ponceau SS at the end of the run. All experiments were carried out in 20 mM Tris-HCl buffer at pH 7.4 and 2% HFIP (v/v) and 32 μM of peptide

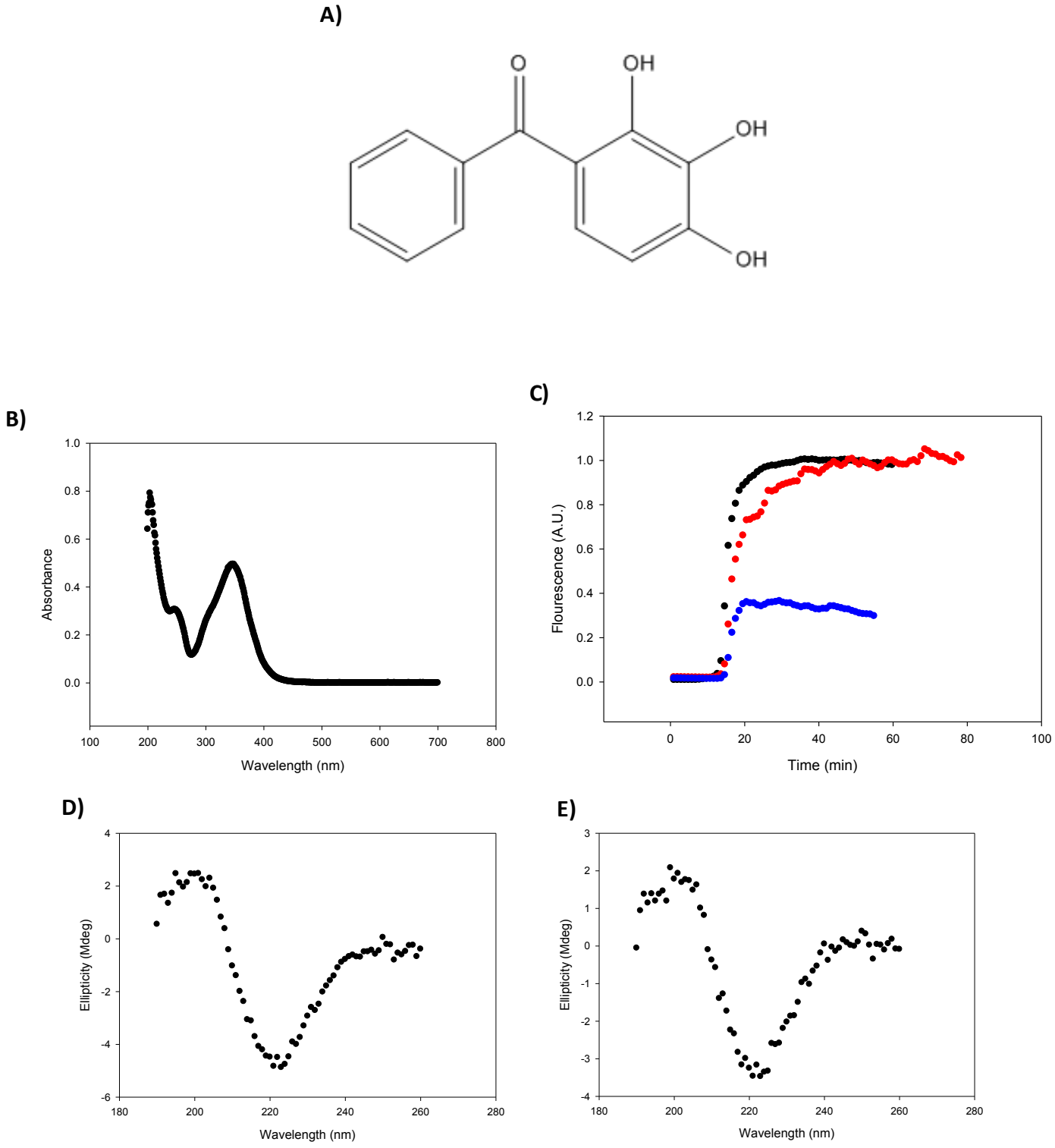

Figure 4-3: A) Structure of Trihydroxybenzophenone. **B)** UV Absorbance Spectra of Trihydroxybenzophenone at 16 µM concentration in 2% HFIP (v/v). **C)** Thioflavin-T based assay of Trihydroxybenzophenone with IAPP. Black is IAPP control at 16 µM. Red indicates IAPP in the presence of Trihydroxybenzophenone at a 1:1 ratio of IAPP: Trihydroxybenzophenone. Blue indicates IAPP in the presence of Trihydroxybenzophenone at a 1:10 ratio of IAPP: Trihydroxybenzophenone. **D)** CD scan of IAPP: Trihydroxybenzophenone at a 1:1 ratio. **E)** CD scan of IAPP: Trihydroxybenzophenone at a 1:10 ratio. Both CD scans indicate β-sheet structure.

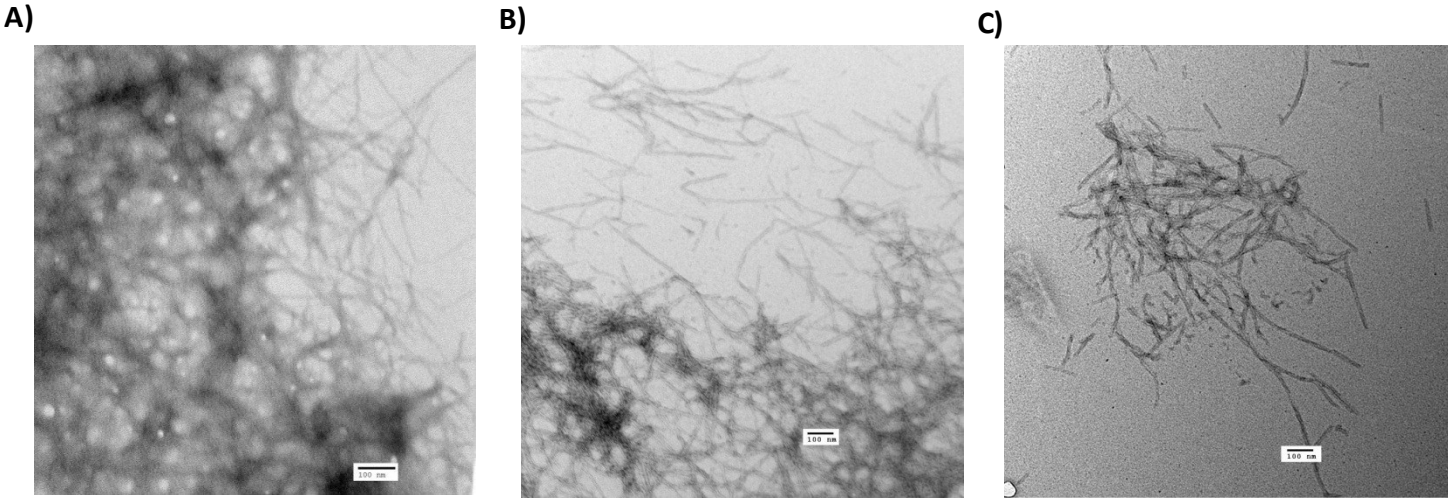

Figure 4-4: A) TEM image of IAPP in the absence of Trihydroxybenzophenone. **B)** TEM image of IAPP in the presence of Trihydroxybenzophenone at 1:1 ratio. **C)** and 1:10 ratio of IAPP:Trihydroxybenzophenone. Scale bars represent 100 nm.

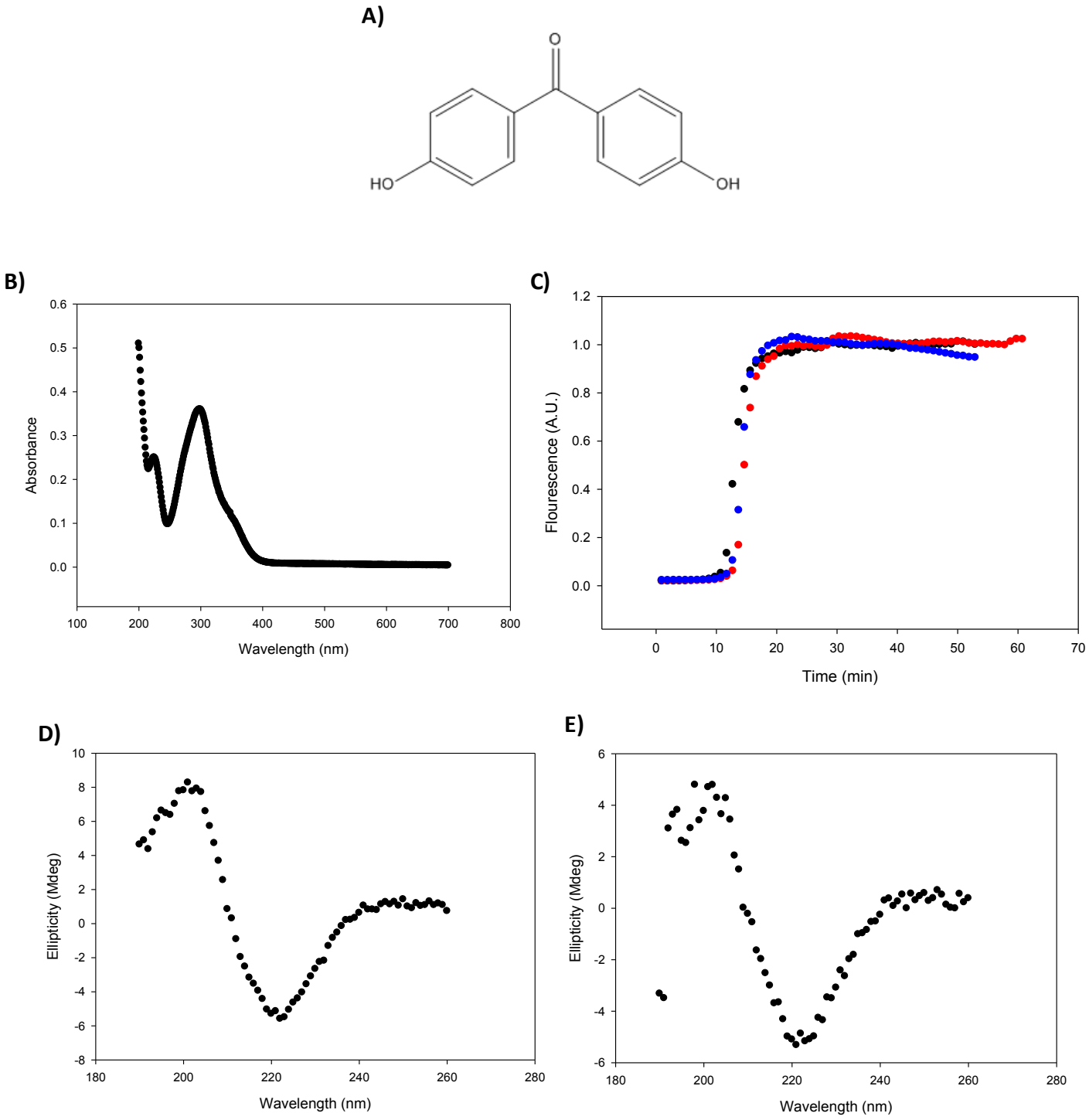

Figure 4-5: A) Structure of Dihydroxybenzophenone. **B)** UV Absorbance Spectra of Dihydroxybenzophenone at 16 μM concentration in 2% HFIP (v/v). **C)** Thioflavin-T based assay of Dihydroxybenzophenone with IAPP. Black is IAPP control at 16 μM. Red indicates IAPP in the presence of Dihydroxybenzophenone at a 1:1 ratio of IAPP: Dihydroxybenzophenone. Blue indicates IAPP in the presence of Dihydroxybenzophenone at a 1:10 ratio of IAPP: Dihydroxybenzophenone. **D)** CD scan of IAPP:Dihydroxybenzophenone at a 1:1 ratio. **E)** CD scan of IAPP: Dihydroxybenzophenone at a 1:10 ratio. Both CD scans indicate β-sheet structure.

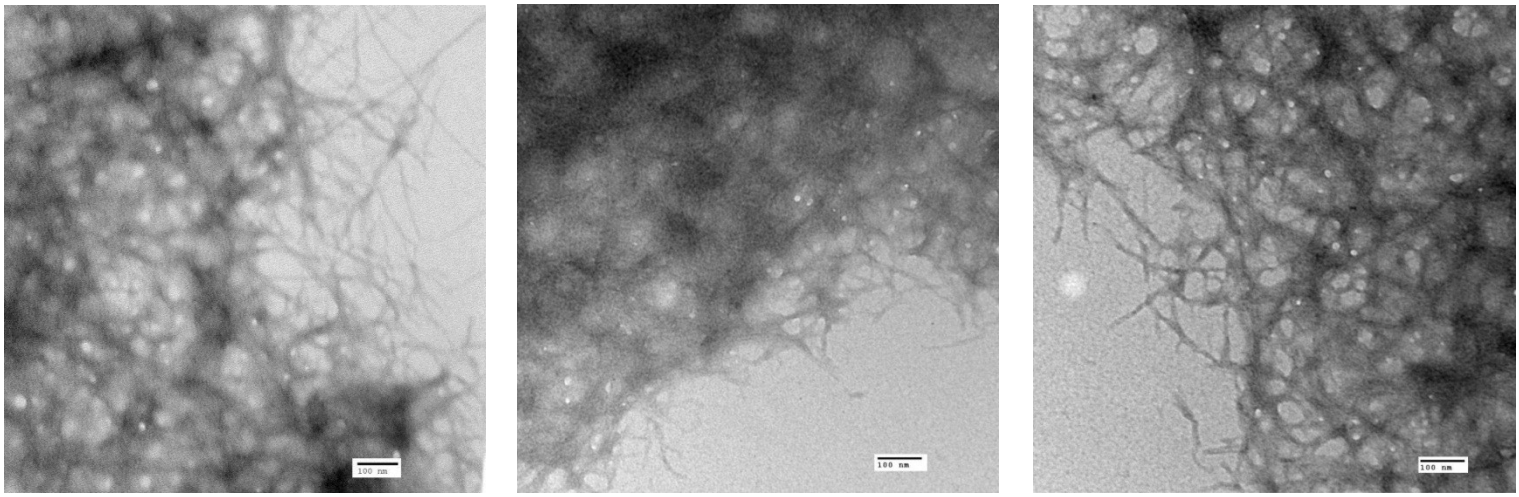

Figure 4-6: A) TEM image of IAPP in the absence of Dihydroxybenzophenone. **B)** TEM image of IAPP in the presence of Dihydroxybenzophenone at 1:1 ratio. **C)** and 1:10 ratio of IAPP:Dihydroxybenzophenone. Scale bars represent 100 nm.

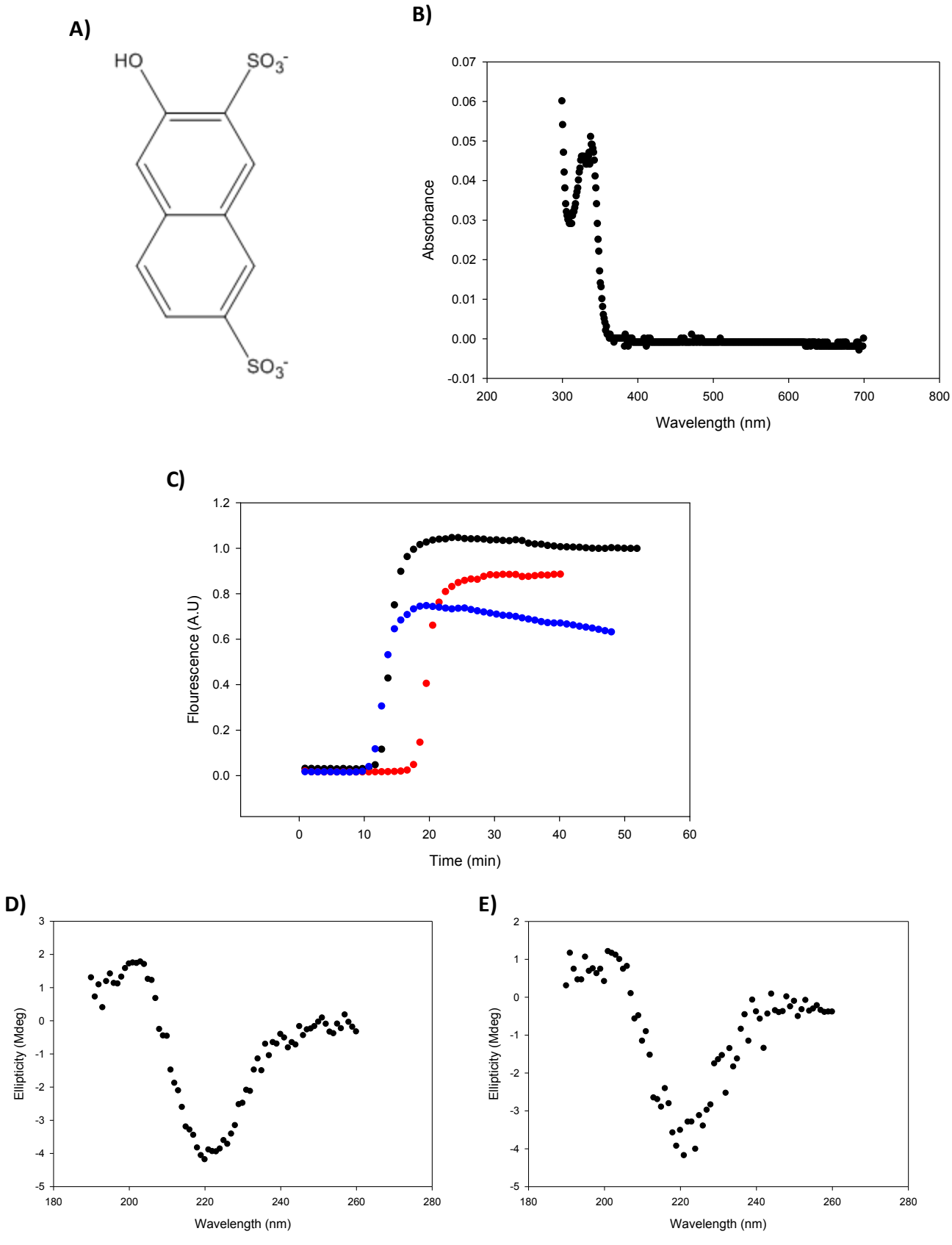

Figure 4-7: A) Structure of 3-Hydroxy 2,7-Naphthalene disulfonic acid disodium salt (HNDSA). **B)** UV Absorbance Spectra of HNDSA at 16 μM concentration in 2% HFIP (v/v). **C)** Thioflavin-T based assay of HNDSA with IAPP. Black is IAPP control at 16 μM. Red indicates IAPP in the presence of HNDSA at a 1:1 ratio of IAPP: HNDSA. Blue indicates IAPP in the presence of HNDSA at a 1:10 ratio of IAPP: HNDSA. **D)** CD scan of IAPP: HNDSA at a 1:1 ratio. **E)** CD scan of IAPP: HNDSA at a 1:10 ratio. Both CD scans indicate β-sheet structure.

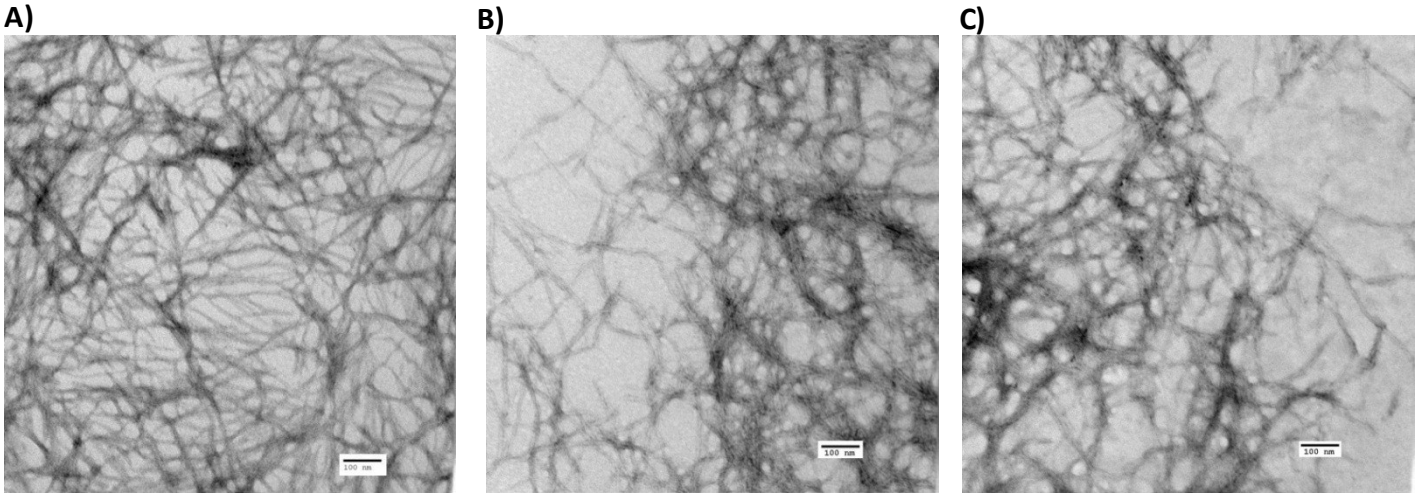

Figure 4-8: A) TEM image IAPP in the absence of HNDSA. **B)** TEM image of IAPP in the presence of HNDSA at 1:1 ratio. **C)** and 1:10 ratio of IAPP:HNDSA. Scale bars represent 100 nm.

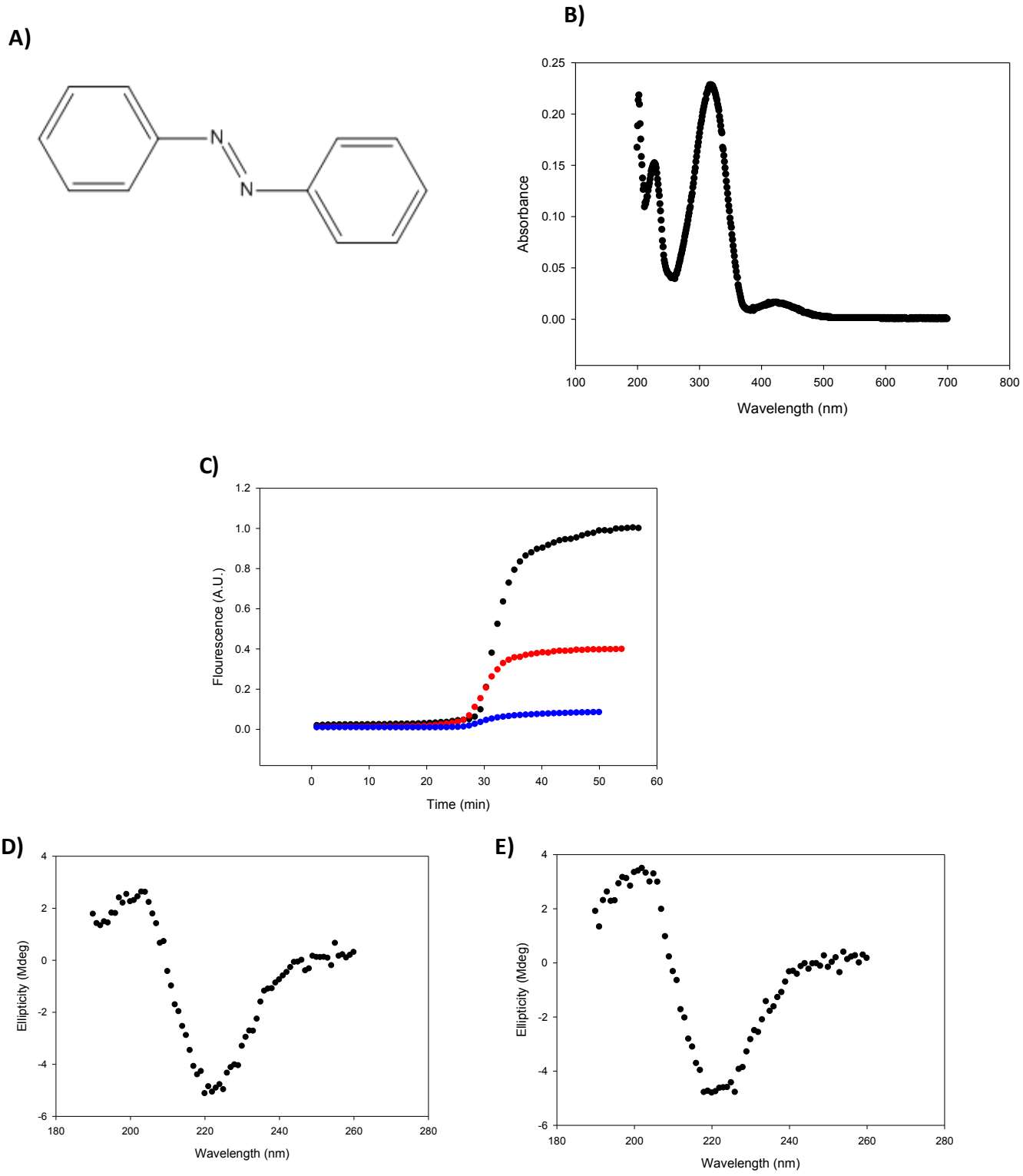

Figure 4-9: A) Structure of Azobenzene. **B)** UV Absorbance Spectra of Azobenzene at 16 μM concentration in 2% HFIP (v/v). **C)** Thioflavin-T based assay of Azobenzene with IAPP. Black is IAPP control at 16 μM. Red indicates IAPP in the presence of Azobenzene at a 1:1 ratio of IAPP:Azobenzene. Blue indicates IAPP in the presence of Azobenzene at a 1:10 ratio of IAPP: Azobenzene. **D)** CD scan of IAPP: Azobenzene at a 1:1 ratio. **E)** CD scan of IAPP: Azobenzene at a 1:10 ratio. Both CD scans indicate β-sheet structure.

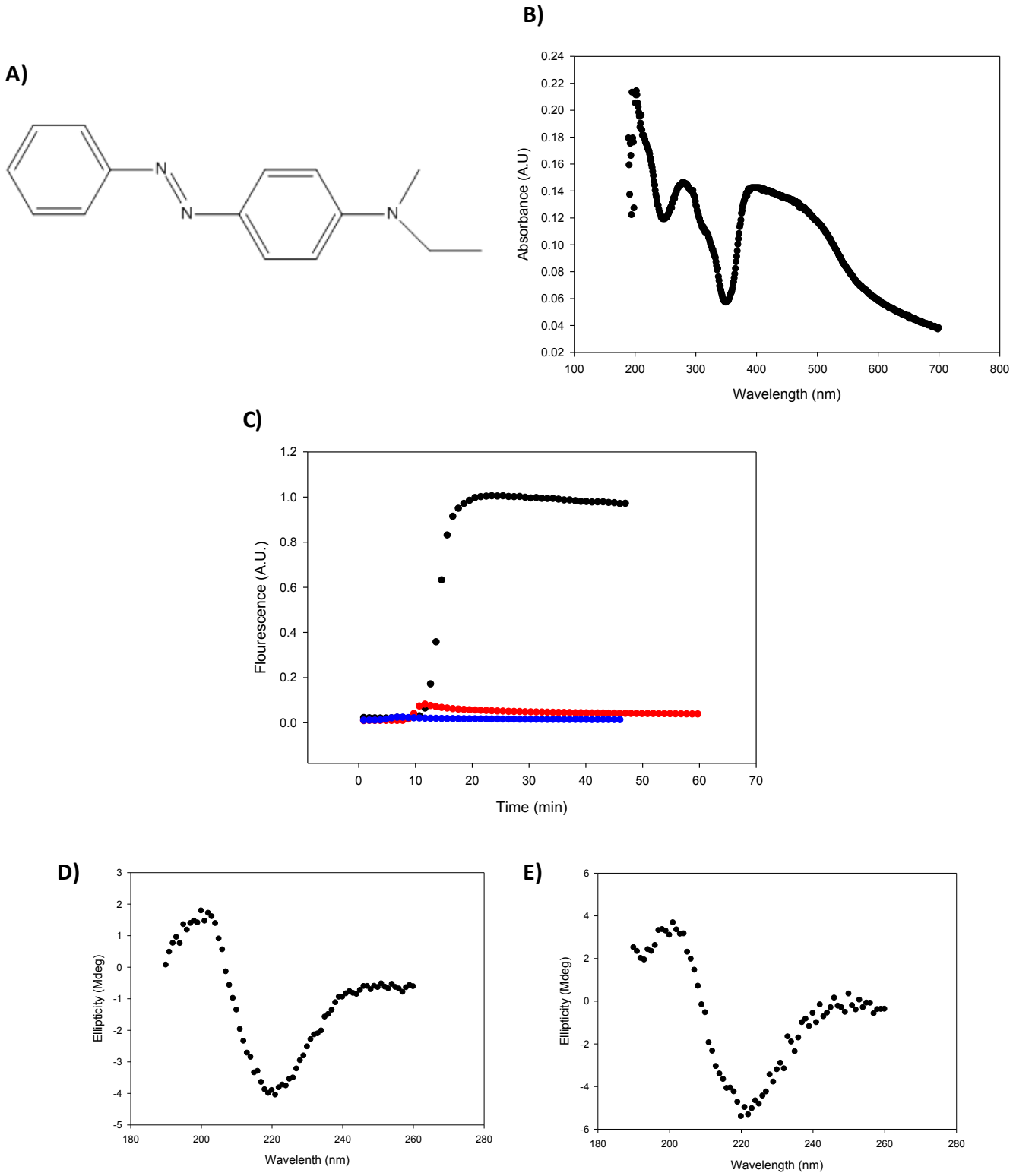

Figure 4-10: A) Structure of N-Ethyl-N-Methylamino(phenylazo)benzonitrile (EMPB). **B)** UV Absorbance Spectra of EMPB at 16 μM concentration in 2% HFIP (v/v). **C)** Thioflavin-T based assay of EMPB with IAPP. Black is IAPP control at 16 μM. Red indicates IAPP in the presence of EMPB at a 1:1 ratio of IAPP:EMPB. Blue indicates IAPP in the presence of EMPB at a 1:10 ratio of IAPP:EMPB. **D)** CD scan of IAPP:EMPB at a 1:1 ratio. **E)** CD scan of IAPP:EMPB at a 1:10 ratio. Both CD scans indicate β-sheet structure.

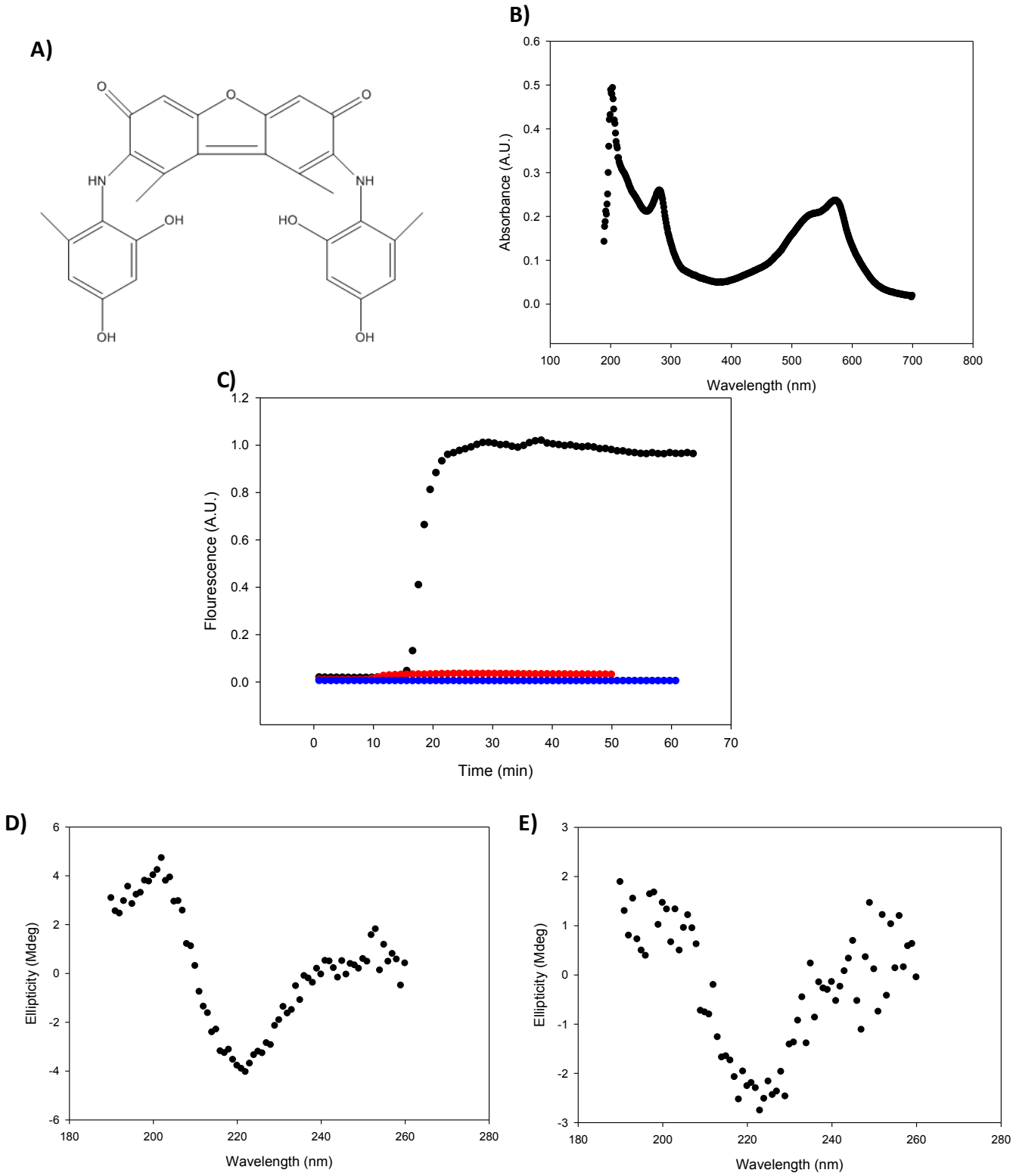

Figure 4-11: A) Structure of Orcein. **B)** UV Absorbance Spectra of Orcein at 16 μM concentration in 2% HFIP (v/v). **C)** Thioflavin-T based assay of Orcein with IAPP. Black is IAPP control at 16 μM. Red indicates IAPP in the presence of Orcein at a 1:1 ratio of IAPP: Orcein. Blue indicates IAPP in the presence of Orcein at a 1:10 ratio of IAPP: Orcein. **D)** CD scan of IAPP: Orcein at a 1:1 ratio. **E)** CD scan of IAPP: Orcein at a 1:10 ratio. Both CD scans indicate β-sheet structure.

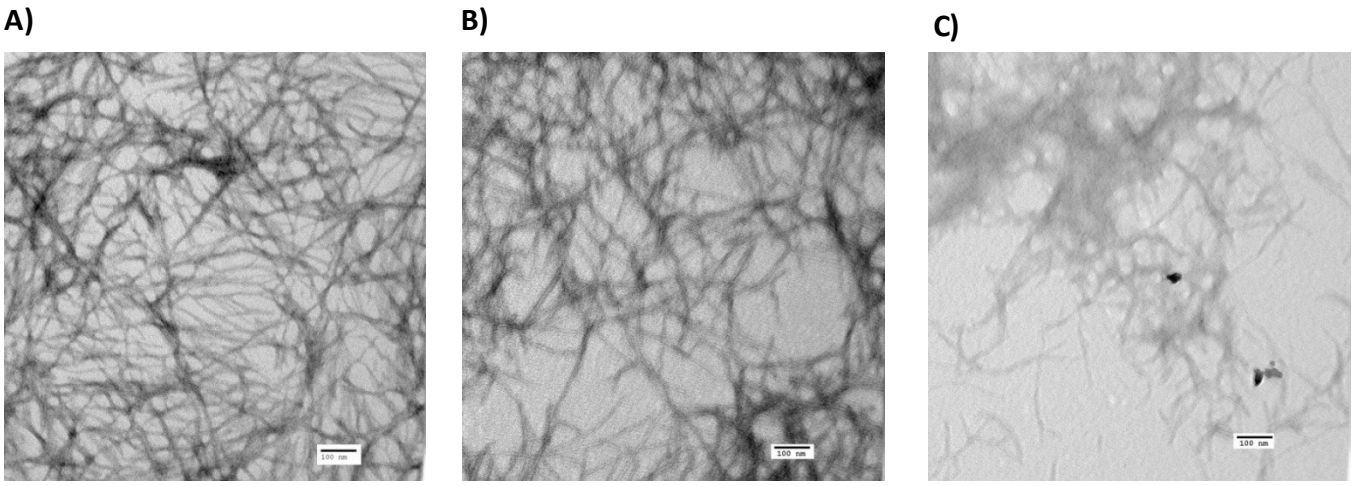

Figure 4-12: A) TEM image IAPP in the absence of Orcein. **B)** TEM image of IAPP in the presence of Orcein at 1:1 ratio. **C)** and 1:10 ratio of IAPP:Orcein. Scale bars represent 100 nm.

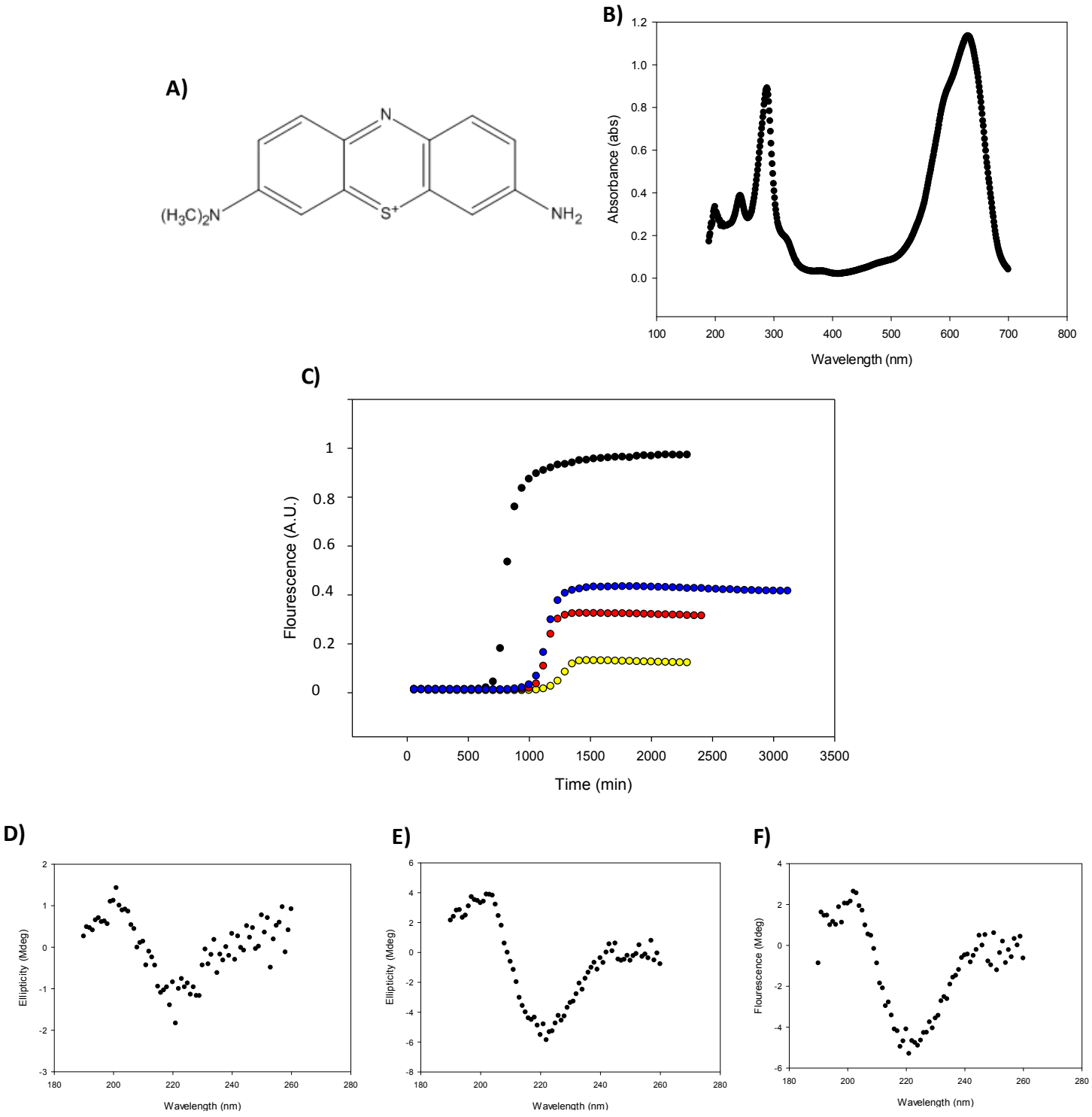

Figure 4-13: A) Structure of Azure A. **B)** UV Absorbance Spectra of Azure A at 32 μM concentration in 2% HFIP (v/v). **C)** Thioflavin-T based assay of Azure A with IAPP. Black is IAPP control at 16 μM. Blue indicates IAPP in the presence of Azure A at a 1:1 ratio of IAPP:Azure A. Red indicates IAPP in the presence of Azure A at a 1:5 ratio of IAPP:Azure A. Yellow indicates IAPP in the presence of Azure A at a 1:10 ratio of IAPP:Azure A. **D)** CD scan of IAPP:Azure A at a 1:1 ratio. **E)** CD scan of IAPP: Azure A at a 1:5 ratio. **F)** CD scan of IAPP:Azure A at a 1:10 ratio. All CD scans indicate β-sheet structure.

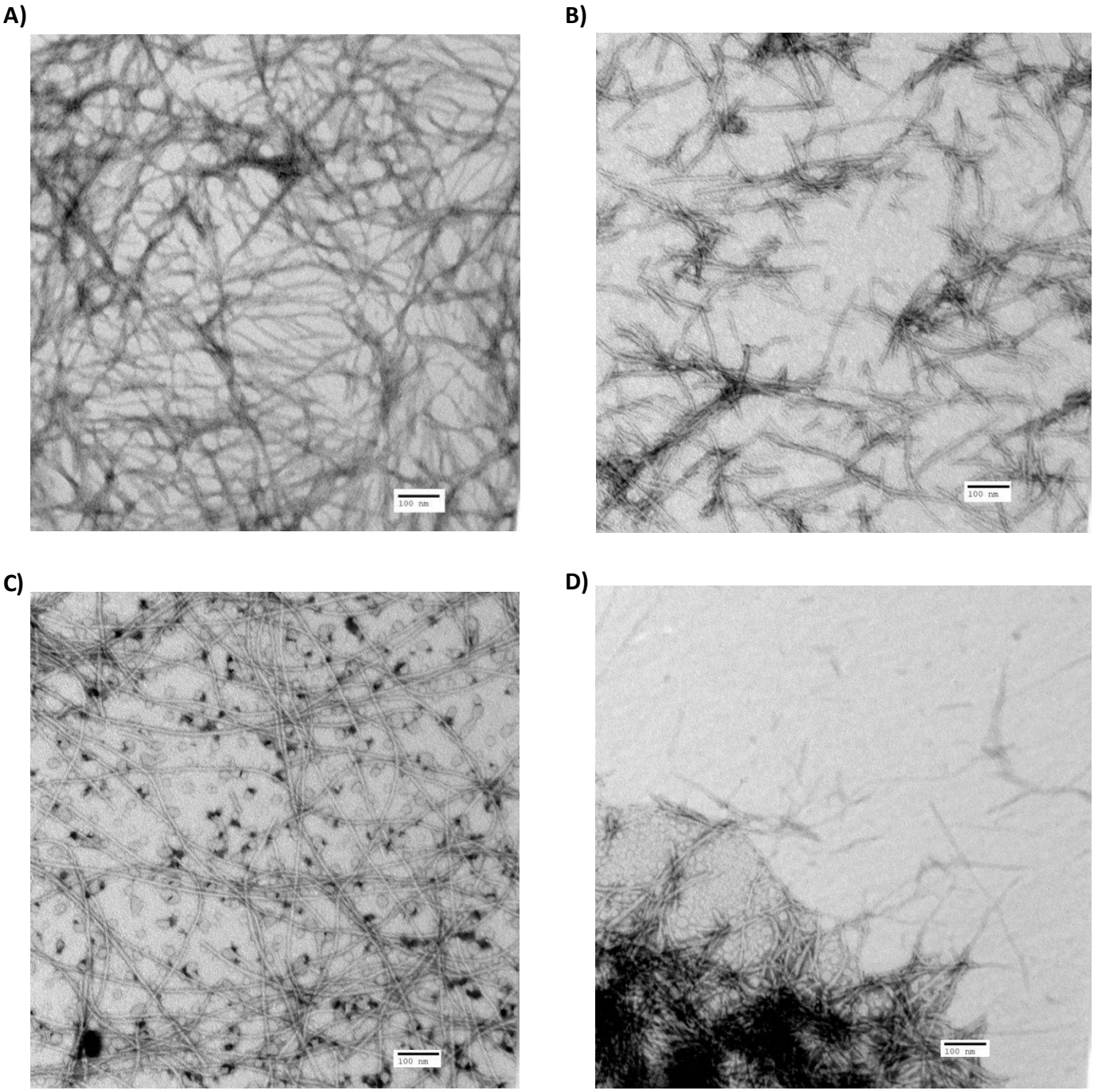

Figure 4-14: A) TEM image IAPP in the absence of Azure A. **B)** TEM image of IAPP in the presence of Azure A at 1:1 ratio, **C)** 1:5 ratio, **D)** and 1:10 ratio of IAPP:Azure A. Scale bars represent 100 nm.

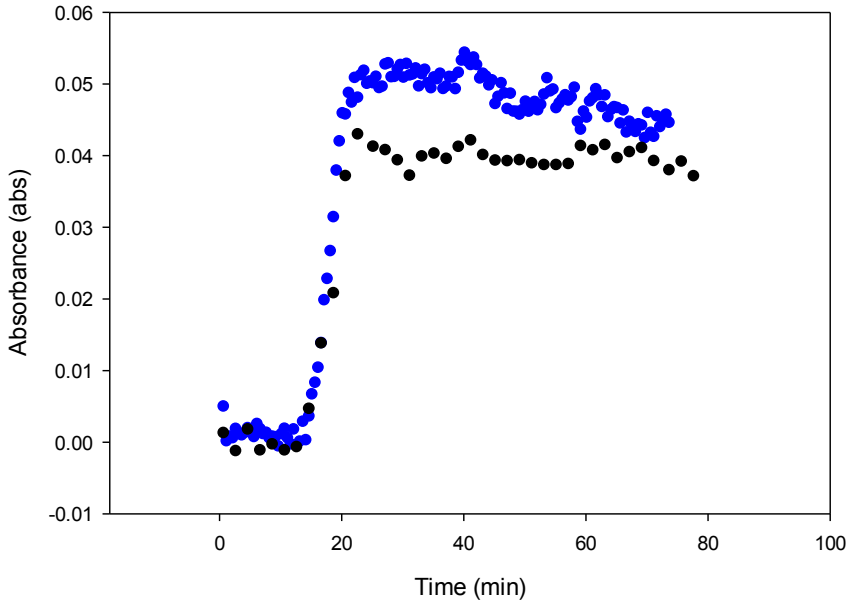

Figure 4-15: Turbidity assay with IAPP in the presence (blue curve) and absence (black curve). The wavelength used is 400 nm. Conditions were 20 mM Tris-HCl buffer and 2% (v/v) HFIP.

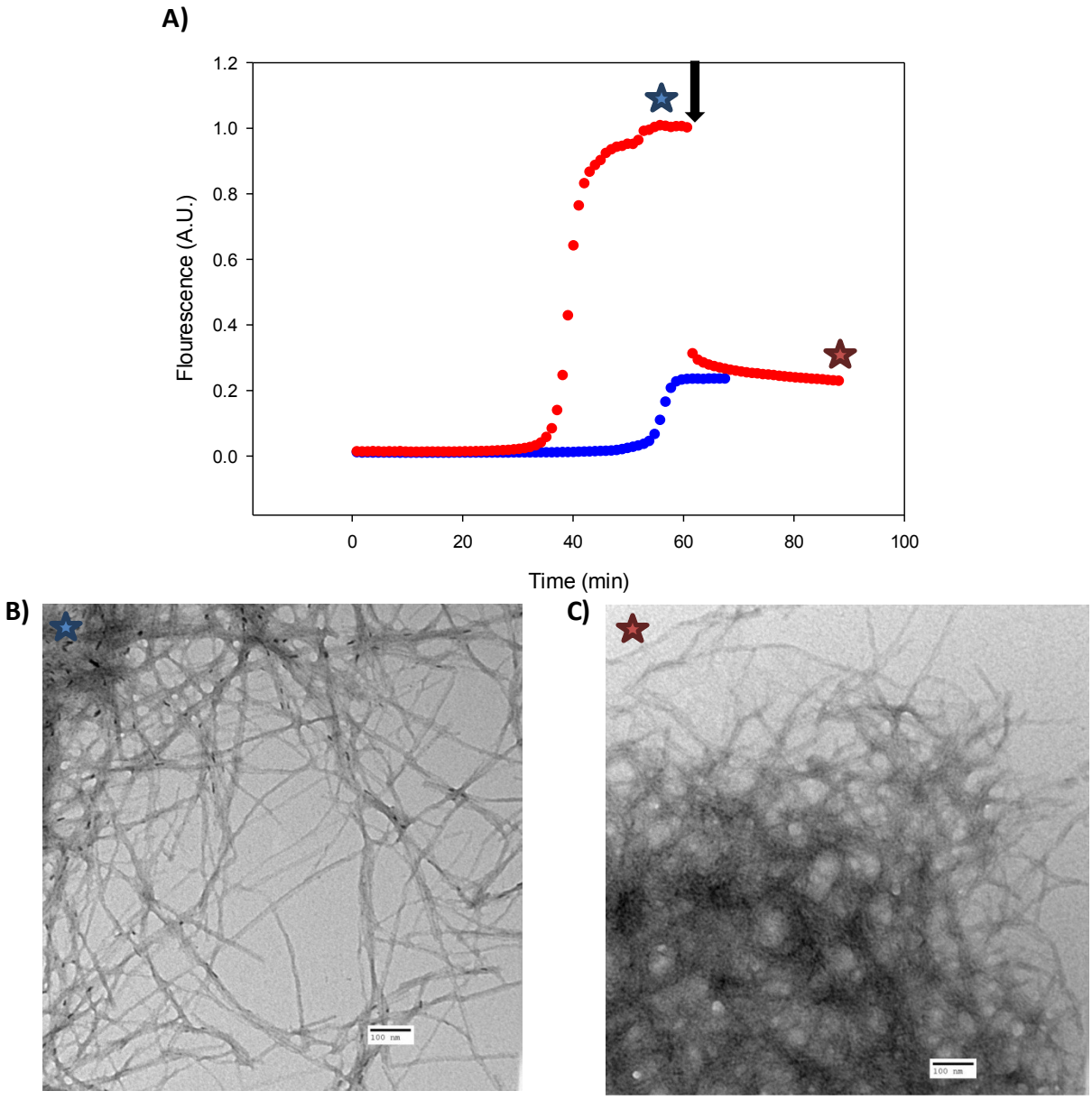

Figure 4-16: A) Thioflavin-T curve of an interruption study performed with Azure A. The red curve indicates the interruption study. The black arrow indicates the addition Azure A at approximately t = 60 min. The blue and red star indicates an aliquot of the assay that was taken for TEM analysis. The blue curve indicates a thioflavin-T assay of IAPP with Azure A at t = 0 min. **B)** TEM image indicated by the blue star prior to addition of Azure A. **C)** TEM image indicated by the red star after the addition of Azure A. Scale bars represent 100 nm.

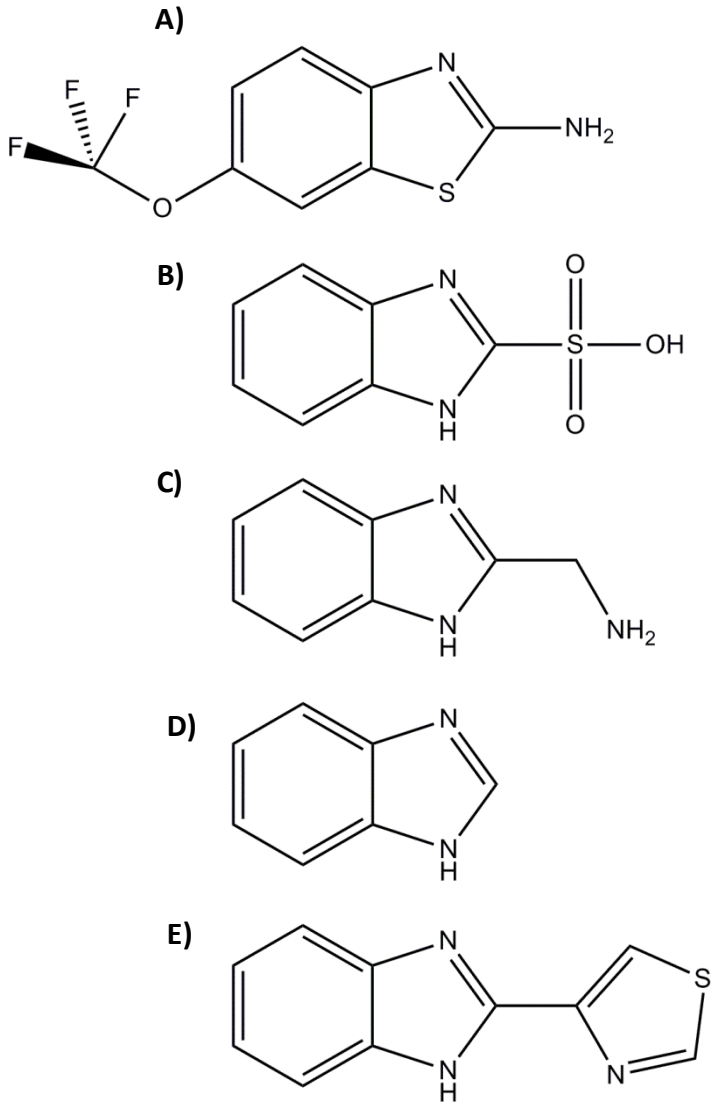

Figure 4-17: Structure of **A)** Riluzole, **B)** 1-H-Benzimidazole-2-Sulfonic Acid (BISA), **C)** Aminomethylbenzimidazol (AMBI), **D)** Benzimidazol, **E)** and Thiabenzdazole.

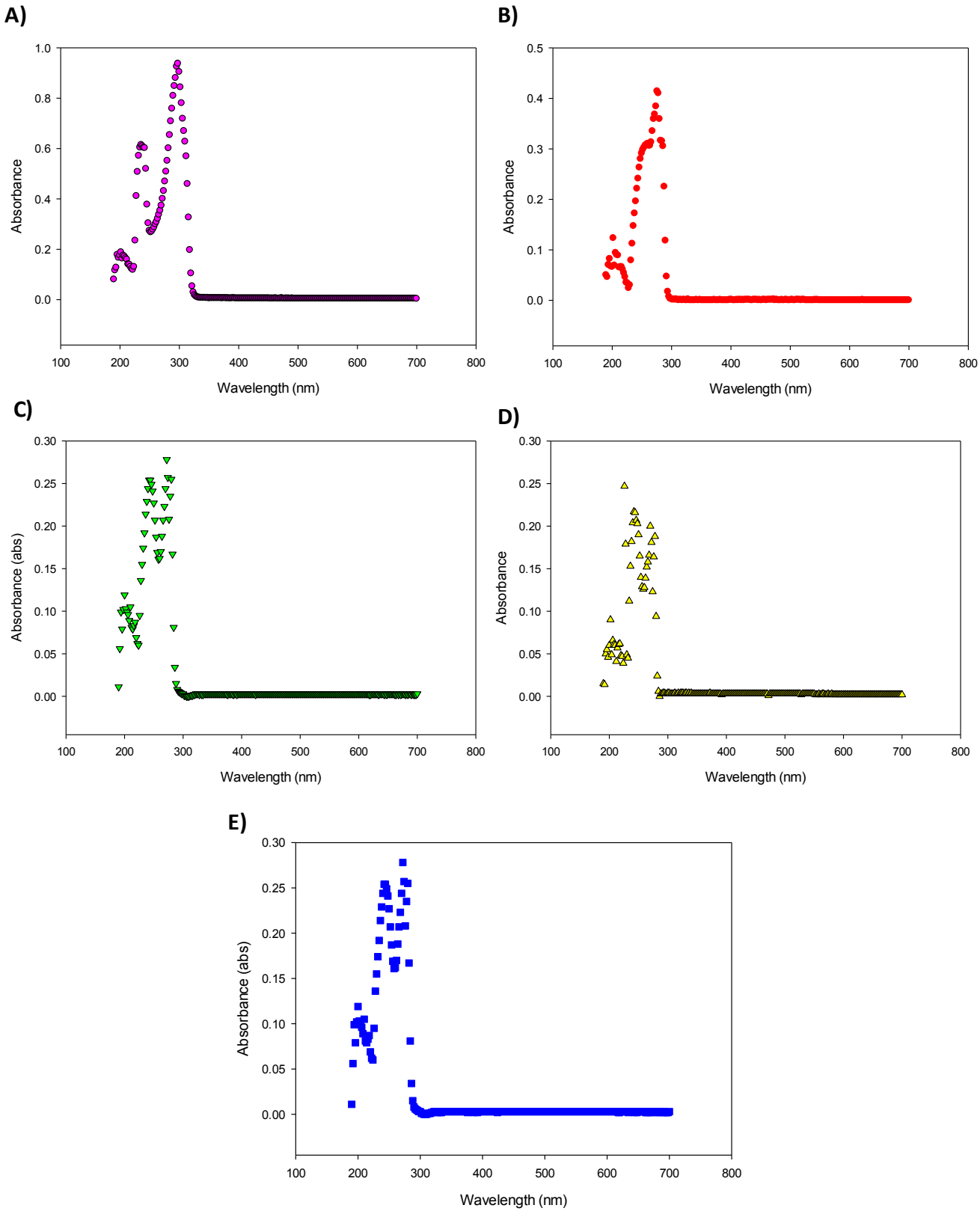

Figure 4-18: UV absorbance spectra of **A)** Riluzole, **B)** 1-H-Benzimidazole-2-Sulfonic Acid (BISA), **C)** Aminomethylbenzimidazol (AMBI), **D)** Benzimidazol, **E)** and Thiabenzdazole. All the small molecule inhibitors were dissolved at 32 µM in 20 mM Tris-HCl buffer and 0.25% (v/v) DMSO.

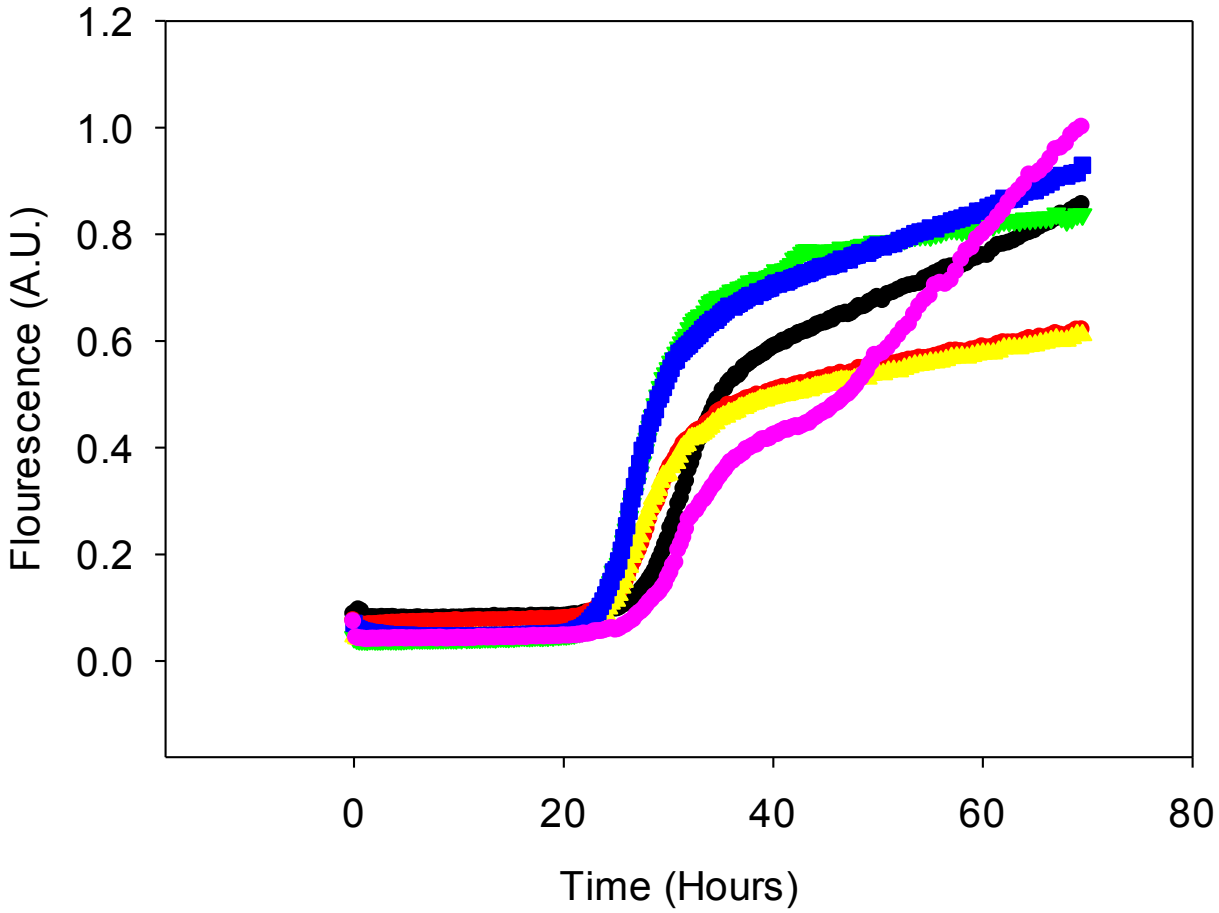

Figure 4-19: Thioflavin-T curves of wild type IAPP in the absence of inhibitor (Black) and in the presence of Riluzole (Pink), 1-H-Benzimidazole-2-Sulfonic Acid (Red), Aminomethylbenzimidazol (Green), Benzimidazol (Yellow), and Thiabenzdazole (Blue). All the small molecule inhibitors were present with IAPP in solution at a 10 fold excess. The conditions were in 20 mM Tris-HCl buffer and 0.25% (v/v) DMSO.

REFERENCES

1. Sipe, J. D. (1994) Amyloidosis, *Crit. Rev. Clin. Lab. Sci. 31*, 325-354.
2. Selkoe, D. J. (2004) Cell biology of protein misfolding: The examples of alzheimer's and parkinson's disease, *Nat. Cell Biol. 348*, 247-252.
3. Kajava, A. V., Aebi, U., and Steven, A. C. (2005) The parallel superpleated beta-structure as a model for amyloid fibrils of human amylin, *J. Mol. Biol. 348*, 247-252.
4. Makin, S. O., and Serpell, L. C. (2004) Structural characterisation of islet amyloid polypeptide fibrils, *J. Mol. Biol. 335*, 1279-1288.
5. Makin, O. S., and Serpell, L. C. (2005) Structures of amyloid fibrils, *FEBS J. 272*, 5950-5961.
6. Sunde, M., Serpell, L. C., Bartlam, M., Fraser, P. E., Pepys, M. B., and Blake, C. C. F. (1997) Common core structure of amyloid fibrils by synchotron x-ray diffration, *J. Mol. Biol. 273*, 729-739.
7. Johnston, N. (2005) Gamma-secretase makes a splash, *Scientist 19*, 24-25.
8. Krebs, M. R. H., Bromley, E. H. C., and Donald, A. M. (2005) The binding of thioflavin-T to amyloid fibrils: Localisation and implications, *J. Mol. Biol. 308*, 783-794.
9. Levine, H. (1995) Thioflavin-T interaction with amyloid beta-sheet structures,, *Amyloid-International Jounal of Experimental and Clinical Investigation 2*, 1-6.
10. Padrick, S. B., and Miranker, A. D. (2001) Islet amyloid polypeptide: Identification of long-range contacts and local order on the fibrillogenesis pathway, *J. Mol. Biol. 308*, 783-794.
11. Jarrett, J. T., and Lansbury, P. T. (1993) Seeding one-dimensional crystallization of amyloid - a pathogenic mechanism in alzheimers-disease and scrapie, *Cell 73*, 1055-1058.
12. Lomakin, A., Chung, D. S., Benedek, G. B., Kirschner, D. A., and Teplow, D. B. (1996) On the nucleation and growth of amyloid beta- protein fibrils: Detection of nuclei and quantitation of rate constants, *Proc. Natl. Acad. Sci. 93*, 1125-1129.
13. Soto, C., Saborio, G. P., and Anderes, L. (2002) Cyclic amplification of protein misfolding: Application to prion-related disorders and beyond, *Trends Neurosci. 25*, 390-394.
14. Westermark, P., Wernstedt, C., Wilander, E., Hayden, D. W., Obrien, T. D., and Johnson, K. H. (1987) Amyloid fibrils in human insulinoma and islets of langerhans of the diabetic cat are derived from a neuropeptide-like protein also present in normal islet cells, *Proc. Natl. Acad. Sci. USA 84*, 3881-3885.
15. Cooper, G. J. S., Willis, A. C., Clark, A., Turner, R. C., Sim, R. B., and Reid, K. B. M. (1987) Purification and characterization of a peptide from amyloid-rich pancreases of type-2 diabetic-patients, *Proc. Natl. Acad. Sci. USA 84*, 8628-8632.
16. Cooper, G. J. S. (1994) Amylin compared with calcitonin-gene-related peptide - structure, biology, and relevance to metabolic disease, *Endocrine Rev. 15*, 163-201.
17. Hay, D. L., Christopoulos, G., Christopoulos, A., and Sexton, P. M. (2004) Amylin receptors: molecular composition and pharmacology, *Biochem. Soc. Trans. 32*, 865-867.

18. Nishi, M., Sanke, T., Nagamatsu, S., Bell, G. I., and Steiner, D. F. (1990) Islet amyloid polypeptide - a new beta-cell secretory product related to islet amyloid deposits, *J. Biol. Chem. 265*, 4173-4176.
19. Hutton, J. C. (1989) The insulin secretory granule, *Diabetologia 32*, 271-281.
20. Kahn, S. E., Andrikopoulos, S., and Verchere, C. B. (1999) Islet amyloid: A long-recognized but underappreciated pathological feature of type 2 diabetes, *Diabetes 48*, 241-253.
21. Clark, A., Lewis, C. E., Willis, A. C., Cooper, G. J. S., Morris, J. F., Reid, K. B. M., and Turner, R. C. (1987) Islet amyloid formed from diabetes-associated peptide may be pathogenic in type-2 diabetes, *Lancet 2*, 231-234.
22. Kahn, S. E., Hull, R. L., Westermark, G. T., and Westermark, P. (2004) Islet amyloid: A critical entity in the pathogenesis of type 2 diabetes, *J. Clin. Endocrinol. Metab. 89*, 3629-3643.
23. Verchere, C. B., Marzban, L., and Park, K. (2003) Islet amyloid polypeptide and type 2 diabetes, *Exp. Geront. 38*, 347-351.
24. Lorenzo, A., Razzaboni, B., Weir, G. C., and Yankner, B. A. (1994) Pancreatic-islet cell toxicity of amylin associated with type-2 diabetes-mellitus, *Nature 368*, 756-760.
25. Clark, A., Wells, C. A., Buley, I. D., Cruickshank, J. K., Vanhegan, R. I., Matthews, D. R., Cooper, G. J. S., Holman, R. R., and Turner, R. C. (1988) Islet amyloid, increased alpha-cells, reduced beta-cells and exocrine fibrosis - quantitative changes in the pancreas in type-2 diabetes, *Diabetes. Res. Clin. Pract. 9*, 151-159.
26. Butler, P. C., Butler, A. E., Janson, J., Bonner-Weir, S., Ritzel, R., and Rizza, R. A. (2003) beta-cell deficit and increased beta-cell apoptosis in humans with type 2 diabetes, *Diabetes 52*, 102-110.
27. Aitken, J., Loomes, K., Konarkowska, B., and Cooper, G. J. S. (2003) Suppression by polycyclic compounds of the conversion of human amylin into insoluble amyloid, *Biochem. J. 374*, 779-784.
28. Westermark, G. T., Westermark, P., Berne, C., and Korsgren, O. (2008) Widespread amyloid deposition in transplanted human pancreatic islets, *N. Engl. J. Med. 359*, 977-979.
29. Teplow, D. B., Kirkitadze, M. D., and Bitan, G. (2002) Paradigm shifts in Alzheimer's disease and other neuro degenerative disorders: The emerging role of oligomeric assemblies, *J. Neurosci. Res. 69*, 567-577.
30. Potter, K. J., Abedini, A., Marek, P., Klimek, A. M., Butterworth, S., Driscoll, M., Baker, R., Nilsson, M. R., Warnock, G. L., Oberholzer, J., Bertera, S., Trucco, M., Korbutt, G. S., Fraser, P. E., Raleigh, D. P., and Verchere, C. B. (2010) Islet amyloid deposition limits the viability of human islet grafts but not porcine islet grafts, *Proc. Natl. Acad. Sci. USA 107*, 4305-4310.
31. Kahn, S. E., Andrikopoulos, S., and Verchere, C. B. (1999) Islet amyloid: A long recognized but underappreciated pathological feature of type-2 diabetes, *Diabetes 48*, 241-253.
32. Sanke, T., Hanabusa, T., Nakano, Y., Oki, C., Okai, K., Nishimura, S., Kondo, M., and Nanjo, K. (1991) Plasmat islet amyloid polypeptide (amylin) levels and

their responses to oral glucose in type-2 (non-insulin-dependent) diabetic-patients, *Diabetologia 34*, 129-132.
33. Kahn, S. E., Dalessio, D. A., Schwartz, M. W., Fujimoto, W. Y., Ensinck, J. W., Taborsky, G. J., and Porte, D. (1990) Evidence of cosecretion of islet amyloid polypeptide and insulin by beta-cells, *Diabetes 39*, 634-638.
34. Castillo, M. J., Scheen, A. J., and Lefebvre, P. J. (1995) Amylin islet amyloid polypeptide - biochemistry, physiology, pathophysiology, *Diabetes Metab. 21*, 3-25.
35. Leighton, B., and Cooper, G. J. S. (1988) Pancreatic amylin and calcitonin gene-related peptide cause resistance to insulin in skeletal-muscle invitro, *Nature 335*, 632-635.
36. Ratner, R. E., Dickey, R., Fineman, M., Maggs, G., Shen, L., Strobel, S. A., Weyer, C., and Kolterman, O. G. (2004) Amylin replacement with pramlintide as an adjunct to insulin therapy improves long-term glycaemic and weight control in Type 1 diabetes mellitus: a 1-year, randomized controlled trial, *Diabetic Med. 21*, 1204-1212.
37. Makin, O. S., and Serpell, L. C. (2004) Structural characterisation of islet amyloid polypeptide fibrils, *J. Mol. Biol. 335*, 1279-1288.
38. Sanke, T., Bell, G. I., Sample, C., Rubenstein, A. H., and Steiner, D. F. (1988) An islet amyloid peptide is derived from an 89-amino acid precursor by proteolytic processing, *J. Mol. Biol. 263*, 17243-17246.
39. Marzban, L., and Verchere, C. B. (2004) Pro-islet amyloid polypeptide and its n-terminally extended intermediate are secreted from both the regulated and constitutive secretory pathways of beta-cells, *Diabetes 53*, A395-a395.
40. Udayasankar, J., Kodama, K., Hull, R. L., Zraika, S., Aston-Mourney, K., Subramanian, S. L., Tong, J., Faulenbach, M. V., Vidal, J., and Kahn, S. E. (2009) Amyloid formation results in recurrence of hyperglycemia following transplantation of human IAPP transgenic mouse islets, *Diabetologia 52*, 145-153.
41. Taniguchi, S., Suzuki, N., Masuda, M., Hisanaga, S., Iwatsubo, T., Goedert, M., and Hasegawa, M. (2005) Inhibition of heparin-induced tau filament formation by phenothiazines, polyphenols, and porphyrins, *J. Biol. Chem. 280*, 7614-7623.
42. Hirohata, M., Ono, K., Naiki, H., and Yamada, M. (2005) Non-steroidal anti-inflammatory drugs have anti-amyloidogenic effects for Alzheimer's beta-amyloid fibrils in vitro, *Neuropharmacology 49*, 1088-1099.
43. Rattanachaikunsopon, P., and Phumkhachorn, P. (2007) Bacteriostatic effect of flavonoids isolated from leaves of Psidium gujava on fish pathogens, *Fitoterapia 78*, 434-436.
44. Bieschke, J., Herbst, M., and Wanker, E. E. (2011) Small-molecule conversion of toxic oligomers to nontoxic beta-sheet-rich amyloid fibrils, *Nature 8*, 93-101.
45. Kapurniotu, A., Yan, L. M., Tatarek-Nossol, M., Velkova, A., and Kazantzis, A. (2006) Design of a mimic of nonamyloidogenic and bioactive human islet amyloid polypeptide (IAPP) as nanomolar affinity inhibitor of IAPP cytotoxic fibrillogenesis, *Proc. Natl. Acad. Sci. USA 103*, 2046-2051.

46. Shoichet, B. K., Feng, B. Y., Toyama, B. H., Wille, H., Colby, D. W., Collins, S. R., May, B. C. H., Prusiner, S. B., and Weissman, J. (2008) Small-molecule aggregates inhibit amyloid polymerization, *Nat. Chem. Biol. 4*, 197-199.
47. Neubig, R. R., and Blazer, L. L. (2009) Small molecule protein-protein interaction inhibitors as CNS therapeutic agents: current progress and future hurdles, *Neuropsychopharmacology 34*, 126-141.
48. Mihara, H., and Takahashi, T. (2008) Peptide and protein mimetics inhibiting amyloid beta-peptide aggregation, *Acc. Chem. Res. 41*, 1309-1318.
49. Abedini, A., Meng, F. L., and Raleigh, D. P. (2007) A single-point mutation converts the highly amyloidogenic human islet amyloid polypeptide into a potent fibrillization inhibitor, *J. Am. Chem. Soc. 129*, 11300-11301.
50. Fraser, P. E., Scrocchi, L. A., Chen, Y., Wang, F., Han, K., Ha, K., and Wu, L. (2003) Inhibitors of islet amyloid polypeptide fibrillogenesis, and the treatment of type-2 diabetes, *Lett. Pept. Sci. 10*, 545-551.
51. Gazit, E. (2002) A possible role for pi-stacking in the self-assembly of amyloid fibrils, *Faseb J. 16*, 77-83.
52. Winter, R., Mishra, R., Bulic, B., Sellin, D., Jha, S., and Waldmann, H. (2008) Small-molecule inhibitors of islet amyloid polypeptide fibril formation, *Angew. Chem. Int. Ed. Engl. 47*, 4679-4682.
53. Porat, Y., Abramowitz, A., and Gazit, E. (2006) Inhibition of amyloid fibril formation by polyphenols: Structural similarity and aromatic interactions as a common inhibition mechanism, *Chem. Biol. Drug. Des. 67*, 27-37.
54. Meng, F. L., Abedini, A., and Raleigh, D. P. (2010) Combination of kinetically selected inhibitors in trans leads to highly effective inhibition of amyloid formation, *J. Am. Chem. Soc. 132*, 14340-14342.
55. Ehrnhoefer, D. E., Bieschke, J., Boeddrich, A., Herbst, M., Masino, L., Lurz, R., Engemann, S., Pastore, A., and Wanker, E. E. (2008) EGCG redirects amyloidogenic polypeptides into unstructured, off-pathway oligomers, *Nat. Struct. Mol. Biol. 15*, 558-566.
56. Tatzelt, J., Rambold, A. S., Miesbauer, M., Olschewski, D., Seidel, R., Riemer, C., Smale, L., Brumm, L., Levy, M., Gazit, E., Oesterhelt, D., Baier, M., Becker, C. F. W., Engelhard, M., and Winklhofer, K. F. (2008) Green tea extracts interfere with the stress-protective activity of PrP(C) and the formation of PrP(Sc), *J. Neurochem. 107*, 218-229.
57. Hasegawa, M., Masuda, M., Suzuki, N., Taniguchi, S., Oikawa, T., Nonaka, T., Iwatsubo, T., Hisanaga, S., and Goedert, M. (2006) Small molecule inhibitors of alpha-synuclein filament assembly, *Biochemistry 45*, 6085-6094.
58. Wanker, E. E., Ehrnhoefer, D. E., Duennwald, M., Markovic, P., Wacker, J. L., Engemann, S., Roark, M., Legleiter, J., Marsh, J. L., Thompson, L. M., Lindquist, S., and Muchowski, P. J. (2006) Green tea (-)-epigallocatechin-gallate modulates early events in huntingtin misfolding and reduces toxicity in Huntington's disease models, *Hum. Mol. Gen. 15*, 2743-2751.
59. Meng, F. L., Abedini, A., Plesner, A., Verchere, C. B., and Raleigh, D. P. (2010) The Flavanol (-)-Epigallocatechin 3-Gallate inhibits amyloid formation by islet amyloid polypeptide, disaggregates amyloid fibrils, and protects cultured cells against IAPP-induced toxicity, *Biochemistry 49*, 8127-8133.

60. Norton, R. S., Chandrashekaran, I. R., Adda, C. G., MacRaild, C. A., and Anders, R. F. (2011) EGCG disaggregates amyloid-like fibrils formed by Plasmodium falciparum merozoite surface protein 2, *Arch. Biochem. Biophys. 513*, 153-157.
61. Bieschke, J., Russ, J., Friedrich, R. P., Ehrnhoefer, D. E., Wobst, H., Neugebauer, K., and Wanker, E. E. (2010) EGCG remodels mature alpha-synuclein and amyloid-beta fibrils and reduces cellular toxicity, *Proc. Natl. Acad. Sci. USA 107*, 7710-7715.
62. Hauber, I., Hohenberg, H., Holstermann, B., Hunstein, W., and Hauber, J. (2009) The main green tea polyphenol epigallocatechin-3-gallate counteracts semen-mediated enhancement of HIV infection, *Proc. Natl. Acad. Sci. USA 106*, 9033-9038.
63. Hasegawa, M., Masuda, M., Nonaka, T., Oikawa, T., Yonetani, M., Yamaguchi, Y., Kato, K., Hisanaga, S., and Goedert, M. (2009) Inhibition of alpha-synuclein fibril assembly by small molecules: Analysis using epitope-specific antibodies, *FEBS Lett. 583*, 787-791.
64. Lansbury, P. T., and Lashuel, H. A. (2006) A century-old debate on protein aggregation and neurodegeneration enters the clinic, *Nat. Cell Biol. 443*, 774-779.
65. Ray, S., Nowak, R., Brown, R., and Lansbury, P. (2005) Small-molecule-mediated stabilization of familial amyotrophic lateral sclerosis-linked superoxide dismutase mutants against unfolding and aggregation, *Proc. Natl. Acad. Sci. USA 102*, 3639-3644.
66. Chen, J., Armstrong, A. H., Koehler, A. N., and Hecht, M. H. (2010) Small molecule microarrays enable the discovery of compounds that bind the alzheimer's Ab peptide and reduce its cytotoxicity, *J. Am. Chem. Soc. 132*, 17015-17022.
67. Akaishi, T., Morimoto, T., Shibao, M., Watanabe, S., Sakai-Kato, K., Utsunomiya-Tate, N., and Abe, K. (2008) Structural requirements for the flavonoid fisetin in inhibiting fibril formation of amyloid b protein, *Neurosci. Lett. 444*, 280-285.
68. Ono, K., Yoshiike, Y., Takashima, A., Hasegawa, K., Naiki, H., and Yamada, M. (2003) Potent antiamyloidogenic and firbil-destabilizing effects of polyphenols in vitro: implications for the prevention and therapeutics of Alzheimer's disease, *J. Neurochem. 87*, 172-181.
69. Kim, H., Park, B., Lee, K., Choi, C., Jang, S., Kim, Y., and Lee, S. (2005) Effects of naturally occurring compounds on fibril formation and oxidative stress of b-amyloid, *J. Agric. Food Chem 53*, 8537-8541.
70. Abedini, A., and Raleigh, D. (2005) Incorporation of pseudoproline derivatives allows the facile synthesis of human IAPP, a highly amyloidogenic and aggregation-prone polypeptide, *Org. Lett. 7*, 693-696.
71. Abedini, A., Singh, G., and Raleigh, D. P. (2006) Recovery and purification of highly aggregation-prone disulfide-containing peptides: Application to islet amyloid polypeptide, *Anal. Biochem. 351*, 181-186.
72. Levine, H. (1995) Thioflavine-T interaction with amyloid beta-sheet structures, *Amyloid 2*, 1-6.
73. Meng, F. L., Marek, P., Potter, K. J., Verchere, C. B., and Raleigh, D. P. (2008) Rifampicin does not prevent amyloid fibril formation by human islet amyloid

polypeptide but does inhibit fibril thioflavin-T interactions: Implications for mechanistic studies beta-cell death, *Biochemistry 47*, 6016-6024.
74. Carver, J. A., Hudson, S. A., Ecroyd, H., and Kee, T. W. (2009) The thioflavin T fluorescence assay for amyloid fibril detection can be biased by the presence of exogenous compounds, *FEBS Lett. 276*, 5960-5972.
75. Cao, P., Tu, L. H., Abedini, A., Levsh, O., Akter, R., Patsalo, V., Schmidt, A. M., and Raleigh, D. P. (2011) Sensitivity of amyloid formation by human islet amyloid polypeptide to mutations at residue 20, *J. Mol. Biol.*
76. Nilsson, M. R., and Raleigh, D. P. (1999) Analysis of amylin cleavage products prodice new insights into the amyloidogenic region of human amylin., *J. Mol. Biol. 294*, 1375-1385.
77. Padrick, S. B., and Miranker, A. D. (2002) Islet amyloid: phase partitioning and secondary nucleation are central to the mechanism of fibrillogenesis, *Biochemistry 41*, 4694-4703.
78. Dunstan, D. E., Brown, P. H., Asimakis, P., Ducker, W., and Bertolini, J. (2009) Shear flow promotes amyloid-beta fibrilization, *Protein Eng Des Sel 22*, 741-746.
79. Eriksen, J. L., Sagi, S. A., Smith, T. E., Weggen, S., Das, P., McLendon, D. C., Ozols, V. V., Jessing, K. W., Zavitz, K. H., Koo, E. H., and Golde, T. E. (2003) NSAIDs and enantiomers of flurbiprofen target gamma-secretase and lower Ab42 in vivo., *J. Clin. Invest 112*, 440-449.
80. Feng, B. Y., Toyama, B. H., Wille, H., Colby, D. W., Collins, S. R., May, B. C. H., Prusiner, S. B., Weissman, J., and Schoichet, B. K. (2008) Small-molecule aggregates inhibit amyloid polymerization, *Nat Chem Bio 4*, 197-199.
81. Abedini, A., and Raleigh, D. P. (2009) A critical assessment of the role of helical intermediates in amyloid formation by natively unfolded proteins and polypeptides, *Protein Eng Des Sel 22*, 453-459.
82. Ling, Y. L., Strasfeld, D. B., Shim, S. H., Raleigh, D. P., and Zanni, M. T. (2009) Two-dimensional infrared spectroscopy provides evidence of an intermediate in the membrane-catalyzed assembly of diabetic amyloid, *J. Phys. Chem. 113*, 2498-2505.